STATUS OF THESIS

Title of thesis	Investigation of Starting Behaviour of a Free Piston Linear Generator Engine

I _____ EZRANN ZHARIF BIN ZAINAL ABIDIN _____

hereby allow my thesis to be placed at the Information Resource Center (IRC) of Universiti Teknologi PETRONAS (UTP) with the following conditions:

1. The thesis becomes the property of UTP

2. The IRC of UTP may make copies of the thesis for academic purposes only.

3. This thesis is classified as

   [ ] Confidential

   [x] Non-confidential

If this thesis is confidential, please state the reason:

_____

_____

_____

The contents of the thesis will remain confidential for _____ years.

Remarks on disclosure:
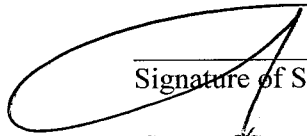
_____

_____

Endorsed by

Prof. Dr. Abd Rashid Abd Aziz
DVC Research & Innovation
Universiti Teknologi PETRONAS

_____   _____
Signature of Author   Signature of Supervisor

Permanent address: _____ .

24, Jalan Burhanuddin Helmi,   Name of Supervisor

Taman Tun Dr. Ismail,   Prof. Dr. Abdul Rashid Abdul Aziz

60000 Kuala Lumpur. Malaysia

Date : 26/12/13   Date : 26/12/13

UNIVERSITI TEKNOLOGI PETRONAS

INVESTIGATION OF STARTING BEHAVIOUR OF A FREE PISTON LINEAR
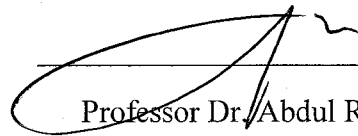
GENERATOR ENGINE

by

EZRANN ZHARIF BIN ZAINAL ABIDIN

The undersigned certify that they have read, and recommend to the Postgraduate Studies Programme for acceptance this thesis for the fulfillment of the requirements for the degree stated.

Signature:
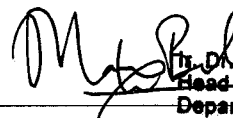
Main Supervisor: Professor Dr. Abdul Rashid Abdul Aziz

Prof. Dr. Abd Rashid Abd Aziz
DVC Research & Innovation
Universiti Teknologi PETRONAS

Signature:

Co-Supervisor: Mr. Saiful Azrin

Signature:

Head of Department: Associate Professor

Ir. Dr. Masri Baharom
Head of Department/Associate Professor
Department of Mechanical Engineering
Universiti Teknologi PETRONAS
Bandar Seri Iskandar, 31750 Tronoh
Perak Darul Ridzuan, Malaysia

Date: 2/1/14

INVESTIGATION OF STARTING BEHAVIOUR OF A FREE PISTON LINEAR

GENERATOR ENGINE

by

EZRANN ZHARIF BIN ZAINAL ABIDIN

A Thesis

Submitted to the Postgraduate Studies Programme

as a Requirement for the Degree of

MASTER OF SCIENCE

MECHANICAL ENGINEERING

UNIVERSITI TEKNOLOGI PETRONAS

BANDAR SERI ISKANDAR,

PERAK

DECEMBER 2013

DECLARATION OF THESIS

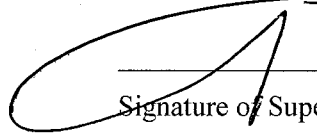| Title of thesis	Investigation of Starting Behaviour of a Free Piston Linear Generator Engine

I _____ EZRANN ZHARIF BIN ZAINAL ABIDIN _____

hereby declare that the thesis is based on my original work except for quotations and citations which have been duly acknowledged. I also declare that it has not been previously or concurrently submitted for any other degree at UTP or other institutions.

Witnessed by

_____
Signature of Author

_____
Signature of Supervisor

Permanent address:_____

 24, Jalan Burhanuddin Helmi,

 Taman Tun Dr. Ismail,

 60000 Kuala Lumpur. Malaysia

Name of Supervisor

Prof. Dr. Abdul Rashid Abdul Aziz

Date : 26/12/13

Date : 26/12/13

iv

DEDICATION

This thesis is dedicated to my family and above all, to my loving late mother Rokiah Bee bt Abu Bakar.

ACKNOWLEDGEMENTS

First and foremost, praise to Allah Almighty for His support and wisdom that gives me strength, patience, insight for me to move forward and complete this research. Without His will, this research would not have been a success, Alhamdulillah.

I would like to convey my sincere appreciation to my supervisor Prof. Dr. Abdul Rashid Abdul Aziz for his invaluable assistance and technical guidance, and also by providing me the opportunity to work with free-piston linear generator engine research team. Special thanks to my co-supervisor Mr. Saiful Azrin for his pioneering work on LG control system while tutoring and assisting on my research towards the end. Only Allah S.W.T can return their tireless effort.

Next gratitude would definitely go to my research partner Dr. Abdulwehab who have helped me a lot in my research progress especially on my thesis writing. I would like to thank Mr. Firmansyah who had helped and advice me on experimental works and understanding on internal combustion engine. Not to forget thank you to all CAREM members.

Furthermore, thanks to MOSTI under the IRPA grant and to MOHE under the FRGS grant to make all of my research possible. The support and assistance from the staffs of Centre for Graduate Studies (CGS) and Research Innovation Office (RIO) are greatly appreciated.

Like they say, keep the best for last hence deepest appreciation goes to my late mother, father, brother and sister for their eternal affection, prayers and support throughout my life. On top of all, to my late mother whose smile promises me a never ending hope for my future endeavors.

ABSTRACT

The current global crisis is now wrapped around the transportation industry whereby emissions and fuel prices are increasing. It is clear that the transportation system have polluted globally with CO, NO_x and soot. Due to the reasons mentioned, environmental policy makers have created laws that limit the emission level produced by the internal combustion engine. As a result, it pushes researchers to develop new methods and technologies to tackle this problem and to come up with a highly efficient internal combustion engine with lower emissions. A two-stroke free piston linear-generator engine (FPLG) as prime mover for electric power generation has been developed to address these issues. A linear engine coupled to a permanent-magnet assembly becomes a linear-generator (LG) which can produce electrical power. Its working principle is based on the free-piston two-stroke engine with direct injection. The piston-rod (translator) assembly consists of two pistons and a rod, with one piston connected to each end of the rod and a magnet assembly at the center. Combustion energy will cause the piston-rod assembly to move freely back and forth between the two engine blocks. Magnetic field from the permanent magnet assembly will cut through conductor coils - which are externally located within the stationary part of the LG (stator iron) - to generate electricity. Thus, electrical power is generated directly from the moving piston. For starting of the generator, the LG is operated in a reverse process - as a motor, whereby current is injected into the coils to produce force to reciprocate the translator against the forces of compression of the engine blocks, in order to produce combustion. Experimental works described in this thesis show promising results on compression and combustion pressure using an upgraded inverter consisting of MOSFETs and gate driver with much increased reliability from previous inverters. It concludes that higher motoring voltage will increase the compression but will reduce compression ratio, exhibiting an inverse relationship between compression pressure and compression ratio. Furthermore, due

to its free-piston characteristic, the combustion pressure will affect the point of TDC in mass fraction burn graph (MFB) and Rate of Heat Release (ROHR). Previous works managed to produce only 9 bar of peak combustion pressure during starting, using 60V battery capacity. With the upgraded system and further engine optimization, the LG managed to produce 12.7 bar of combustion pressure and a higher maximum IMEP of 0.92 bar.

ABSTRAK

Krisis global semasa kini dikelilingi industri pengangkutan di mana pelepasan dan bahan api harga semakin meningkat. Ia adalah jelas bahawa sistem pengangkutan telah mencemarkan dunia dengan CO, NOx dan jelaga. Oleh kerana sebab-sebab yang dinyatakan, pembuat dasar alam sekitar telah mewujudkan undang-undang yang menghadkan tahap pelepasan yang dihasilkan oleh enjin pembakaran dalaman. Akibatnya, ini telak menaikan semangat penyelidik untuk membangunkan kaedah dan teknologi baru untuk menangani masalah ini untuk menghasilkan enjin pembakaran dalaman yang sangat berkesan dengan pelepasan rendah. Satu prototaip omboh bebas dua lejang enjin penjana linear (FPLG) menjana kuasa elektrik telah dibangunkan untuk menangani isu-isu ini. Sebuah enjin linear ditambah pula dengan perhimpunan - magnet kekal menjadi enjin penjana linear (LG) yang boleh menghasilkan kuasa elektrik. Prinsip kerja adalah berdasarkan pada enjin omboh bebas dua lejang dengan suntikan langsung. Omboh rod (penukar) terdiri daripada dua omboh dan satu rod dimana satu omboh disambungkan kepada setiap hujung rod dan pemasangan magnet di tengah-tengah batang. Pembakaran tenaga akan menyebabkan pemasangan rod omboh ini bergerak bebas dan berulang-alik antara kedua-dua blok enjin. Medan magnet yang dihasilkan oleh magnet kekal akan dipotong melalui gegelung pengalir - yang luaran yang terletak di dalam bahagian yang bergerak dari LG (besi pemegun) - untuk menjana elektrik. Oleh itu, kuasa elektrik yang dijana terus dari omboh bergerak. Untuk memulakan penjanaan, LG dikendalikan dalam proses terbalik - seperti motor dimana arus elektrik disuntik ke dalam gegelung untuk menghasilkan kuasa untuk menentang kuasa-kuasa mampatan blok enjin untuk menghasilkan pembakaran. Kerja-kerja eksperiment yang dinyatakan di dalam tesis ini menunjukkan keputusan yang menjanjikan pada mampatan dan tekanan pembakaran menggunakan MOSFET yang dinaik taraf sebagai 'inverter' dan pemandu MOSFET yang sangat handal. Thesis juga membuat kesimpulan bahawa voltan permotoran

yang lebih tinggi akan meningkatkan tekanan mampatan tetapi akan mengurangkan nisbah mampatan maka hubungan songsang antara tekanan mampatan dan nisbah mampatan. Tambahan pula, disebabkan ciri-ciri omboh bebas, tekanan pembakaran akan menjejaskan titik TDC dalam Pecahan Jisim Membakar graf (MFB) dan Kadar Haba Realease (ROHR). Kerja-kerja sebelum ini berjaya menghasilkan hanya 9bar tekanan pembakaran dengan menggunakan 60V kapasiti bateri. Dengan sistem dinaik taraf dan pengoptimuman enjin lagi , LG berjaya menghasilkan 12.7 bar tekanan pembakaran dan IMEP tertinggi 0.92 bar.

In compliance with the terms of the Copyright Act 1987 and the IP Policy of the university, the copyright of this thesis has been reassigned by the author to the legal entity of the university,

Institute of Technology PETRONAS Sdn Bhd.

Due acknowledgement shall always be made of the use of any material contained in, or derived from, this thesis.

TABLE OF CONTENT

LIST OF FIGURES

LIST OF TABLES

CHAPTER 1

INTRODUCTION

1.1 Background

Internal combustion engines (ICE) have been a power unit for numerous applications for the past 200 years. It converts chemical energy to a working mechanical output, a process which is still widely used until today. The high-pressure gas produced by the combustion of air and fuel mixture inside the cylinder will apply force to a piston reciprocates it. The piston when coupled to a crank shaft through a connecting rod will convert the reciprocating motion to a rotating mechanical output. This mechanical output can be used for a variety of applications including coupling it to a generator to produce electrical power. To date, the major use of the ICE is still in the transportation industry as a propulsion unit.

The current global crisis is now wrapped around the transportation industry whereby emissions and fuel prices are increasing. It is clear that the transportation system have polluted globally with its CO, NO_x and soot. Volatile organic compounds (VOCs) were also identified as one of pollutants of the environment [1]. Due to the reasons mentioned, environmental policy makers have created laws that limit the emission level produced by the internal combustion engine. As a result, it pushes researchers to develop new methods and technologies to tackle this problem and to come up with a highly efficient internal combustion engine with low emissions.
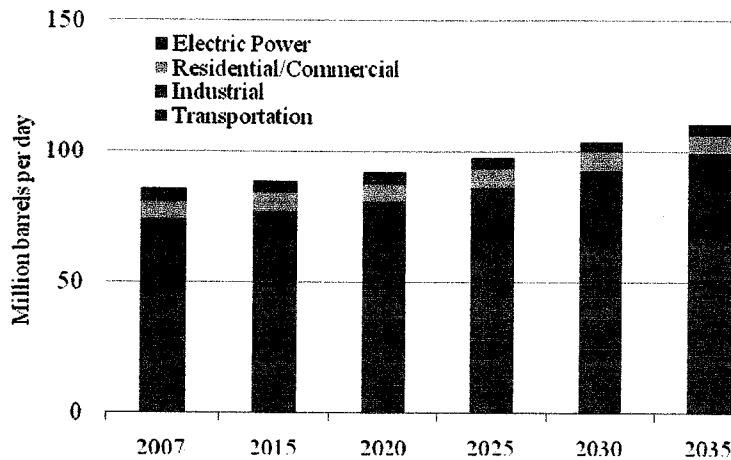
Figure 1.1: World liquids consumption by sector 2007 - 2035 [2]

These environmental issues drive the global direction to produce renewable and alternative forms of energy. Hence, more focus is concentrated in the internal combustion engine since it is a major energy consumption and contributes the highest impact on environmental pollution. This leads researchers to produce internal combustion engines that have low emissions, better mechanical and thermal efficiency at part load operation and improved fuel efficiency [3]. Another group of researchers claim that improvement on engine technology can be accomplished by using free-piston engine technology. The reason is that a free-piston engine has the characteristic of simple structural design, flexibility, high mechanical and thermal efficiency [4-8]. This could develop a new standard in order to achieve global effort to produce a zero-emission engine.

A free-piston linear generator fueled by hydrogen is promising technology to produce electrical energy efficiently with zero emissions. Due to its free-piston motion, a great challenge exists in order to design a control system that could run complex engine operations to address piston motion cyclic variation problems, two-stroke performance issues, and combustion technology (SI or DI). A great number of researchers are attending to these issues for many of years and a few prototypes were reported [9-15].

This thesis here will presents research work done at Universiti Teknologi PETRONAS (UTP) on a free piston linear generator (FPLG) engine that is designed and developed by *UTP FPLG* team. The objective of this project is to produce an

2

environmentally friendly power unit to charge a battery bank on board a series hybrid electric vehicle (SHEV). The prototype is based on two-stroke cycle engine in which hydrogen fuel will be injected directly into the cylinder (DI). A number of parameters are variables of the system such as injection timing and duration, ignition timing, motoring voltage and piston/translator position. All of these parameters and engine operations are monitored and controlled by a complex control system. This research is focused on the behaviour of engine operation and performance by varying the variables above.

1.2 Problem Statement

Starting mechanism of the free-piston linear generator (FPLG) is a great challenge to overcome. The FPLG will be operated as a motor during starting. It will draw current from the battery bank and starts to reciprocate. It could not motor the engine to reach the required full amplitude to ignite the air-fuel mixture. The reason for this is the intricate force and position feature of the system which comes from the interaction of the electromagnetic force with the engine [5]. According to previous studies [11], motoring with higher battery voltage (which relates to higher motoring force) would allow the engine to motor at full amplitude(higher compression ratio) to achieve higher compression pressure; thus, higher combustion pressure of air and fuel mixture is possible. Furthermore, the instants of injection and ignition need to be optimized in order to produce higher combustion pressures to reach engine idling.

1.3 Objectives

The objectives of this research are:

- To study and upgrade the current system to allow higher motoring voltage.

- To verify engine behaviour before and after upgrading.

- To investigate starting behaviour and the effect of battery voltage on the starting operation of the engine through experimental analysis.

1.4 Methodology

This thesis is focused on experimental approach to investigate starting behaviour of the Free-Piston Linear Generator engine. The prototype engine is based on a dual-piston setup with two-stroke direct-injection engine and fueled by high-pressure hydrogen gas. At the center of the prototype device lies a coil and permanent magnet assembly which is very unique since it can operate as both motor and generator but this study only concentrates on motoring. A high-speed data acquisition system is connected to the engine in which monitors crucial engine operations such as the piston position, in-cylinder pressure of both the cylinder and amount of current parameters consumed by the engine during motoring. Preliminary data was taken to look at the maximum performance of the engine when motoring with combustion at 36 V and 50V and to identify items to be upgraded in order to cater for higher motoring voltage. Once identified, upgrading works are carried out on the MOSFETs and IGBT-stage inverter and further studies are implemented to verify behaviour before and after the upgrade. IGBT inverter drive was not chosen due to high electromagnetic interference (EMI) emitted in the system which disrupts engine behaviour. Experiments continued with higher ratings of MOSFET inverted. Once completed, works involving higher than 50V motoring which is 62V and 74V including combustion are executed and data collected. The raw data is analyzed to look at the behaviour and performance through several methods such as the indicated mean effective pressure (IMEP), rate of heat release (ROHR), mass fraction burn (MFB), pressure-volume (PV) curve, coefficient of variance (COV) and thermal efficiency.

1.5 Scope

The main objective of this research is on examining characteristics and starting behaviour of the free-piston linear-generator engine by varying the motoring voltage which relates to higher motoring force. Other parameters such as injection duration and timing, ignition timing and piston position are varied to achieve highest in-cylinder combustion pressure fueled by hydrogen gas while assisted by motoring. It is

conducted on UTP's free-piston linear-generator engine prototype through experimental analysis.

1.6 Thesis Organization

This thesis consists of five chapters. The chapter starts off with introduction, followed by literature review, methodology, results and discussion, conclusion and recommendations. Experimental work are performed and analyzed to meet objectives of the research.

Chapter 1 briefly discusses background of this research that led inventors at UTP to develop the free-piston linear-generator engine. The problem statement and objectives are stated and explained in this chapter.

Chapter 2 describes the concept and types of free-piston engine. Basic operating principles of internal combustion engine and combustion technology are explained. The effects of hydrogen as fuel in combustion engines are also described together with a brief description of electromagnetic inference (EMI).

Chapter 3 presents the running prototype of free-piston linear generator engine together with its experimental setup. The methodology of the experimental works is outline. Finally the fundamental equations for analyzing the experimental data are included.

Chapter 4 is dedicated to present all of experimental data obtained, discussion and findings on the behaviour of the free-piston linear-generator engine. Furthermore, fundamental equations used to analyze performance of the engine are presented.

Chapter 5 concludes the whole outcome of this experiment and provides recommendations to optimize the engine and for further study in this research.

CHAPTER 2

LITERATURE REVIEW

2.1 Introduction

Much research has been done on free-piston engines. This chapter goes through few papers regarding development of the free-piston engine with different configurations. Early development begins with using compressed air and high-pressure gas as a working fluid. The configuration of the setup is mostly dependent on the working fluid or the desired type of energy output. The most complicated is the free-piston linear-generator which will produce electrical energy from combustion, due to the absence of a flywheel which requires complicated control strategy to control and start the engine. The following section discusses challenges and works done on the free-piston engine as well as behavior of hydrogen in an internal combustion engine. This review is essential since the free-piston prototype operates using Hydrogen gas as fuel.

2.2 Types of Free-Piston Engine

Most research is narrowed to 4 concepts. The biggest difference between each other is the output that it produces. It varies from pressurized working fluid to electrical energy. Albeit the differences, the common thing among the 4 concepts is that it runs on a two-stroke cycle basis, due to the need of power stroke for every cycle. Due to the free-piston characteristic, the top dead centre (TDC) and bottom dead centre (BDC) can vary, giving rise to different volume for the working fluid to expand and compress.

The configurations also play an important role for different working fluids [16]. Few designs were made using an opposed piston with a single expansion chamber, single piston with dual expansion chambers and single-piston, single-expansion chamber. A common setup with one piston and dual combustion chambers is used for the free-piston linear generator application [4]. Most setups with single piston are used for hydraulic applications [17].

2.2.1 Free-Piston Linear-Generator Engine

A free-piston linear-generator translates chemical energy to mechanical energy and lastly to electrical energy. This electrical energy is then used to power directly an electric motor in a series hybrid electric vehicle (SHEV) or to charge its onboard battery pack. The combustion of an air and fuel mixture in the combustion chamber produces a reciprocating motion of the dual-piston assembly called the translator. The magnet assembly located at the center of the translator will travel back and forth through several coils. The process of cutting magnetic flux produces electric power. It is one of intricate designs of a free piston due to the existence of cogging force due to the permanent magnet and stator iron laminations coil acting on the translator [5,11]. Challenges faced with this type of design are the complex control system. A complex control strategy needs to be implemented in order to control motion of the piston at startup and running [4,18]. There is a potential in the future that this design is a suitable power unit to be used in a hybrid electric vehicle (HEV) [9] and micro power generator system for portable power applications [5,20,21].

2.2.2 Free-Piston Air Compressor

Free-piston air compressors are among the earliest efficient working prototype that works with variable range [22]. These compressors have few different arrangements, either a horizontal or vertical setup shown in Figure 2.1 and 2.2 [23,24]. The pressurized air is used for pneumatic purposes. A multi-stage air compressor system needs to be implemented to achieve high compression pressure

using the free-piston air compressor. It is mentioned that to compress air to higher than 7 bar, a multi-stage system is required [25,26].
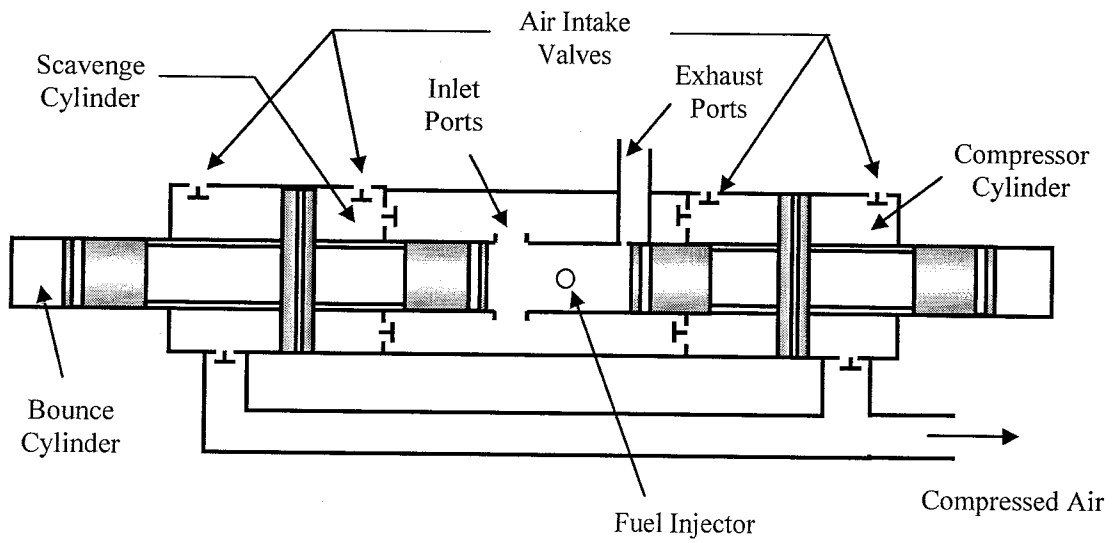
Figure 2.1: Horizontal setup free piston air compressor
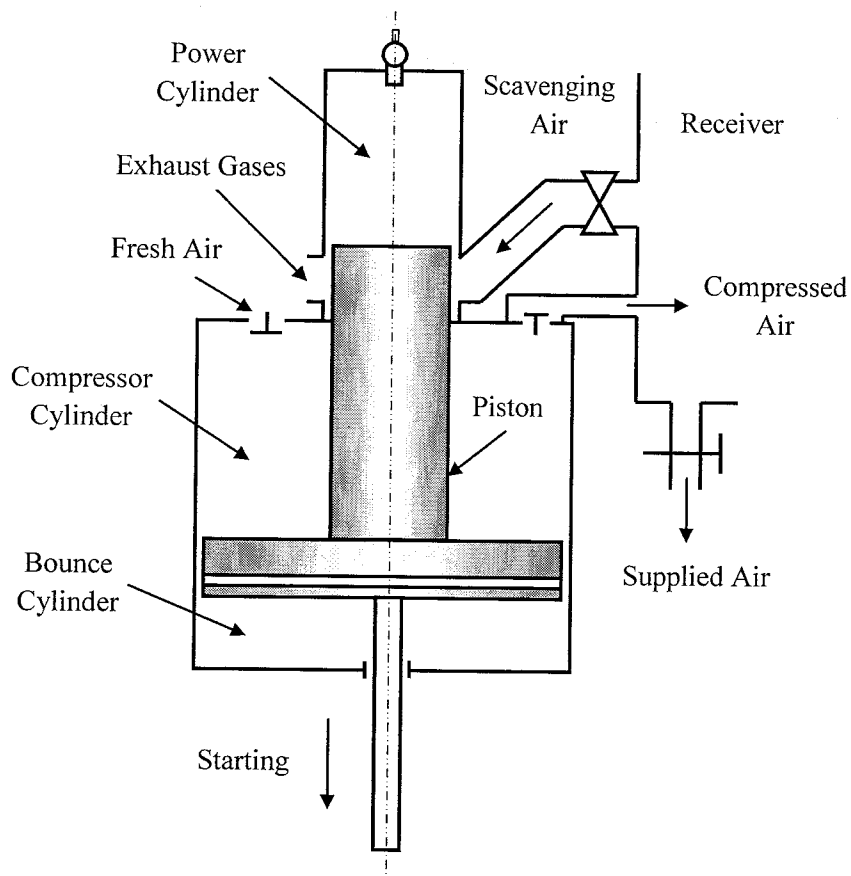
Figure 2.2: Vertical setup free piston air compressor

2.2.3 Hydraulic Free-Piston Engine

Hydraulic free-piston works as a hydraulic pump whereby chemical energy from air and fuel mixture produces combustion pressure that is then applied on the piston to pump the hydraulic fluid to a certain level of pressure. The free piston is directly connected to the hydraulic pump [27]. A typical horizontal setup with linear motion of free piston hydraulic pump is shown in Figure 2.3.

The combustion will only produce pressure in one direction, therefore a compression accumulator is required to push the piston back and forth. Due to hydraulic characteristic (incompressible and accurate delivery of pressure), the hydraulic free piston therefore has the easiest force-position feature [5,28].
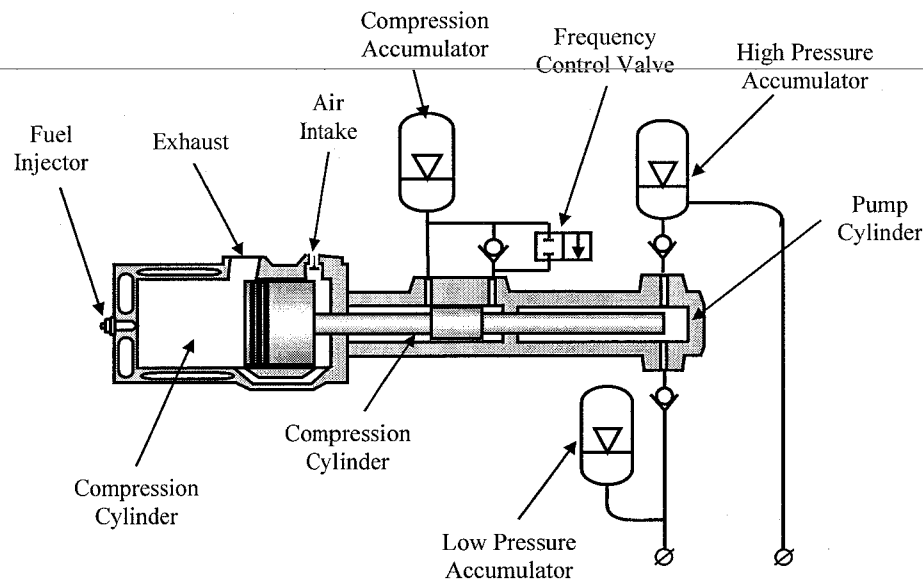
Figure 2.3: Typical hydraulic free piston pump [29]

2.2.4 Free-Piston Gas Generator Engine

Gas generator free-piston engine is almost similar to the air compressor but few modifications are made so that the air compressor piston works as a force induction system supplying pressurized air to the combustion chamber. The combustion process will later produce a high pressure hot gas with pressure slightly lower than compressed air to allow scavenging process to work. Energy in the hot gas will be

harvested by channeling the hot gas burned from the combustion chamber to a turbine, as shown in Figure 2.4 [30].

It is favorable to couple a free-piston gas generator to a turbine, rather than a conventional gas turbine. Conventional gas turbines produce only 1/3 usable power output while the remaining balance is used to drive the compressor impeller. While for free-piston gas generator, the compressed air is produced in a gasifier. In this case, it manages to produce lower temperature for the inlet of the turbine. Low temperature for the inlet of the turbine making material such as iron steel is a potential option to be used as the impeller for the turbine which is not possible with conventional gas turbine [31].
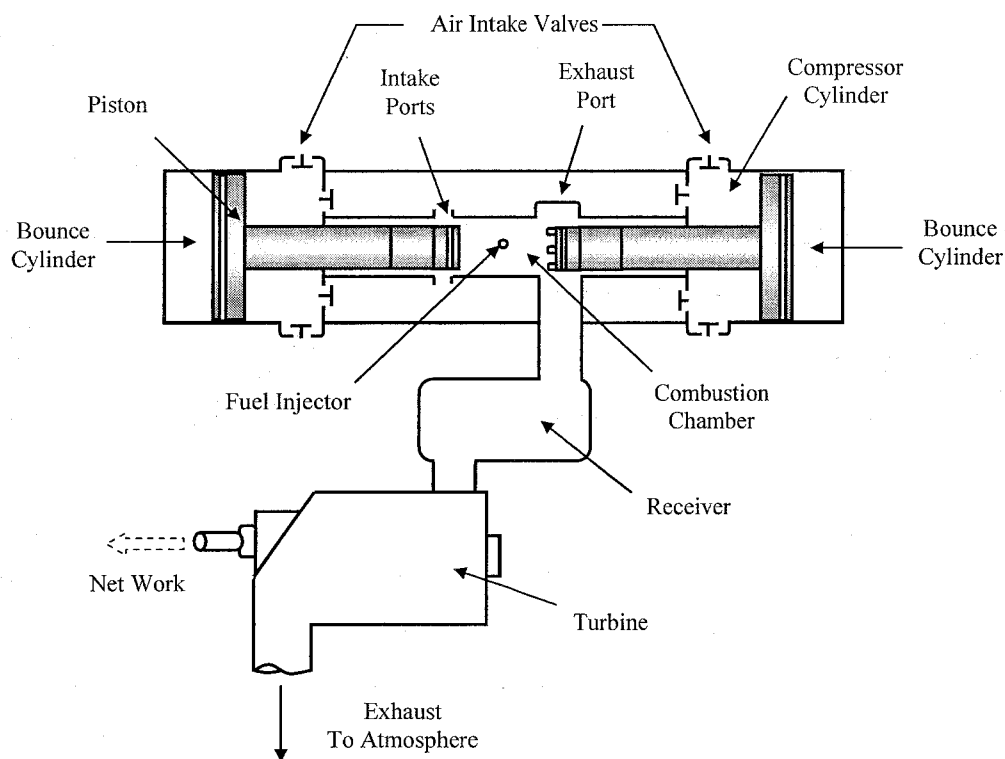
Figure 2.4: Free-Piston Gas Generator [30]

2.3 Free-Piston Linear Generator (FPLG)

As mentioned previously, a free-piston linear-generator is among the most complex configurations of free piston technologies. It has many types of architecture

and each configuration has a different characteristics. The operating principle is somewhat different than conventional engines and the work output is not the same, depending on specific type of FPLG.

2.3.1 Configuration of Free Piston Engine

A substantial amount of reports is available on the setup of the FPLG configuration. There are a set of most common configurations that are widely applied ranging from a single piston, dual piston, and opposed piston. For dual-piston setup, it can have one or two combustion chambers. Hydraulic setups were heavily focused by Achten [32] for which few configurations were discussed and evaluated in a detailed. While Toth-Nagy and Clark in [33], explain different configurations of the free-piston engine.

One of the simplest configurations is the single piston with a single combustion chamber, as shown in Figure 2.5. It is reported that with this setup, the motion is easier to control and it is completely balanced, giving rise to vibration-free operation. With a single piston vertically setup, it is used as a gasifier but it is more effectively used as a hydraulic free-piston engine [32,34]
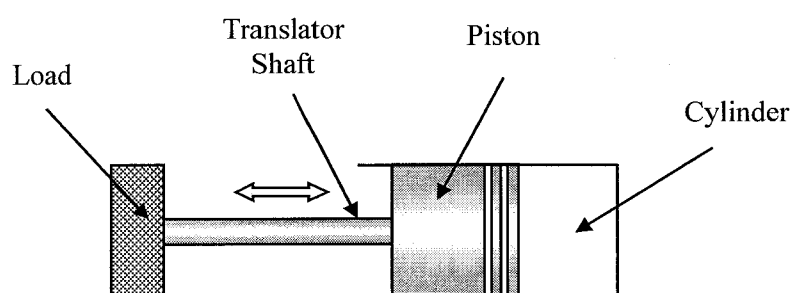
Figure 2.5: Single piston with single combustion chamber configuration

There are two configurations which use using two pistons. One is the dual-piston configuration which consists of two combustion chambers and another is an opposed piston which consists of one combustion chamber. Apart from the main difference in terms of number of combustion chambers, the position and motion of the pistons are to be considered. The motion of both pistons for the dual piston will always be

synchronous since they are connected to a center shaft (Figure 2.6). As for the opposed-piston, motion of one piston is always opposite the other. The opposed-piston configuration (Figure 2.7) has the most balanced setup due to the opposite forces and the inverse motion of the pistons. Even so, motion of the pistons must be synchronized by using a link mechanism or toothed rack on a pinion gear [35].
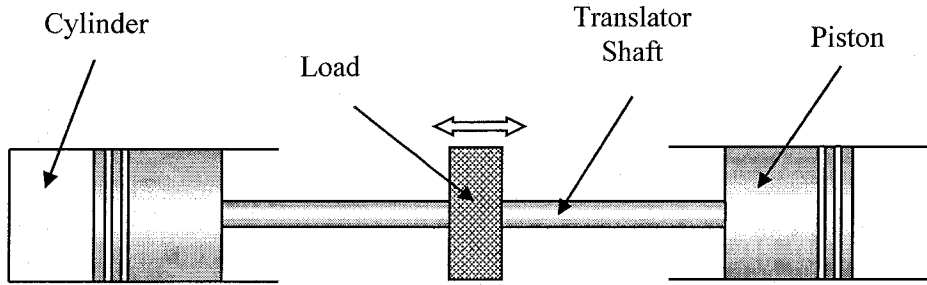
Figure 2.6: Dual piston with two opposite placed combustion chamber
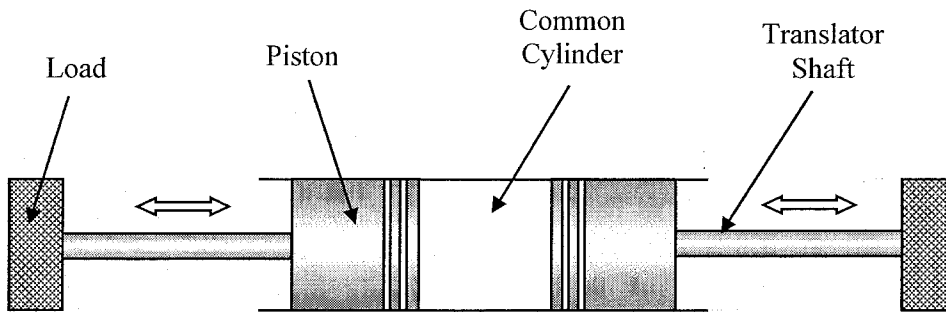
Figure 2.7: Opposed pistons with single combustion chamber placed at the center

In Figure 2.7, a typical opposed-piston configuration is shown. In [26,37], it is mentioned that with this configuration, the engine is simpler, less costly, lighter and more space effective than the dual-piston setup. According to [31], power generated by the opposed piston is higher than dual piston since the weight of the assembly for the dual piston is much larger affecting the rate of oscillation and thus its power output [31].

2.3.2 Operating Principles of the Free-Piston Engine

The basic operating principle for most free-piston engines is very straight-forward. Air and fuel mixture will combust based on a two-stroke cycle. Pressure produced will eventually push the piston, which is connected to a load directly via a translator shaft. It will continuously reciprocate in one axis (linear) to produce work. The load varies from a compressor or pump, to a generator. For free-piston engine with dual piston configurations, there are two combustion chambers that can create two different vectors of forces in one axis. As for the single-piston arrangement, a bounce chamber is required to create an opposite movement of the piston after the combustion process. The bounce chamber consists of air which will store energy during compression (when the piston is in expansion stroke) and release the energy back to the piston (when the piston is in compression stroke). Kinetic energy from the piston is absorbed by the load and the bounce chamber, ignoring energy losses due to friction [5].

2.3.2.1 Intake and Exhaust System

Operating principle of the free-piston engine needs a power stroke for every cycle of the engine. This is only possible with the two-stroke cycle method, hence, an intake and exhaust system is designed based on the two-stroke system. It requires two ports: one for intake and one for exhaust. A one-way flow reed valve is attached at the intake port to create a uni-flow system. Two-stroke systems provide the engine with simple approach with less complexity compared to a four-stroke engine which requires a camshaft and valves. During the expansion/power stroke, the exhaust port will be exposed first before the intake port. This is to allow exhaust gas to exit the cylinder first and once the intake port opens, fresh charge is drawn from the intake port by the momentum of the exhaust gas exiting the cylinder. This process is called scavenging whereby exhaust gas will be flush out of the cylinder completely and fresh air charge will fill up the cylinder.

2.3.2.2 Engine Control System

Free-piston engines work linearly without any crankshaft or flywheel to guide its motion, in contrast to a conventional internal combustion engine. Due to this main reason, the term free-piston is used whereby the piston is not bonded to any motion limitations thus having variable top dead centre (TDC) and bottom dead centre (BDC). With the crankshaft and flywheel removed, a complicated control system coupled with a suitable control strategy is required in order to control the motion of the piston. It is mentioned that if the TDC value is low due to failure of the piston motion, the engine cycle will stop because combustion can't be sustained due to compression drop [38]. Unstable TDC would also create problem, high TDC leads to higher combustion temperature and pressure that would damage the mechanical design of the engine. In this study, controlling the TDC and BDC limits is very important and thus a reliable and effective control system is crucial for a stable operating engine.

Free-piston engines create a number of control parameters due to the lack of crankshaft and flywheel. To control the motion of the piston, parameters such as compression ratio, BDC, TDC and frequency are determined [29]. Desirable stroke length is achieved by controlling the fuel input during the combustion process. Longer stroke relates to more fuel injected and shorter stroke requires less fuel. Furthermore, during the generation process of the free-piston electric generator, the electrical braking force will act against the translator thus increasing the fuel needed to sustain operation [16]. For hydraulic free-piston engines, a pulse pause modulation (PPM) control method can be implemented to control frequency of the engine in order to handle work output of the engine [34].

2.3.2.3 Bounce Chamber

A bounce chamber is used as an energy storage device due to absence of the flywheel in a free-piston engine. The need of a bounce chamber in a free-piston engine is to create an opposite motion/force for the compression cycle. In the expansion stroke, the piston will compress air in the bounce chamber thus storing

14

energy. The energy stored later will be used to push back the piston in the compression cycle. Air in the bounce chamber will be compressed and expand (similar to a pneumatic process) in that chamber without transporting the working fluid to another place [5]. Huber [39] mentions that it is utterly impossible for collision between the piston and the bounce chamber to occur due to the result of 'spring mass' effect obtained by compressing the air. This safety operation is also based on a few design criteria mentioned by the author.

2.3.2.4 Starting of the free-piston engine

The absence of flywheel in a free-piston engine is a great challenge to overcome. Flywheel is needed to start and stabilize cyclic variations in an internal combustion engine and also as energy storage. Thus, a different starting strategy is required in a free-piston engine. A starting method is proposed in [6] for a fre-piston engine, which states that it should be started/ignited at the first stroke, achieved by impulsing the piston. A common starting strategy which is commonly applied at large engines is to push the piston towards top dead centre and then high-pressured air is supply rapidly into the bounce chamber to push the piston at highest velocity possible. This strategy is widely applied in free-piston air compressor and gasifier as well. As for hydraulic free-piston engines, starting is achievable with a hydraulic pump. On the other hand, many starting problems arise with the free-piston linear generators. A number of starting methods using an electric motor are implemented in [18,40], while research using a spring-mass system for starting the engine was proposed in [41].

A two-stroke spark-ignited free-piston linear generator engine prototype was designed and built for research purpose at West Virginia University (WVU). A pair of starter solenoid coils were taken from a heavy-duty engine and attached to the connecting rod to start the engine [10]. The mechanism works successfully on proving motoring force for the prototype but more space is required to place the solenoids. Experiments were carried out and a conclusion drawn was that unthrottled operation of the engine is desirable for the spark-ignited prototype to ease the engine operation and thus the next step was to develop a new diesel type for free-piston

linear generator [43]. Following the second version of the engine, the diesel prototype with an alternator as a motoring device, it could not motor due to problematic starting process which causes a number of transistors to burn out.

A study was conducted by Arof et. al [44] whereby few methods were tested to reduce cogging force and starting method for the free-piston linear generator. Cogging force is a type of interaction force between permanent magnets on the translator and iron core/laminations of the stator. It is an unwanted force because it contributes a resistive force on the motion of the translator and causes a problem to the starting process of the engine. Two methods were determined: first is to add an extra coil to the starter assembly; direct current is injected into the main coils and at the same time an opposite-polarity current is injected in the extra coil. The second method involves the two main coil assembly of the generator being split into four sub-coils. The second method provides easier controlling technique to supply current and different values and polarities to the coils.

Starting of the free-piston linear-generator is a challenge therefore many researchers are looking into this matter. Zulkifli et. al. [18] studied some starting methods and control strategy. The coils on the free-piston linear generator are energized with different strategy, which is the open-loop and rectangular current commutation. Electrical current will energize a pair of coils to drive the piston to compress the air-fuel mixture to a point where combustion occurs. It is mentioned that with a constant force applied to the translator in the direction of motion, the system could reciprocate and reach full required amplitude. It is mentioned that this prototype works through simulation successfully with combustion assisted by motoring. The amount of electrical current injected into the coil is directly proportional to the motoring force, thus supplying higher current will motor the engine at higher frequency.

2.3.3 Linear Generator versus conventional Internal Combustion Engine

New invention always tries to present an alternate solution to a current problem. A large number of researchers are searching for a power unit that is more efficient and versatile than to a conventional crank-slider engine. A free-piston is one of the options that have high potential to create an efficient power unit. Advantages of the free-piston engine are repeatedly mentioned in a number of papers such as simple design with less moving parts, compact, wider range of operation, multi-fuel capability, low maintenance and many more. Piston motion in a free-piston engine is highly dependable on gas pressure acting on the piston [5], which enables the engine to be free from limiting factors that exist in spark-ignition (SI) and compress-ignition (CI) engines.

One of the limiting factors of a crank-slider internal combustion engine is the fixed physical property of compression ratio. To many researchers, it can be a disadvantage since compression ratio brings a very big impact on engine performance. During part load operation of a standard SI engine, it is desirable to have variable compression ratio to fully optimize engine power output [3]. It is impossible to use a high compression ratio in an SI engine due to auto ignition property of gasoline. Due to that, most SI engines are having the most optimized compression ratio of 10 while one knows if the engine were capable of increasing its compression ratio, the efficiency will increase as well. A typical example is the CI engine which uses diesel as fuel, which has 22 as a common compression ratio value; it is more efficient than a spark-ignited engine. Thus, with the free piston-engine, compression ratio is a variable parameter, which relates to higher efficiency, wide operating range and multi-fuel capabilities. In one literature, a free-piston engine was tested to be working with a compression ratio of 40 to 60 [45].

Another big advantage of a free-piston engine is that there is less friction in the system compared to a conventional crank-slider engine. The operating principle of a crank-slider engine and a free-piston is not much different from, but the absence of crank motion in a free-piston creates a unique engine characteristic and compactness. Heywood [46] elaborates that presence of crankshaft, connecting rod and bearing contributes to friction losses in the common crank-slider engine. The highest friction

17

losses are at the piston skirt (side load) during conversion of motion from rotary to linear and vice versa. These major parts are not present in a free-piston engine and due to the two-stroke design which has less moving parts(no camshaft, valves, etc), the free-piston engine has much lower friction losses compared to a crank slider engine.

Furthermore, dynamic balance of the pistons can be accomplished hence reducing noise and vibration. This is possible due to less moving parts as mentioned previously. Possibility of the engine to run at high compression ratio will lead to advantages in thermal efficiency by operating at higher pressure. The free-piston low friction capabilities, together with less moving parts also contribute to a higher thermal efficiency. Advantages gained will not sacrifice the thermodynamic performance of free-piston engines.

2.3.4 Reported Works

Free-piston linear-generator engines are still under development. Most researchers have a great challenge to start the prototype due to absence of the conventional flywheel. Furthermore, majority of them states the importance of a control system in order to achieve precise control of a stable running prototype.

2.3.4.1 West Virginia

Researchers at West Virginia have developed a two-stroke, free-piston linear generator engine prototype which produces electric energy. Studies on the engine were done numerically and experimentally [10,47,43, 48-51]. Nandkumar [10] did experimental investigation on an engine with a 36.5mm bore while varying applied load and ignition timing. The applied external load to create resistance to the shaft was replaced with a friction brake system instead of the old linear alternator. The applied load force followed simulation data of the force that linear alternator would apply to the shaft. The experimental results of few cases by varying ignition timing and braking load are clearly shown. Under high friction load and retarded spark

ignition, the prototype managed to work and produce 780 W of net positive power. Additional studies were done which managed to obtain stable operation of the combination of linear alternator with linear internal combustion engine and achieved 316 W of electrical power at 23.1 Hz [48,52].
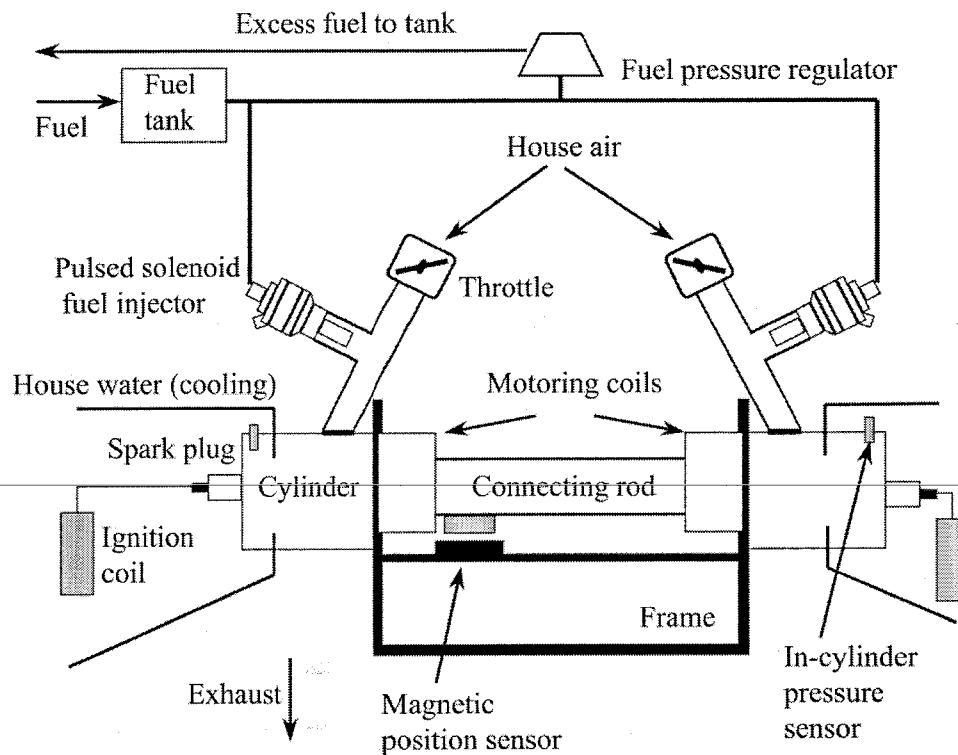
Figure 2.8: West Virginia University two stroke, spark ignition linear engine [10]

2.3.4.2 Sterlzer Free Piston Engine

An interesting innovation was proposed by Frank Stelzer [53], whose design of the engine consists of one compression chamber and two combustion chambers. The compression chamber is placed at the center of the engine and the other two combustion chambers are placed at the opposite of both ends. Figure 2.9 shows the configuration of the engine. The compressor chamber acts as a force induced by supplying charged air to the combustion chamber. What makes this engine special is that it compresses the air and fuel mixture first and later the charged air will be supplied to the combustion chamber through a flow channel. When ignited, the author stated the engine resonated at a high frequency of 500Hz.

19
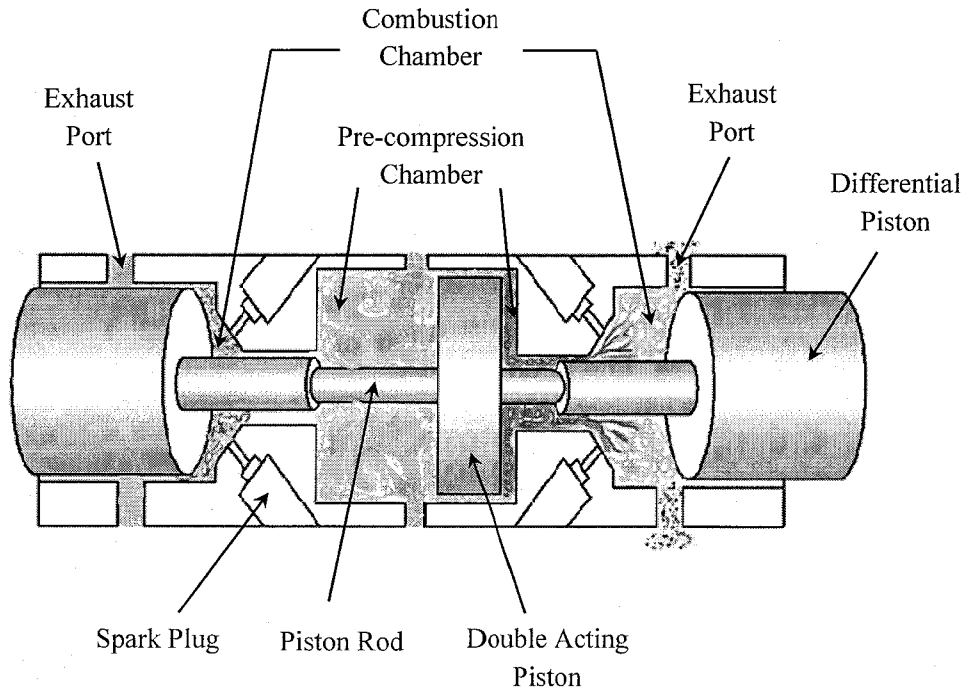
Figure 2.9: Stelzer Free-Piston Engine [53]

2.3.4.3 Sandia National Laboratories

Sandia National Laboratory is driven by strict policies to provide high energy conversion with low emissions. It led them to the development of experimental and numerical investigations of free-piston linear generator engine by using lean mixtures and a homogeneous charge compression ignition (HCCI) combustion concept [55-56].

Experimental works were done using their own prototype which is the rapid compression expansion machine. Eight types of fuels with low equivalence ratio ($\square$~0.35) and initial air intake temperature of 25°C, 50°C and 70°C was investigated [56]. Comparison studies were carried out between the fuels, the effect of lean equivalence ratio and HCCI combustion. The result was then processed and presented as indicated thermal efficiency and exhaust emissions level versus compression ratio. It is discovered that with high compression ratio HCCI free piston, constant volume combustion behaviour in Otto-cycle can be achieved. This would also produce higher indicated thermal efficiencies compared to SI engines. Additionally, low NOx

emissions were produced while CO and HC emission did not achieve the criteria which must be decreased after treatment technologies. The temperature varying test shows that by increasing the intake air temperature, HC and CO emissions decreases and NOx emissions increased with over compression. The fastest combustion duration was showed by hydrogen fuel with higher NOx emission level. The overall thermal efficiency are between 50% to 60% for all the fuels tested [56].

2.4 Internal Combustion Engine

An internal combustion engine is a heat engine which converts chemical energy to mechanical energy. The first practical internal combustion engine was a two-stroke cycle engine which is fueled by a mix of hydrogen and carbon monoxide gases and it was done by J.J.E Lenoir in 1860 [57-60]. Seven years later in 1867, Nicolaus A. Otto and Eugen Langen produced a free piston engine [57,58]. Later years in 1876, the first four-stroke crank-slider engine was produced by Otto which has efficiency up to three times better and less noise compared to the free-piston engine [58]. Most internal combustion engines operated using two-stroke cycle before the invention of four-stroke engine in 1876. Joseph Day in 1891 successfully builds a basic version of two-stroke engine with the crank-case scavenged design. A more efficient engine was later found by Rudolf Diesel in 1892 [57-59]. The new design was based on a compression ignition engine which produces up to 26% efficiency [59].

2.4.1 Two Stroke Cycle

As described previously, the first built engine was operating with two-stroke cycle. This type of engine has the highest power to weight ratio owning to the power stroke occurring every revolution, compared to a four-stroke engine which only has one power stroke in every 2 revolutions. A part from that, two stroke engines have a simpler design and construction, making it compact, lighter, cheap, easy to maintain and more reliable, due to less moving parts [58, 60]. It is also very robust and widely used from small engine model to large ships [58,60,61]. Even though several issues arise from the two-stroke design, specifically its high thermal stress, fuel short

circuiting and poor scavenging performance, it still remains in the market due to its simplicity and high power to weight ratio.

Ports are a type of hole that are used as a path way of the inlet and exhaust gas in a two-stroke engine instead of the conventional valves in a four-stroke engine. These port openings and closing operations are controlled by the piston skirt design. A reed valve is attached at the air inlet of the engine to create a uniflow system for the engine [61].

At TDC, when spark is ignited and air fuel mixture is combusted, the piston moves down towards BDC and the exhaust ports start to expose itself to allow the process of exhaust blow-down period. This is also the beginning of the gas exchange period. While the piston is still moving towards BDC and exhaust is being blow down through the exhaust port, the intake ports starts to open which allows fresh charge to fill up the combustion chamber by displacing the exhaust gas. This is the scavenging period. When the piston is moving upwards, it will firstly close the intake port and later the exhaust port. Once the exhaust port is fully closed, it marks the end of the scavenging and gas exchange period.

The two-stroke cycle is still accepted in the current market as a power plant due to its compact, low cost, robust and simple design. The scavenging process optimization is crucial towards a better efficiency two-stroke engine with low emissions.

2.4.2 Starting

Flywheel is an energy storage system which connects directly to a crank shaft. It is a vital component of an engine during starting to achieve idling. The starter motor which cranks up the engine during starting links directly to the flywheel and it supplies a minimum starting speed required for the engine to achieve combustion and then idle. The common starting speeds for SI engines are from 60 to 90 rpm for a two cylinder engine [62]. During the starting process, the flywheel speed starts to speed up and turn the crank shaft. The energy stored in the flywheel provides additional torque by accelerating the crankshaft towards the equilibrium cranking speed. A cyclic

variation in torque exists due to compression stroke and later absorbed slowly by the inertia of the flywheel.

For a single cylinder engine, the energy provided by the starter motor will be stored in the flywheel. The energy will be used during the compression stroke and stored back in the flywheel during the expansion stroke. This will increase the kinetic energy in the crankshaft and provide energy for the next compression stroke. Therefore, inertia of the rotating mass which is the flywheel is a vital component to eliminate cyclic speed variation during the compression stroke [63] and achieve a stable speed to start up the engine and reach idling.

Due to the absence of flywheel in a free-piston linear engine, starting is a great challenge. Therefore, few attempts were done by impulsing the piston to provide it with ample energy to reciprocate towards TDC or to gain sufficient compression [4]. A number of methods were implemented for the free-piston engine starting which is by controlling the timing for ignition, releasing a wound spring and pre-charging the rebound device [5].

2.4.3 Hydrogen in internal combustion engine

In this green technology era, hydrogen gas as a fuel in internal combustion engine is favorable due to its 'green' characteristics which produces clean emissions. Furthermore, this gaseous fuel have wide flammability range, high anti-knock properties which makes a high compression ratio engine possible, with higher thermal efficiency and clean emissions.

2.4.3.1 The hydrogen-fueled internal combustion engine: technical review

This paper discuses about the combustion characteristics, problems, future development and optimization of a Hydrogen-fuelled internal combustion engine (H$_2$ICE) to achieve better performance and near zero emission. The ability of H$_2$ICE to burn cleanly and operate efficiently is due to the unique combustion characteristics

of hydrogen that allow ultra-lean combustion with dramatically reduced NOx production and efficient low-engine load operation [64].

It is said that the main problem with using hydrogen is the pre-ignition (since hydrogen has low ignition energy) which is caused by engine hot spots such as spark electrodes, valves or engine deposits, which can lead to engine peak power output reduced by 50% compared to operation with gasoline. Therefore, for practical application, the maximum equivalence ratio (Φ) and consequently, peak power output can be limited by the pre-ignition limit. This problem can be minimized using cold-rated spark plugs, low coolant temperature, optimized fuel-injection timing and advance engine control strategies such as intake charge cooling, variable valve timing for effective scavenging of exhaust residuals, advanced ignitions systems and hydrogen direct injection (DI) [64].

The direct injection H_2ICE has long been viewed as one of the most attractive advanced H_2ICE options. The view is based on the high volumetric efficiency (since hydrogen is injected after intake valve closing) and the potential to avoid pre-ignition. It is known that the potential of DI-H_2ICE power density to approximately 115% that of the identical engine operated on gasoline. The challenge with DI-H_2ICE is that in-cylinder injection requires hydrogen-air mixing in a very short time. Experimental evidence demonstrates that complete mixing in an engine takes approximately 10ms [64].

Another interesting fact is that if the H_2ICE is used to drive an alternator that generates electricity, it can be operate and optimize for single speed operation at maximum power [64].

2.4.3.2 The Performance characteristics of a hydrogen-fuelled free piston internal combustion engine and linear generator system

This paper describes the performance of a Free Piston Engine (FPE) with engine capacity of 150.8cc or 100.5cc depending on 2 types of fuel application that is compress natural gas (CNG) and hydrogen. When CNG fuel is use, the piston stroke

is elongated half of the original stroke to draw more useful work out from the generator. The engine speed is controlled mainly by the ignition timing on the fixed piston location [65].

It can be seen throughout the experimental data's, the peak cylinder pressure with combustion using CNG as a fuel is around 25-30 bar with piston frequency of 13Hz and a few misfires recorded in the experiment. With the use of hydrogen as a fuel, the test engine was operated at 13Hz with peak cylinder pressure of 30-35bar. The increase in pressure was much higher when using hydrogen due to high combustion speed of hydrogen. From the rate of heat release graph, the combustion duration is longer for CNG compared to hydrogen. All the combustion heat released recorded is before the piston's TDC. Ignition timing was adjusted to adjust the position of the peak cylinder pressure to occur after TDC but due to instability of the engine, it stops after few minutes of operation [65].

2.4.4 Combustion Technology

Years of developments of a power unit base on combustion leads to widely used combustion types such as the spark ignition (SI) and compression ignition (CI). The petrol and diesel engines are commonly refer as otto, SI and CI engines [57]. In the recent years, homogeneous compression charge ignition (HCCI) and direct injection spark ignition (DI-SI) are being developed. The reason for the HCCI and DI developments are to have the best of both worlds (SI and CI) and to produce engine with higher engine efficiency (not possible with SI since limited by knocking) with lower emissions (CI engine have poor emissions).

A mixture of air and fuel are ignited by a spark plug at the end of a compression stroke for SI engine to produce combustion [21]. The ignition is a time dependant process which is drive by reactants and develops towards a steadily burning flame [66]. While for CI engines, the temperature of the compress air by the end of the compression stroke is high enough to auto ignite the diesel once it is injected into the cylinder. Auto ignition is not favorable in SI engines and can cause engine damage.

The fresh charges in Homogenous Charge Compression Ignition will combust when the mixture will reach the auto-ignition temperature. The result is HCCI will produce low emission and better fuel economy. HCCI engines have low fuel consumptions, low emissions especially NOx and an indicated efficiency is around 50% [5,8,20,21,54,56,59].

Another technology which is able to reduce fuel consumption at part load by 15% to 25% is the direct injection (DI) system [67]. DI system originated from diesel engine due to the ability to reduce fuel consumption and reduced CO_2 emissions. DI system injects fuel directly into the combustion cylinder which improves volumetric efficiency by 10%, decrease knock occurrence and engine compression ratio can be increase by 1 to 1.5 units [67].

The main problem for a two stroke engine is that the short circuiting issues which causes bad emissions. This can be resolve by adopting DI system to a two stroke engine [57,59,68]. Fuel will be injected directly into the cylinder once the exhaust port is completely close hence no air fuel mixture will exit to the environment. This solution is possible with complicated and fast control system in order to make sure the delivery of the fuel is accurate and fast.

2.5 IGBT inverter drive and noise interference

Bipolar junction transistors (BJT) and MOSFETS have characteristics that complement each other in some respects. BJTs have lower conduction losses in the on state, especially in devices with larger blocking voltages, but have longer switching times, especially at turn-off. MOSFETs can be turned on and off much faster, but their on-state conduction losses are larger, especially in devices rated for higher blocking voltages. These observations have led to attempts to combine BJTs and MOSFETs on the same silicon wafer to achieve a circuit or even perhaps a new device that combines the best qualities of both types of devices which is the insulated gate bipolar transistor (IGBT). [69]

Contrary to the progress of IGBT's, electromagnetic interference (EMI) noise caused by high dV/dt, high di/dt switching exerts adverse effect over other systems. These papers stated that noises created by switching transients may cause trip and false alarm. Sharp voltage gradients act as stimulus for high power IGBT modules, which can exhibit a potentially instable high frequency behavior. As noise filters are essential, the design of these filters is explained, simulated and experimented to prove its effectiveness in running an IGBT inverter drive [70-74].

2.6 Free-piston Linear-Generator Engine Prototype developed by UTP

A group of researchers in UTP together with Universiti of Malaya (UM) and Universiti Kebangsaan Malaysia (UKM) did a collaboration to develop a free-piston linear-generator as a power unit to charge battery banks on board of hybrid electric vehicle [2, 11, 79] . They have developed a direct injection two-stroke linear-generator engine with dual-piston configuration. Detail specification of the prototype will be discussed in the next chapter.

Researches in UTP have reported several works on FPLG engine [11, 15, 16]. Saiful [11] have developed a transient starting process modeling in Matlab Simulink platform together with efficient control strategy using National Instruments Labview platform. These allow the FPLG to operate in motoring mode while allowing users to change parameters on the fly. Razali [16] reports combustion behaviours using compress natural gas (CNG) and hydrogen (H_2). Important parameters such as piston position, ignition and injection timing were determined to produce high combustion pressure while motoring at 60 V battery capacity. Abdulwehab [15] presents numerical simulation model which consist of motoring, cogging force and FPLG models. The artificial neural network (ANN) was showed to be valuable addition to engine modeling in order to predict the expected results. Rare experimental gasoline data was reported.

The problem remains to be in the starting mode whereby the compression pressure is not suitable to produce high combustion pressure in order to reach idling. The experimental setup was limited up to 60 V battery capacity due to MOSFETs inverter

drive property. Through Saiful's simulation [11], it is reported that with higher motoring voltage, higher compression pressure is achievable. In order to produce higher compression pressure experimentally, the system requires higher motoring voltage which is beyond the capabilities of the current inverter. Hence, to conduct further experimental analysis to produce higher compression pressure, upgrading an inverter drive to allow higher motoring voltage is necessary.

CHAPTER 3

RESEARCH METHODOLOGY AND EXPERIMENTAL SETUP

3.1 Introduction

A prototype was built by a team of researchers in UTP to address to the current global issues to produce highly efficient power unit. Free piston linear generator engine was design, fabricated and tested in order to study the behaviour of the engine by providing important experimental data for further research on this prototype. This chapter will give in depth detail of the research flow, engine prototype and methods used to process experimental data. Through this method, behaviour of the engine can be analyzed and explained.

3.2 Research Flow and Experimental Method

The main research target is to idle the engine but as mention previously, the engine could not reach idling due to low combustion pressure. The overall research flow is shown in Figure 3.1 and detail troubleshooting method is illustrated in Figure 3.2. Experimental works were implemented by a series of matrix shown in appendix A.
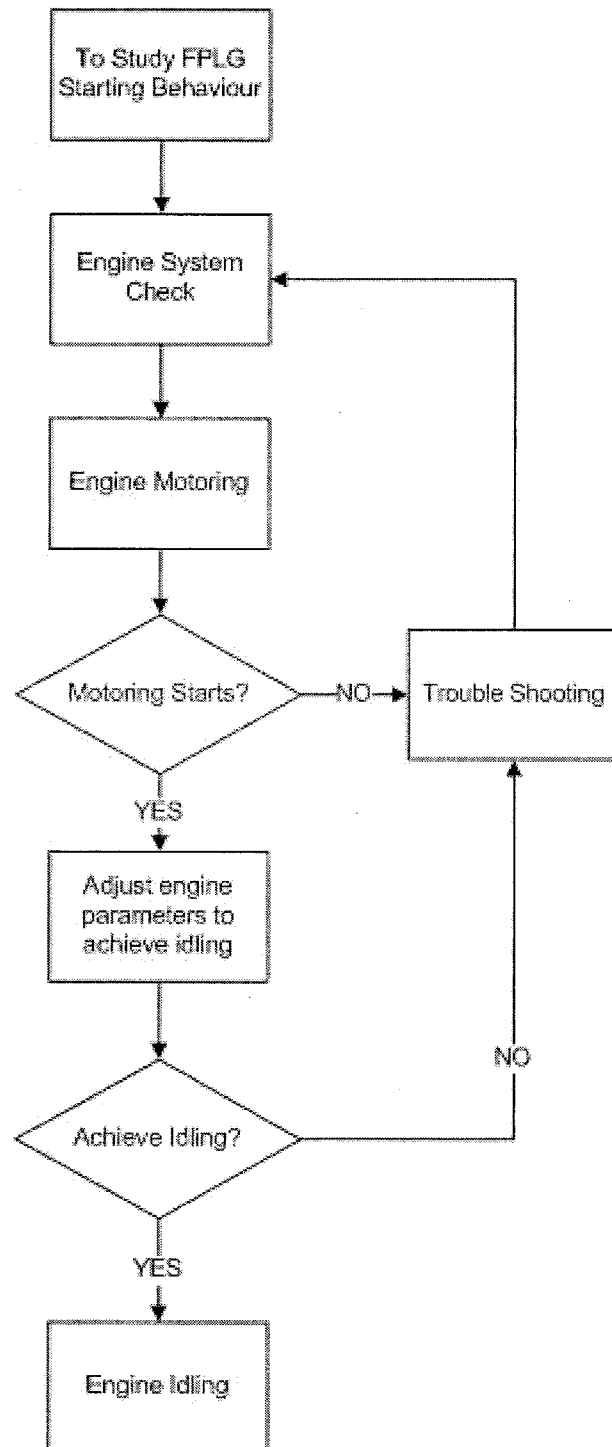
Figure 3.1: Overall research flow
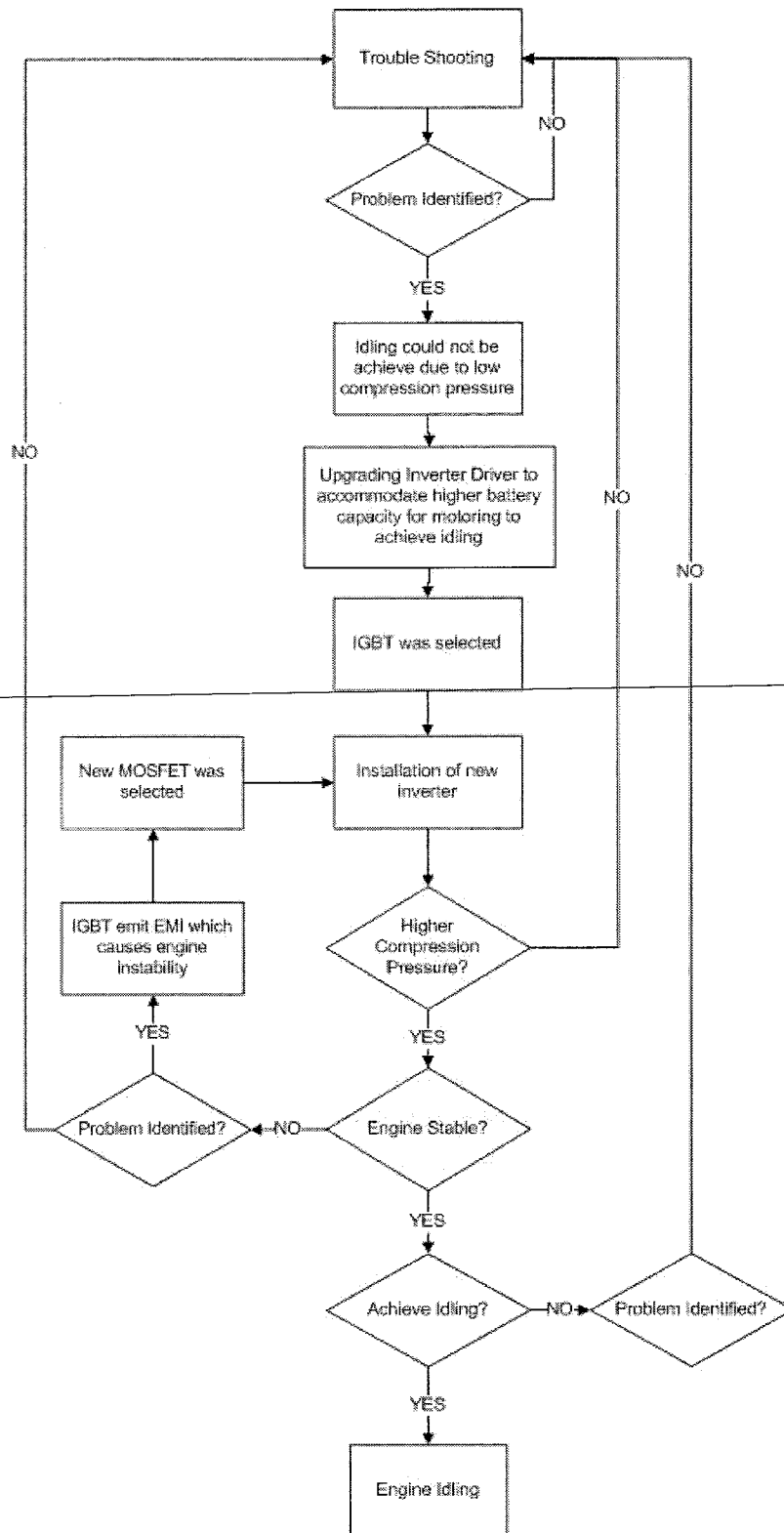
Figure 3.2: Trouble shooting flowchart

31

3.3 Free Piston Linear Generator Engine Prototype

A prototype was built base on a two stroke cycle with direct injection technology and fueled by hydrogen gas. With this particular setup, it can be clearly seen that this engine was design to have low manufacturing cost by having less weight, fuel efficient and clean emission. The prototype is a combination of two crucial mechanisms that is the linear engine and the linear alternator. This combination will convert from chemical energy to electrical energy to charge a battery power bank on a SHEV. The main components of the engine consist of the translator shaft which will connect two pistons, the stator assembly where magnets and coils are placed, and the combustion chamber. A cross sectional view of the engine is shown in Figure 3.3. The engine bore and stroke are 76mm and 69mm respectively which makes a 313cc engine capacity per cylinder. The combustion will produce high combustion pressure on one cylinder which will push the piston assembly (translator) towards second cylinder and the process repeats in which this reciprocating motion will cut the magnetic flux at the center of the prototype where the stator assembly is located. To minimized development time, the cylinder block and head, pistons were taken from an aircraft glider and were modified to suit the prototype.
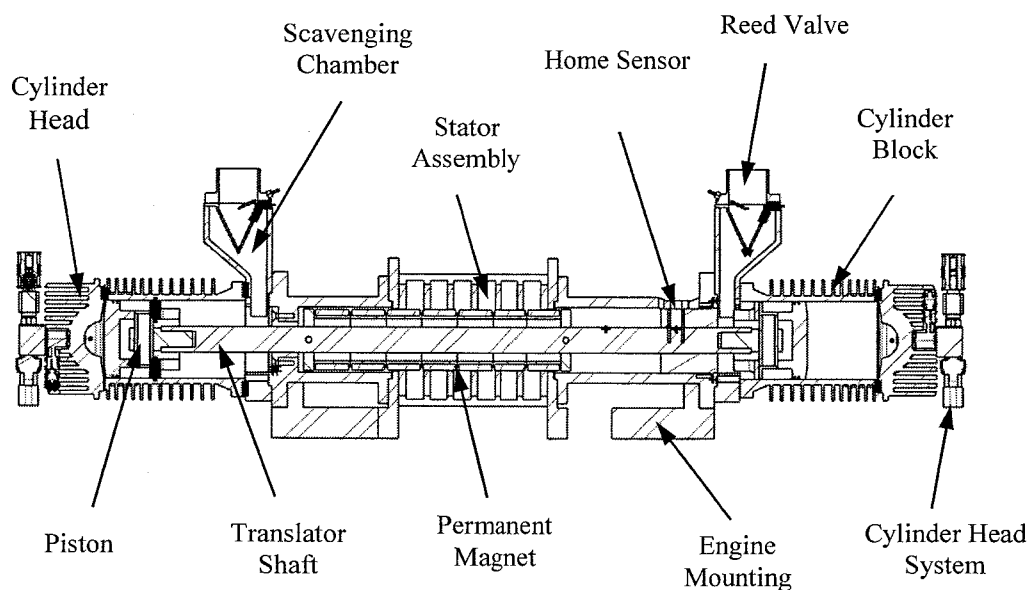
Figure 3.3: Cross-sectional view of UTP Free Piston Linear Generator Engine

Table 3.1: The specifications of UTP free-piston linear generator engine prototype

No.	Description	Specification
1	Engine type	Two-stroke, Spark Ignition, Direct Injection
2	Number of cylinders	2
3	Bore x Maximum Stroke	76mm x 69mm
4	Engine Capacity	313cc /cylinder
5	Max Compression Ratio	14
6	Exhaust Port Start Opening (relative to origin 0 mm)	-5.5 mm (Cylinder 1) 5.5 mm (Cylinder 2)
7	Exhaust Port length	28.5mm
8	Intake Port Start Opening (relative to origin 0 mm)	-22 mm (Cylinder 1) 22 mm (Cylinder 2)
9	Intake Port length	12mm
10	Moving mass	6kg
11	Power (kW)	5 kW at 2000 cpm

The total stroke of the engine is 69 mm hence dividing it to two gives a position reading of ± 34.5 mm. When the translator is at far left of the engine, the position is said to be at -34.5 mm while at far right, it is at +34.5 mm. The origin of the translator position is at 0 mm which is at the center of the engine geometry. At this point, both the exhaust and intake ports are closed. A detail view on the positioning system can be seen in Figure 3.4 including the intake and exhaust ports dimensions.

A rig was constructed to place the prototype on a test bed. The test bed was design to reduce the vibrations during the operation of the engine. The test bed consists of linear bearings, springs and dampers to absorb vibrations as shown in Figure 3.5.

Cylinder 2

Figure 3.4: Linear position scale in relation to cylinder 2 geometry and origin position

[16]
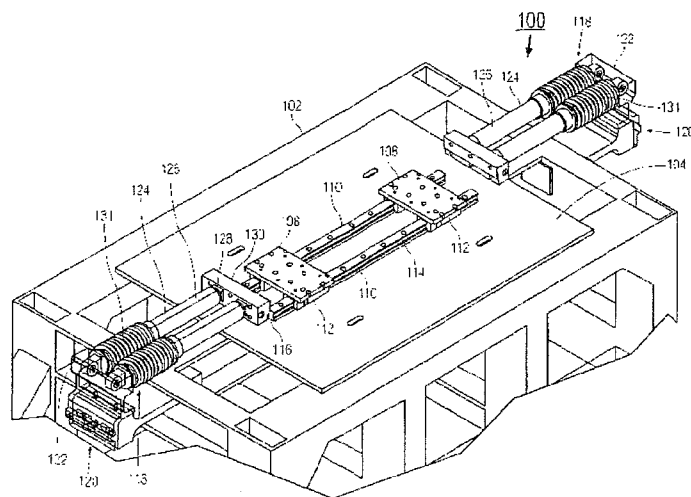
Figure 3.5: Free Piston Engine Support

3.3.1 Linear Alternator

A linear alternator is a piece of device which will convert mechanical energy to electrical energy. It was designed and developed by UM research teams [75-77]. The linear alternator is divided into two parts, one is the permanent magnet and the stator. The permanent magnet is located at the translator with a quasi halbach system while the stator is located at the center of the engine. The stator consists of pi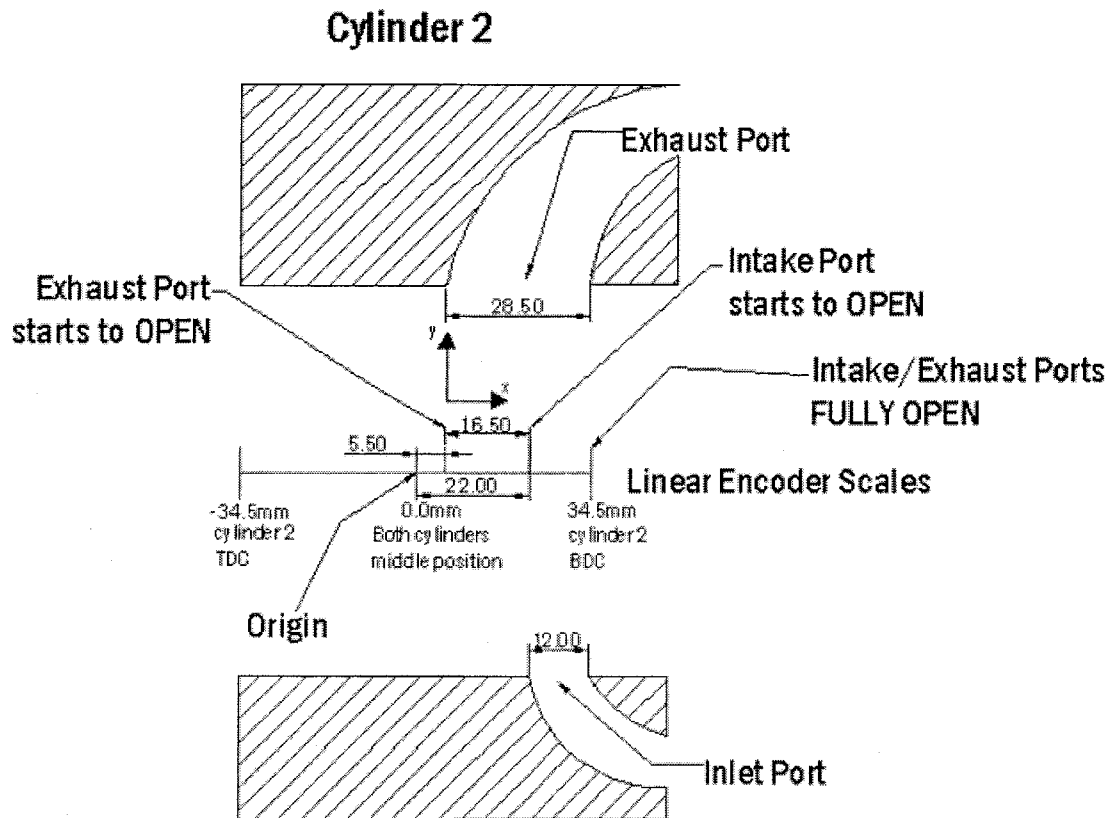eces of silicon steel laminations and 6 coils with a 3 phase layout. At the center of the translator or shaft lays a permanent magnet assembly with a combination of radial and axial magnet for a quasi halbach system. This alternator can be operated as a motor and a generator. The alternator first will run as a motor whereby current is being induced by the system to reciprocate the translator in order to build compression pressure to achieve combustion. Once combustion is initiated, the translator will now move base on the combustion pressure and the linear alternator will change its mode to generator to generate electrical power from the motion of the translator. Load is connected to the output terminals of the coils and current will flow thus power is extracted from the alternator. The generated power will be used to charge a power bank on a SHEV.

Table 3.2: The specifications of the linear generator [75-77]

No.	Part	Specifications
1	Shaft radius (non permeable material)	12.5 mm
2	Magnet (axial and radial) inner radius	12.5 mm
3	Radial Magnet length	22.5 mm
4	Iron ring thickness	1 mm
5	Radial Magnet thickness	11 mm
6	Axial Magnet length	12 mm
7	Axial Magnet thickness	12 mm
8	Air gap	1 mm
9	Tooth width	6 mm
10	Stator back iron	6 mm
11	Slot width	17 mm
12	Slot depth	102 mm
13	Wire AWG#	12

| 14 | Number of turn per coil | 312 |
| 15 | Power Generated | 5kW at 2000cpm |

3.3.2 Working Principles

This prototype which is build by UTP research team is based on a two stroke cycle engine hence power is produced for every complete revolution. One cycle is the intake and exhaust stroke and another is the compression and power stroke. During starting, the piston will be push to an initial position at far left of the engine so that during motoring, the piston could gain higher velocity to compress the air fuel mixture to a higher compression pressure when moving to the far right of the cylinder (compression and power stroke for right cylinder). At the far right, fuel is injected directly into the cylinder and spark is ignited to combust the mixture hence will push the piston back towards the far left (intake and exhaust stroke for right cylinder). During these processes, current is being induced by the system to move the translator to a desired position and controlled by the control system. The cycle repeats until combustion is stable to achieve idling. During the expansion process, cutting of magnetic flux at the center of the prototype occurs repetitively thus producing electrical power.

3.3.3 Engine Control System

The basic of a control system is to retrieve and send parameters to the engine. This process should be done in high speed in order to have accurate engine control. Due to this, a National Instrument (NI) PXI embedded controller was chosen to be the control system platform for the prototype in order to control the engine parameters and simultaneously acquiring data of the engine performance and electrical machine parameters for further analysis. The NI PXI have a specifications of 2.2 GHz, Pentium 4 - based, industrial PC platform PXI-8186 embedded controller with the additional modules which is the SCXI-1102C (analogue input for measurements of current and pressure) and PXI - 6602 (for linear position sensor and gate driver control).

Labview 7.0 is a graphic user interface (GUI) software which was developed by National Instruments in order to design and produce highly efficient and complicated control strategy with real time capabilities. There are several control loops in the systems which is the starting, speed, current control, throttle, speed control and combustion control loop. These loops enables users to controlled the engine by varying parameters such the ignition timing, fuel amount and injection timing, current limit flowing in the coil and the linear position of translator. During motoring of the engine, the starting control loop is enable and it will control the translator position in respect to energizing the correct pair of coils to produce required motoring force and direction. Switching of inverter gate drivers are based on the translator position. This inverter will deliver a 3 phase power supply from a battery bank to energize the correct coils. This process will be done by the control loop based on the linear position parameters keyed in by the user. Figure 3.6 show a control diagram for the UTP free piston linear generator engine.

As mention previously, the control system acquires data during experimental testing making it a real time data acquisition system (DAQ). Data is logged at a frequency of 10 kHz to attain precise and accurate data for post processing. Data logged including in cylinder pressure for both side, translator position sensor, intake air flow rate and temperature and manifold absolute pressure.
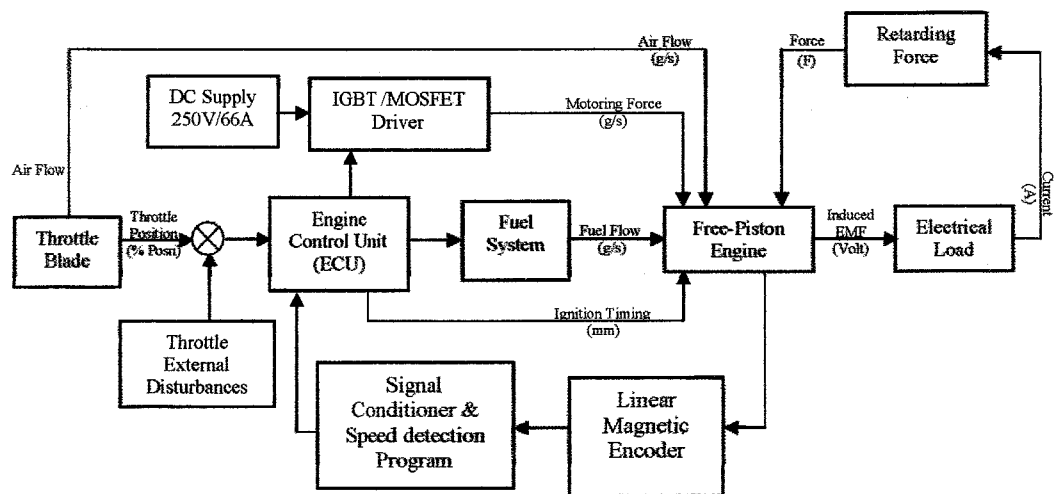
Figure 3.6: Free-piston linear generator engine control system block diagram [11]

37

3.3.4 Starting of the Engine

The linear alternator coils are charged up by injecting current to produce electromagnetic force hence moving the translator was achieved. Proper energizing of coil base on the translator position is crucial to produce stable motoring process hence a six step commutation developed by UTP research team was implemented [11,18]. Six step commutations will energize two coils simultaneously with different polarity. The control system will control the motion of the translator by the switching the inverter (MOSFET or IGBT) gate drivers which is base on the six step commutations relative to translator position. The inverter will later energize designated coils to move the translator hence motoring is achieve to initiate the combustion. The six step commutations switching profile of the coils are shown in Figure 3.7. Furthermore, the switching strategy was developed and incorporated in the control system [11,18]. The switching strategy mentioned enables the engine to run in stable motoring condition.
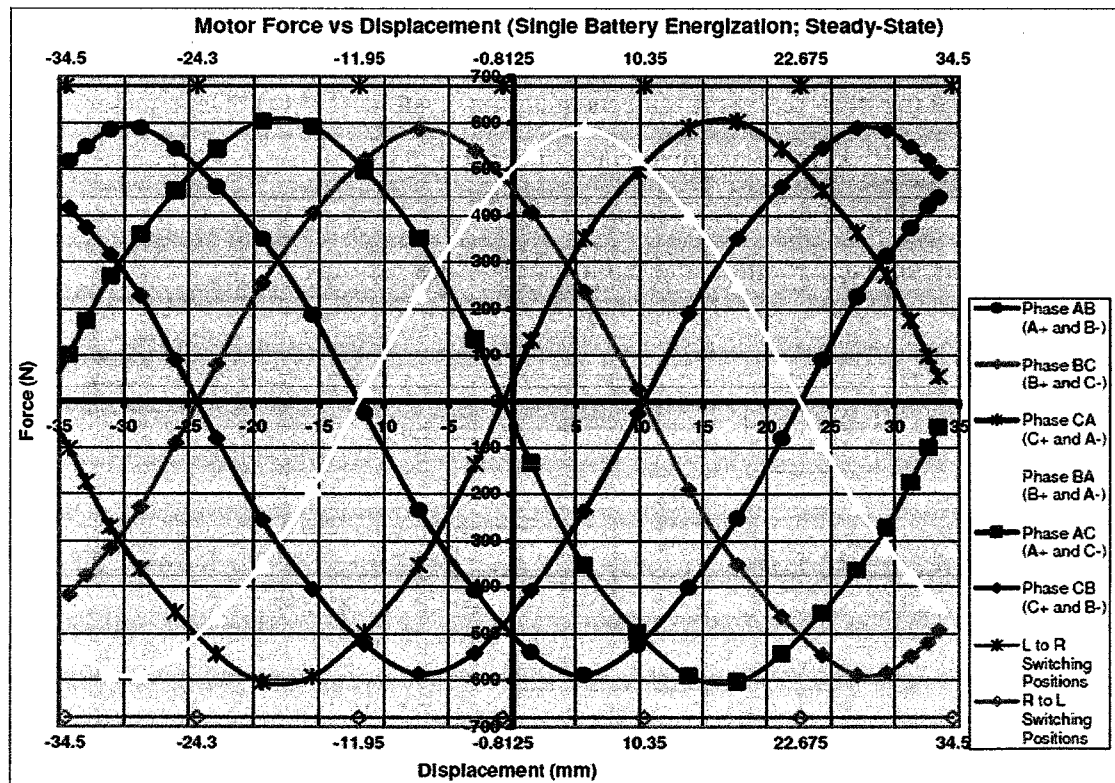
Figure 3.7: Motoring Force vs. Displacement for Single 12V Battery Energization
(25Amp Steady State Current): 6-Step Commutation [11]
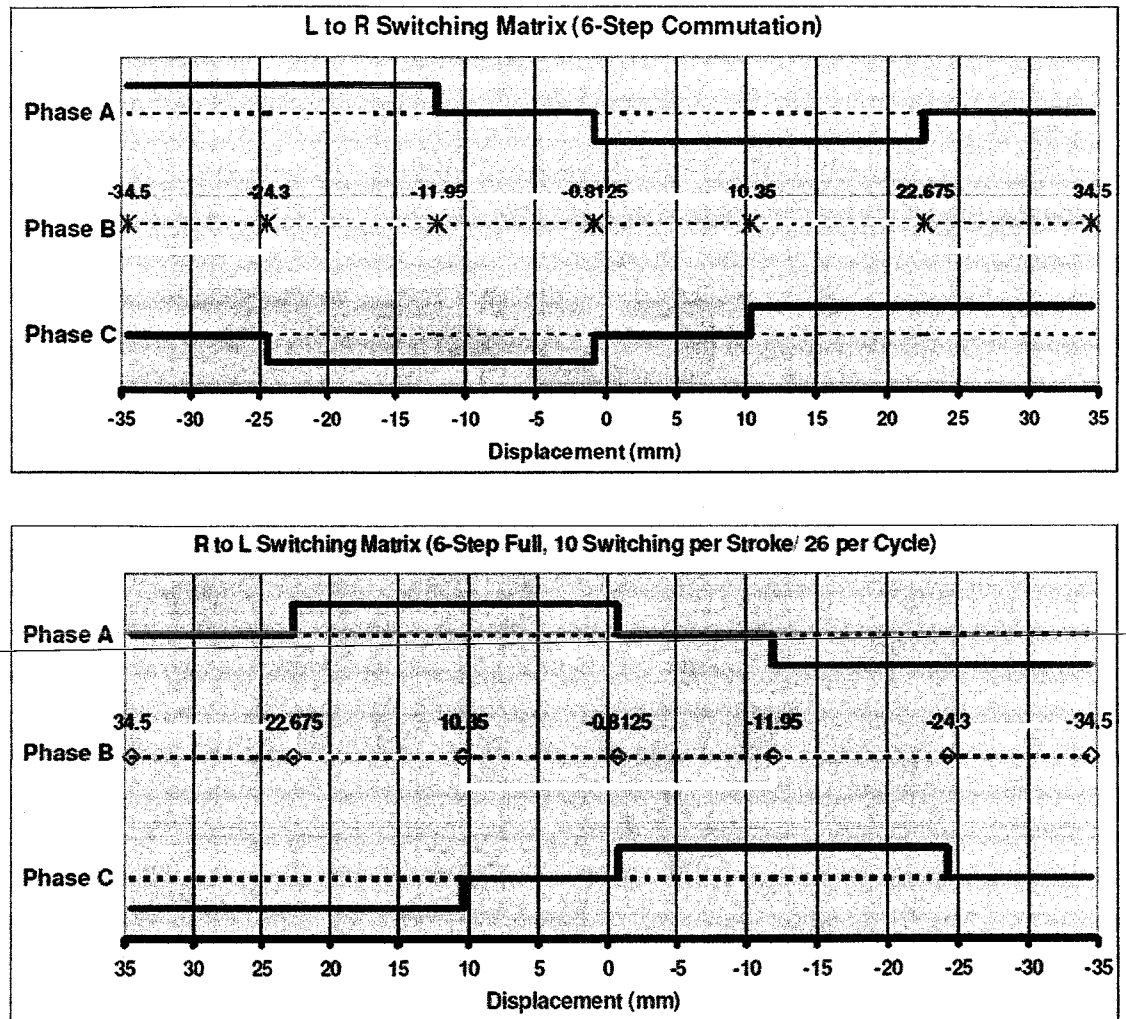
Figure 3.8: Switching Matrix for 6-Step Commutation: Both directions [11]

3.3.5 Intake and Exhaust System

In a two-stroke engine, valves are replaced by ports and the opening and closing is controlled by the piston skirt geometry design relative to its motion. This will allow the gas exchange of fresh charge into the cylinder and at the same time to displace the combusted mixture. Once the air fuel mixture is ignited, the expansion stroke takes place. During this process, the motion of the piston will travel away from TDC and exposing the exhaust port earlier than the intake port. This will allow the burned gas to flow out of the cylinder partially. Furthermore once the intake port is open, the fresh charge is drawn into the combustion cylinder and at the same time to scavenge

39

the remaining burned gas out of the cylinder. In Figure 3.9, the Free Piston Linear Generator intake system is displayed. Intake air will be filtered before flowing into the laminar flow element which will make the intake air to flow into the engine under laminar flow and at the same time to measure the intake air flow rate. Filtered air will be stored in the blue intake box before supplying it into the combustion cylinder via a hose connected between these two zones.
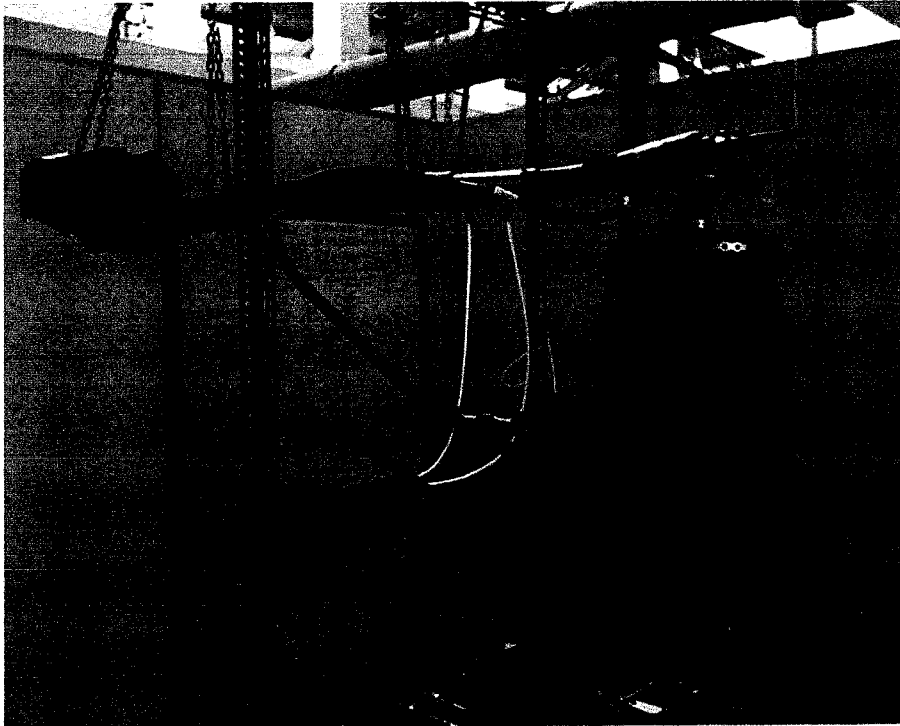
Figure 3.9: FPLG Air intake system [15]

3.3.6 Fuel Supply and Injection System

Hydrogen gas is used as a fuel for combustion. Therefore the fuel supply and injection system was setup base on the high pressure gaseous setup. The Hydrogen supply tank will supply 200 bar of pressure and will be reduced and regulated to 20bar through a multi stage fuel pressure regulator that will be supplied directly to the injectors. A direct injection system using a pair of Synerject high pressure direct injector is mounted on the two combustion chambers with 79° exit angle. These injectors will inject 20 bar of Hydrogen directly into the combustion cylinder and controlled by the NI control system. A fuel flow meter is placed along the fuel line to

measure accurate fuel metering. Accurate fuel metering is essential for the combustion process in order to control the combustion at different engine operations. The specification of micro-motionmass flow meter is included in the Table 3.3. Figure 3.10 and 3.11 shows the complete fuel supply system together with the Synerject injectors.

Table 3.3: Micro-motion fuel flow meter specifications

No	Parameter	Specifications
1	Flow accuracy	+/-0.05% of flow rate
2	Gas accuracy	+/-0.35% of flow rate
3	Density accuracy	+/-0.0002 g/cc
4	Wetted materials	304L, 316L Stainless Steel or Nickel Alloy
5	Temperature rating	-400 to 800°F (-240 to 427°C)
6	Pressure rating	100 to 413bar
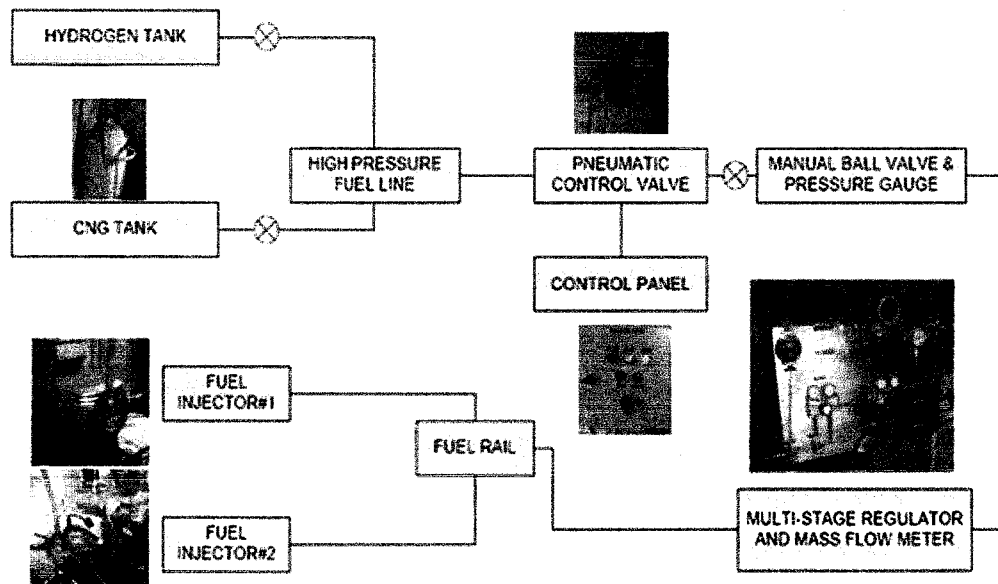
Figure 3.10: Fuel supply and injection systems [16]
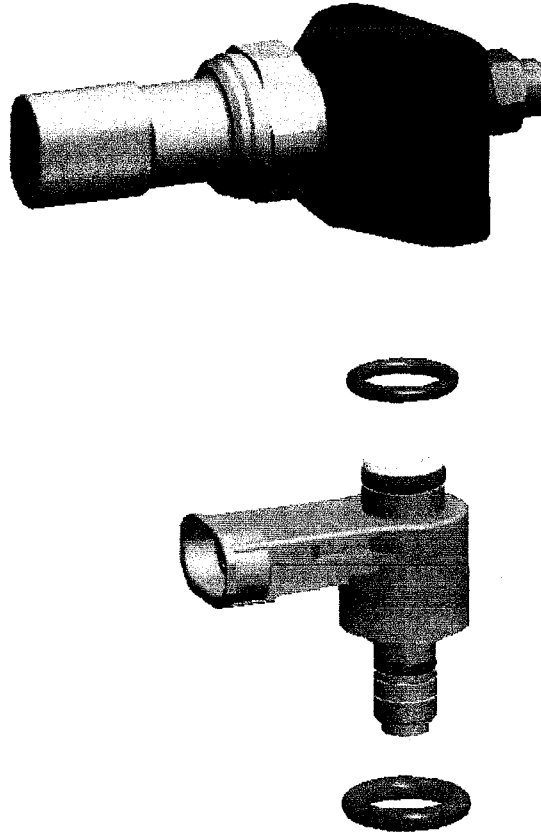
Figure 3.11: UTP Fuel injector systems [15]

3.3.7 Ignition System

Special ignition coils manufactured by Marshall (ME52-78 with 40 kV) are used in the experiment to supply high voltage to the NGK PZF6H platinum spark plugs. These ignition coils are electronically controlled by the control system to ignite the mixture in the combustion chamber. The point of ignition is one of the parameters which are controlled by the user through the NI control system.

3.3.8 Inverter and Gate Driver

Inverters such as the MOSFET and IGBT (insulated gate by polar transistor) are used for this prototype to drive the linear alternator. These technologies are widely used today in modern power electronics equipments. These inverters are capable to work at high switching frequency and at high voltage. In order to operate a single

MOSFET or IGBT gate, a gate driver is needed to supply a voltage across the gate-source junction. This will allow the on and off operations of the inverters. Figure 3.12 and Figure 3.13 shows the experimental setup for the inverters together with its gate driver and the specification of the inverters are listed in Table 3.4. The 'Old MOSFETs' was the current setup and upgrading to IGBT was needed due to increase in motoring voltage. The IGBT allows the maximum voltage up to 900 V but due its instability in motoring process which will be describe later in this thesis, further upgrading method takes place where by the 'New MOSFET' was chosen. The 'New MOSFET' has lower voltage and current ratings than the IGBT but it is sufficient for the experimental activities. Due to its simple design, it is very stable therefore 'New MOSFET' was chosen to proceed with further experimental task.

Table 3.4: Inverter Specifications

	Old MOSFET	IGBT	New MOSFET
Model	IRFP1405	SKiiP 342 GB120-3DUL	IRFP4110PBF
Max operating voltage	55 V	900 V	100V
Max operating current	95 A	300 A	180 A
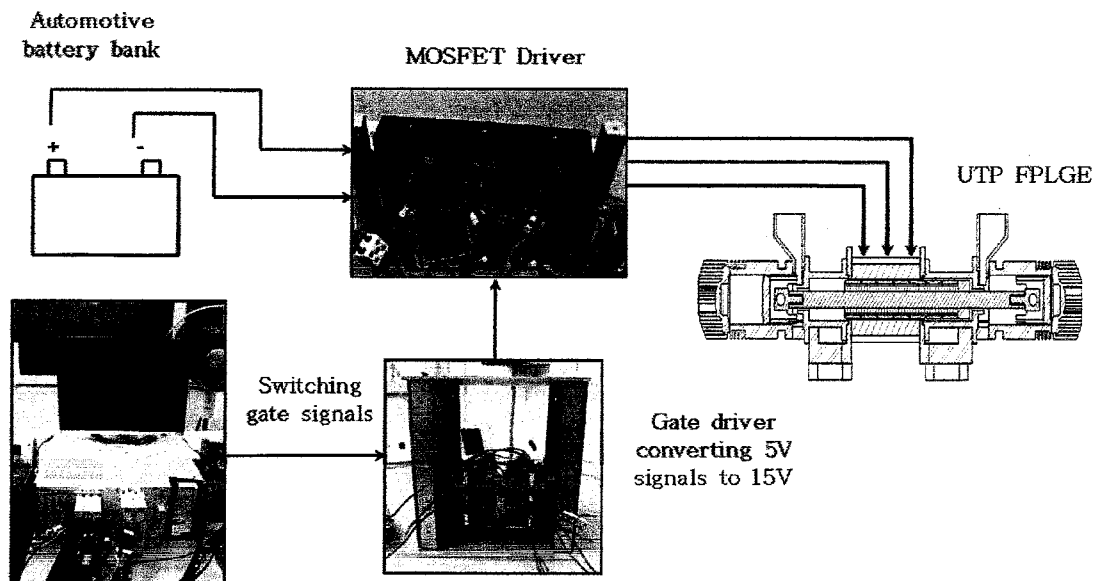
Figure 3.12: Experimental setup of MOSFET driver for free piston linear generator engine
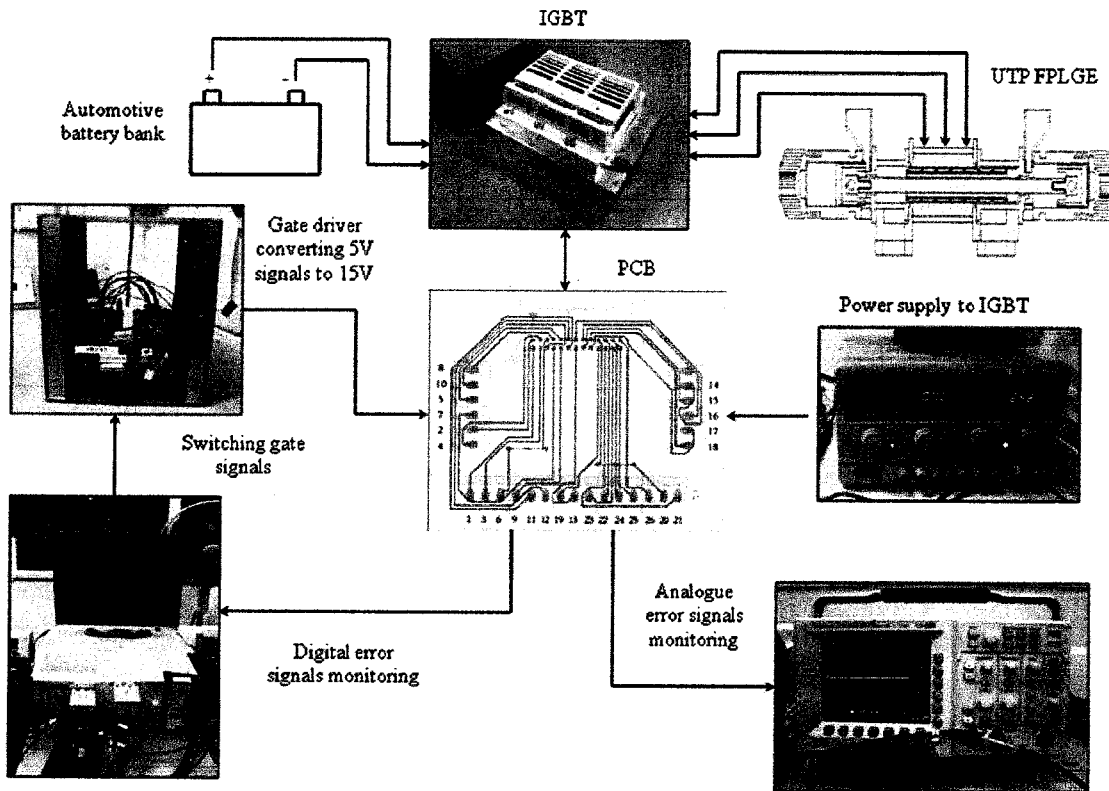
Figure 3.13: Experimental setup of IGBT driver for free piston linear generator engine

3.3.9 Instrumentation and Measurements

All the engine parameters are measured and recorded during the experimental testing. The parameters such as the instantaneous linear translator position, in-cylinder pressure, engine temperature, electrical current and voltage were measured. The energizing of coils to move the translator is highly dependable to the linear position sensor. Furthermore, the injection and ignition points too depends on linear position readings. Hence, linear position reading is very crucial for smooth motoring and combustion operations. While for the other parameters, it is for the purpose of experimental analysis to measure and evaluate the performance of the engine.

3.3.10 Linear Position Measurement

In a conventional crank rotating engine, the positions of the pistons are described in angular form since it is circular. It is wholly a different scenario for the free piston linear generator engine. Since it is in linear configuration, a different type of sensor will read the position linearly thus expressing the readings in (mm). This linear position reading is the most crucial part of the engine. This data will be the input to the control system which later the control system will determine the switching of the coils to energize to put the translator in motion, when to inject the fuel and finally to ignite the air fuel mixture. If the engine received false linear position reading, the whole engine operations will stall.

Two sensors are used to determine the location of the translator via linear position system. One is the linear encoder which will read multiple signals from a magnetic strip and another is the proximity sensor which will read one signal to indicate homing or zeroing (0 mm) point. The linear encoder used is the Baumer MLFK-08T7101 with a resolution of 0.125mm. The signal from this sensor is capable to not only give the position (displacement) reading, but direction of the translator motion as well due to a 2-channel (A-B) signal. Both of these sensors will produce the final position reading in millimeters (mm). This reading will be the input to the control system.

3.3.11 In-Cylinder Pressure Measurement

Free piston linear generator with dual piston configuration has two cylinder heads thus two pressure sensors to measure pressure on each cylinder head separately. A pressure sensor located on top of the cylinder head which is the Kistler 6061B (0 bar - 300 bar) piezoelectric pressure transducer which is connected to a Kistler charge amplifier type 5037B measures the in cylinder pressure and sends the signal in a form of analogue voltage value to the NI control system. The pressure of the intake air and manifold absolute pressure were gathered by TMAP sensor.

3.3.12 Temperature Measurement

The temperature of the engine was monitored during the experiment. A temperature sensor was placed on the cylinder head to measure the temperature of the engine. A Synerject 366-055 will measure the temperature in the range of -20°C to 200°C. Additionally, the temperature of the air intake also was monitored by using a TMAP sensor by Synerject with model name TMAP07 with temperature range of -40°C to +125°C.

3.3.13 Current and Voltage Measurements

The battery bank using multiple battery banks are connect directly to the inverter and from the inverter, it supply the power to the prototype. A current clamp meter is connected in between the power bank and the inverter to measure the current flow from the power source to the prototype. The measurement is measured by KYORITSU 2003A AC/DC (0-400A) current clamp meter. A multi meter is used to measure the state of charge of the battery bank during running. During combustion, a back electromagnetic force is generated (EMF) and this is also measured by the current clamp meter.

3.3.14 Lubrication and Cooling System

Lubrication is important to keep the engine working smoothly and reducing its friction losses. It is also crucial in terms of keeping the engine temperature low. Free piston linear generator engine works on a two-stroke cycle hence it adapts the conventional two-stroke engine lubrication and cooling system. The lubrication oil will be injected into the incoming air hence the intake air consist of a fine mist of lubrication and will mix with the air. This oil will stick to the surface of the cylinder wall providing the piston with smooth surface to slide on. An oil pump by Mikuni (ESOSP-03) was used to inject oil at a rate of 250cm3/hr. Furthermore, the cylinder head and cylinder block are design with fins to be cooled using forced air.

3.4 Data Processing

Raw data which were taken directly from the data acquisition system embedded in the National Instrument control system are processed in Microsoft excel. Every data was logged at a 10 kHz sampling rate to obtain accurate and precise data to study the behaviour and performance of the prototype.

3.4.1 Pressure, Displacement vs. Time, p-V Diagram

Raw data which is taken directly from the data acquisition system is plotted directly. The control system records in cylinder pressure and position (displacement) against time in real time mode at a frequency of 10 kHz. Graphs for pressure vs. time, position vs. time and pressure vs. displacement are plotted in excel directly to study the behavior. Selected data will then be analyzed further to obtain the performance characteristic.

3.4.2 Indicated Mean Effective Pressure

Indicated Mean Effective Pressure (IMEP) is a useful relative measurement of engine performance. It represents the average combustion pressure per unit volume. The value is independent to engine size when compared to power and torque of an internal combustion engine. Hence it was a suitable parameter to use in order to evaluate the overall engine performance when running at different type of battery capacity.

IMEP is one important engine fundamentals which is derived from the cylinder pressure reading and the numerical integration of the cylinder pressure. The work done per cycle can be obtain from a pressure vs. volume graph. The area under the graph as illustrated in Figure 3.14 shows that by integrating area under the curve, IMEP can be calculated over the entire engine cycle. Since this prototype engine would not be producing any mechanical output, the work per cycle was evaluated from the p-V graph.
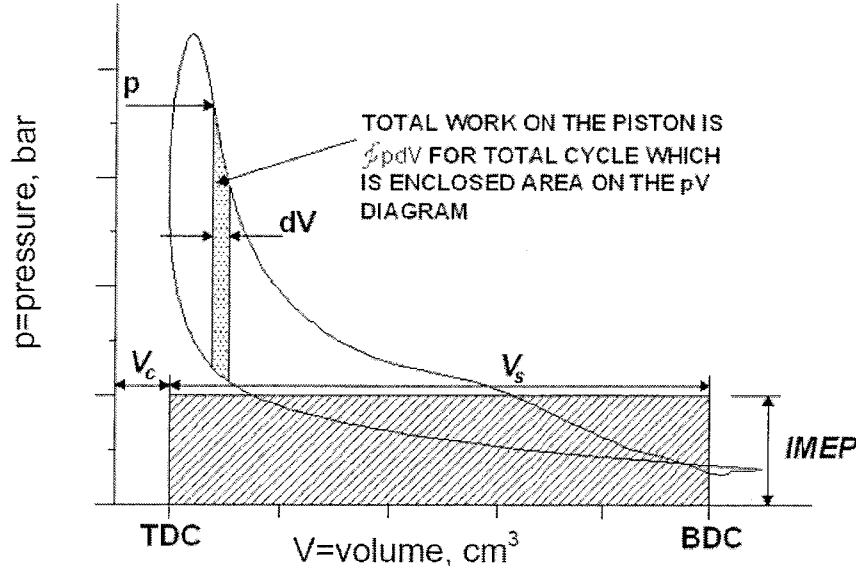
47

Figure 3.14: IMEP representation from a p-V diagram [61]

Additional methods were evaluated and it can be used to calculate IMEP numerically from the experimental data obtain in a time based manner instead of the angle based [19].

$$IMEP = \frac{\Delta t}{V_s} \sum_{i=n1}^{n2} p(i) \frac{dV(i)}{dt} \tag{3.1}$$

A simple formula is then derived below to calculate the indicated power output by inserting values such as the IMEP, displacement volume and engine speed as follow:

$$P_i = IMEP \times V_s \times N \tag{3.2}$$

3.4.3 Coefficient of Variance (COV)

Coefficient of variance is a useful method to determine the stability of the engine. It measures the cycle to cycle variation of the IMEP. The variation of the IMEP is expected to be high during lean operation and at low speed (idling). Calculation of the COV is as below. Firstly the average IMEP is calculated is equation 3.3. Next the standard deviation of the IMEP is calculated in equation 3.4 and finally the COV is then obtain using equation 3.5.

48

$$IMEP_{ave} = \frac{1}{n}\sum_{i=1}^{n} IMEP_i \tag{3.3}$$

where n = number of samples

$$\sigma_{IMEP} = \frac{1}{n}\sqrt{\sum_{i=1}^{n}\frac{(IMEP_{ave}-IMEP_i)^2}{n-1}} \tag{3.4}$$

$$COV_{IMEP} = \frac{\sigma_{IMEP}}{IMEP_{ave}} \tag{3.5}$$

Typical value for COV is usually less than 10% which represents a stable combustion characteristic for a conventional internal combustion engine [46].

3.4.4 Rate of Heat Release (ROHR) and Mass Fraction Burn (MFB)

The heat release by the combustion process in the combustion cylinder increases the pressure and temperature of the burning gasses thus expansion of gasses and work is done on piston. Experimental data from engine sensors such as the in-cylinder pressure and volume/displacement will be analyzed to obtain the rate of heat release (ROHR) and mass fraction burn (MFB)

3.4.4.1 Rate of Heat Release (ROHR)

Assumptions were made in an ideal Otto cycle whereby the combustion process is assumed to be in a constant volume state. Whereas, the experimental pressure vs. time diagram shows that it is a time dependent process. The pressure and volume data are important for combustion process analysis. In Figure 3.15, initial conditions of the combustion process was stated and a heat release was derived by Blair [61].
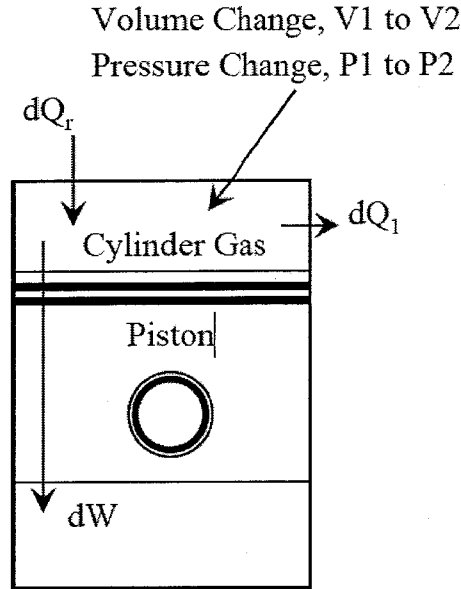
Figure 3.15: The initial state of in-cylinder thermodynamic during combustion [61]

Due to the absence of crank shaft in free piston engine, a different kind of approach was used for the combustion analysis. Hence, the derivation will be adapted to neglect the crank angle term which resulted in the equation below [61].

$$dQ_r = \left((P2 - P1) \times V_r^n\right) \times \left[\left(\frac{V2}{(\gamma - 1)}\right) + \left(\frac{V2 - V1}{2}\right)\right] \qquad (3.6)$$

Whereby dQr is incremental heat release, P1 and V1 are initial pressure and volume, P2 and V2 are pressure and volume at certain time dt respectively, γ is specific heats ratio, Vr is incremental volume ratio which is calculated by V1/V2 and n is polytrophic exponent. Another equation was derived by Rassweiler and Withrhow and it is shown below.

$$dQ_r = \left((P2 - P1) \times V_r^n\right) \times \left(\frac{V2}{(\gamma - 1)}\right) \qquad (3.7)$$

Summations of dQr will determine the total heat release within a combustion period, tb, which will give the total heat release Qr. The total heat release will be defined below:

$$Q_r = \sum_{t=ts}^{t=te} dQ_r \qquad (3.8)$$

50

The summation of dQr begins with the start of combustion, ts, and end of combustion is te. The start of combustion can be determined when the net heat release starts to become positive while the end of combustion marks the point when the net heat release is negative [61].

3.4.4.2 Mass Fraction Burn (MFB)

Mass fraction burn (MFB) is a ratio of the total fuel burned from the start of combustion which is 0, and to the end of combustion which indicates the value of 1. It expressed the energy conversion throughout the combustion process [R68,R69]. MFB at every time step was determined by the calculation of the ratio of the heat release illustrate below.

$$MFB = \frac{\sum_{t=t_s}^{t=t_e} dQ_r}{Q_r} \qquad (3.9)$$

Additionally, MFB can be compute based on Rassweiler and Withrow procedure [42,57,78]. It was mentioned that pressure rise is due to two factors which are due to combustion (Δp_c) and another is due to change of in cylinder volume (Δp_v).

$$\Delta p = \Delta p_c + \Delta p_v \qquad (3.10)$$

Assuming that the heat added to the in cylinder pressure is directly related to the pressure rise Δpc during the time interval, the value of MFB at the end of i-th interval can be compute from equation below.

$$MFB = \frac{m_b(i)}{m_b(total)} = \frac{\sum_0^i \Delta p_c}{\sum_0^N \Delta p_c} \qquad (3.11)$$

Whereby 0 represents the start of combustion and N is the end of combustion. The polytropic equation that could be used to calculate the Δp_v is as shown below.

$$\Delta p_v = p_{i+1} - p_i = p_i \left[\left(\frac{V_{i+1}}{V_i} \right)^n - 1 \right] \qquad (3.12)$$

51

3.4.5 Thermal Efficiency

Thermal efficiency is measured by the total workout over the total work in as shown in equation. The total work out (equation 3.13) was derived from the highest IMEP per cycle and the work in (equation 3.14) is from the fuel mass flow rate per cycle.

$$W_{out} = IMEP \times V_d \times N \qquad (3.13)$$

Whereby IMEP value per cycle was taken to be compute together with displacement volume (Vd) and the engine speed in cpm (N) as shown in equation 3.13.

$$Q_{in} = \dot{m}_f \times Q_{LHV} \qquad (3.14)$$

Equation 3.14 is the work in per cycle where by mass of fuel in kg/s and Hydrogen lower heating value (Q_{LHV}) which is 122 MJ/kg are inserted to get the work in value.

$$= \frac{W_{out}}{Q_{in}} \qquad (3.15)$$

The final equation will give the thermal efficiency value as shown in equation 3.15.

3.5 Summary

The prototype with a specification of two-stroke, direct injection, fueled by Hydrogen gas, free piston linear generator engine was explained in detail. The bore and stroke is 76mm and 69mm respectively which make up 313cc/cylinder engine capacity. The engine is mounted on a test rig to reduce vibration during operation. The linear alternator is design n fabricated specifically for the engine which will produce 5kW output at 2000 cpm. This power will charge the battery power bank on a SHEV. A National Instrument (NI) PXI embedded controlled with Real Time Labview construct a fast and reliable control system to control the operation of the

engine simultaneously records engine operating data for further experimental investigation.

Furthermore, raw data which was recorded were processed accordingly to determine the behaviour and performance of the prototype through analysing p-V, IMEP, ROHR, MFB and thermal efficiency.

To conclude, every part of the engine was described in detail including the engine inverter, fuel supply and lubrication systems. Data processing of recorded raw data was also presented.

CHAPTER 4

RESULTS AND DISCUSSION

It have been explained in previous chapters on how the fundamentals of this prototype and the methodology of the experimental works and previous studies have been done up to 60 V and faced problems moving towards more than 60V [16]. Initial works was to identify the problem and then to proceed with experimental works to validate the new component that is integrated to LG control system and to proceed testing with more than 60 V. This chapter discusses the experimental data's from identifying the problem, LG modification and to completing experimental works up to 84 V. Raw combustion data is shown in appendix B. Combustion analysis were done as well to look at the effect of LG performance when varying parameters such as the battery capacity and equivalence ratio. Combustion analysis includes Indicated Mean Effective Pressure (IMEP), Mass Fraction Burn (MFB), Rate of Heat Release (ROHR) and Thermal Efficiency.

4.1 Preliminary Data

Before any modification is made, preliminary data was taken to analyze existing setup and to identify the problem.
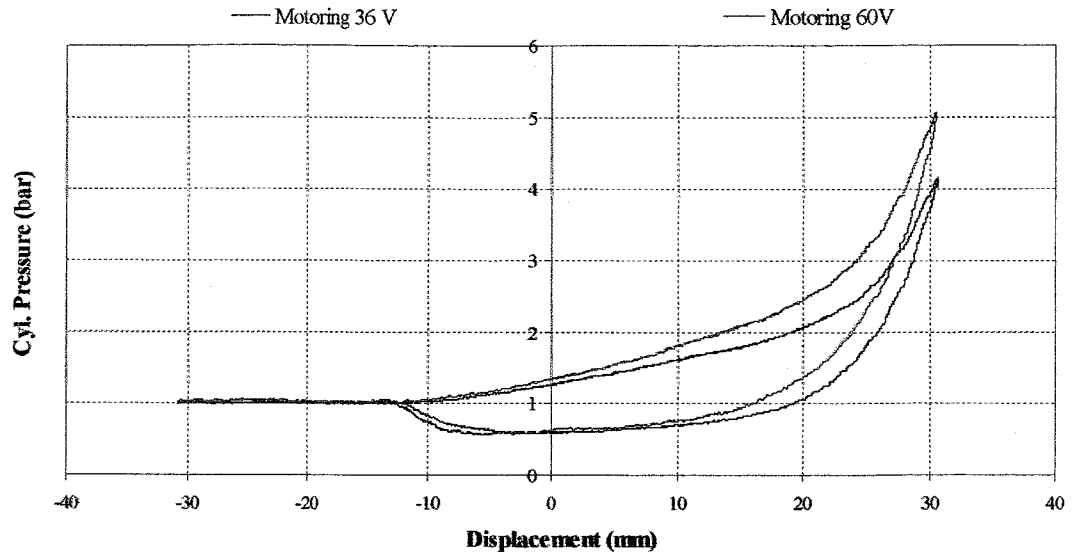
Figure 4.1: Motoring only 36 V and 60 V

Figure 4.1 above shows a comparison of two motoring profile which have different battery capacity. With 36 V, LG operating frequency is at 4 Hz and with 60 V, 5.87 Hz. From visual analysis, the peak for both graphs have differences in x and y axis. The graph for 36 V shows longer stroke/further TDC at 32mm while for 60 V is at 31mm. Whereas for the y-axis, a significant difference in compression pressure up to 1 bar can be seen. Preliminary work shows that by increasing the battery capacity, higher compression pressure can be produced but with a shorter stroke whilst shorter stroke relates to lower compression ratio.
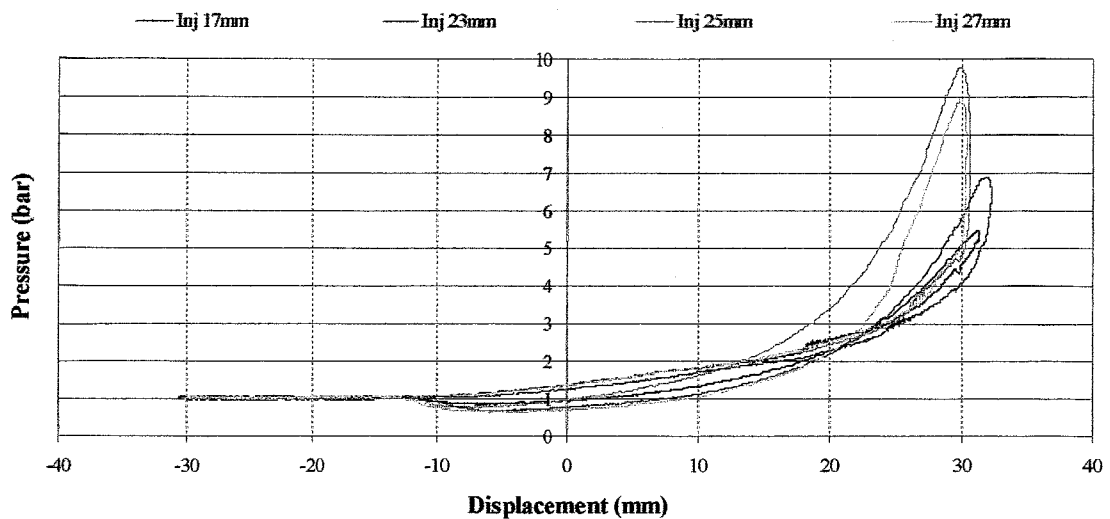

Figure 4.2: Motoring with combustion PV diagram for various injection points with 60 V with constant 1.6 equivalence ratio

Few combustion experiments were done on 60 V by varying the injection timing as shown in figure 4.2. The peak combustion pressure was produced highest at 25mm injection due to optimum time for air fuel mixing which later will be describe in this chapter. Injection at 17mm and 23mm produce lower peak pressure due to too early injection which reduce the volumetric efficiency by dissipating fresh air from the chamber. Too late injection (27mm) also is not appropriate whereby insufficient time required mixing air and fueling mixture.
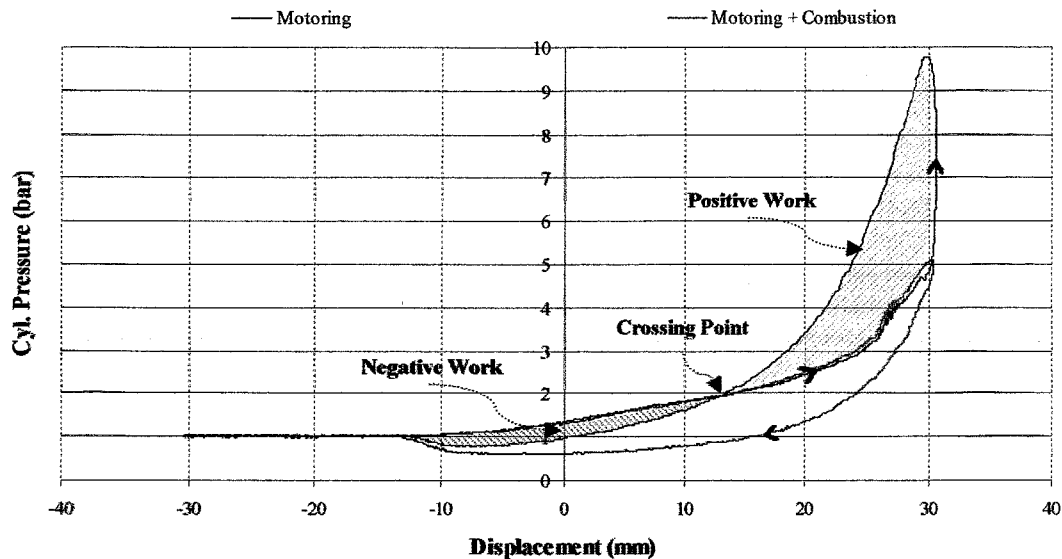

Figure 4.3: PV diagram motoring with combustion for 60 V

Figure 4.3 is plotted to illustrate 2 separate graphs for motoring and motoring with combustion. The combustion PV shows the best pressure that LG could get using 60 V battery capacities. It can be seen that a crossing point separates to 2 areas in the PV curve. One is to represent positive work (combustion) from the engine while another reflects a negative work (motoring), introducing work into the engine. Even with the best combustion settings, energy is not enough to sustain throughout cycle.
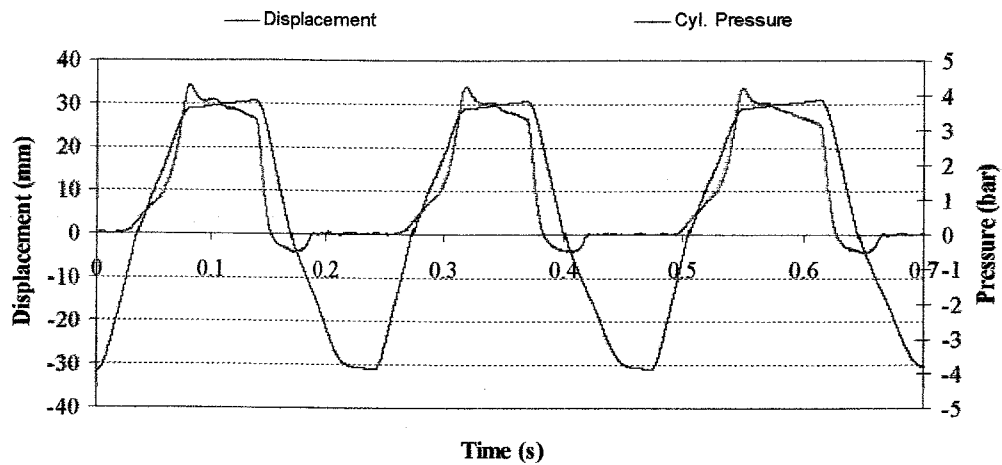
Figure 4.4: Motoring with 60 V showing irregularities

It is known that LG could not travel more than 29mm to produce high compression pressure due to low motoring voltage as shown in figure 4.4. For the above experiment, LG TDC was set to 30mm to achieve higher compression ratio thus higher compression pressure but it did not manage to do so. Higher power which means higher voltage is required to motor LG more than 29mm and produce higher compression pressure than 5bar. With only 5 bar of compression pressure, 9.8 bar combustion pressure are produced. Higher compression pressure is crucial to produce higher combustion pressure. Base on the previous simulation results [11], 60 V battery produced 5.7 bar of compression pressure. A difference of 12.3% comparing experimental and simulation results are noticed. From the simulation as well, higher voltage produce higher compression pressure. The current setup using MOSFETs only allow the maximum voltage of 60 V. Due to that, works are being done to accommodate higher voltage being induced into LG to produce higher compression pressure.

4.2 Integration and Experimental Works on Insulated-Gate Bipolar Transistor (IGBT)

Insulated-gate bipolar transistor is chosen due to high voltage and high current characteristic. A printed circuit board was design and built to intergrate the new IGBT into the current control system. The new IGBT can accommodate up to 900V and 300A.
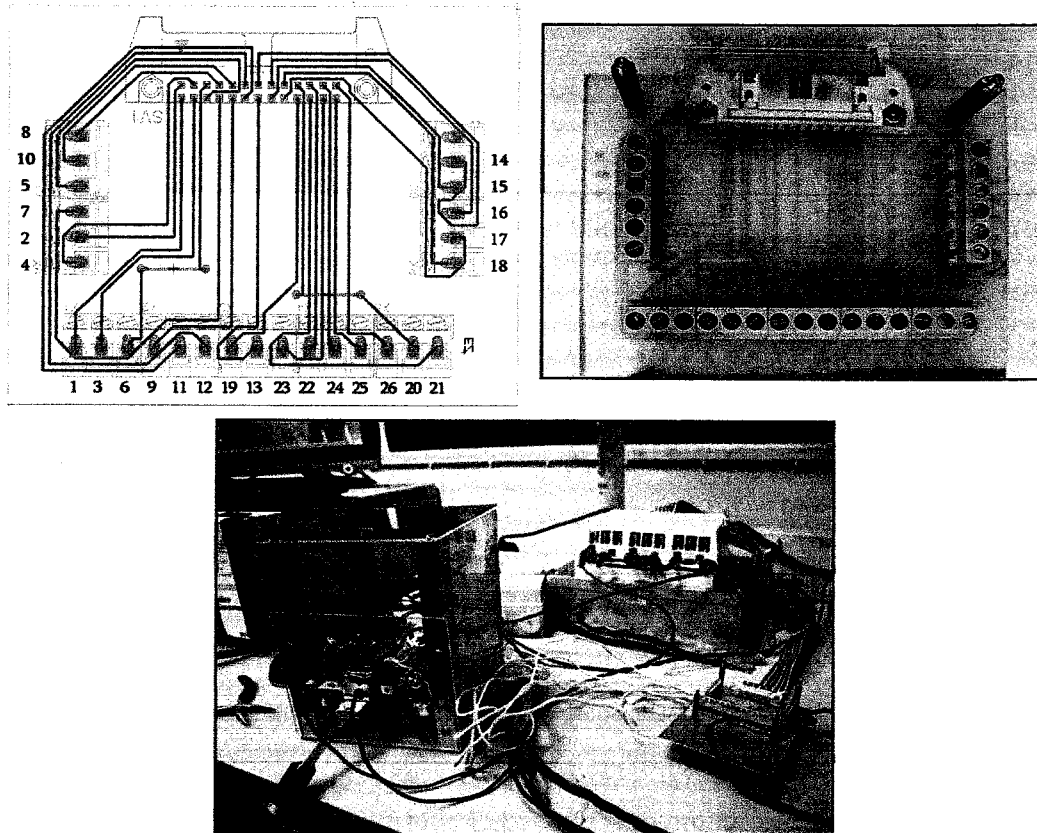
Figure 4.5: PCB model was built and integrated into the control system

Figure above shows a crucial modification made so that installation of the new IGBT is possible. Figure 4.5 shows a schematic of a printed circuit board (PCB) which was design using Eagle 5.1 software and fabricated by the electrical department lab. The installation was done so that the communication between the gate driver and IGBT is feasible.

4.2.1 Motoring with 36 V

After the installation of the new IGBT, experimental works on motoring with 36 V are done and are plotted below.
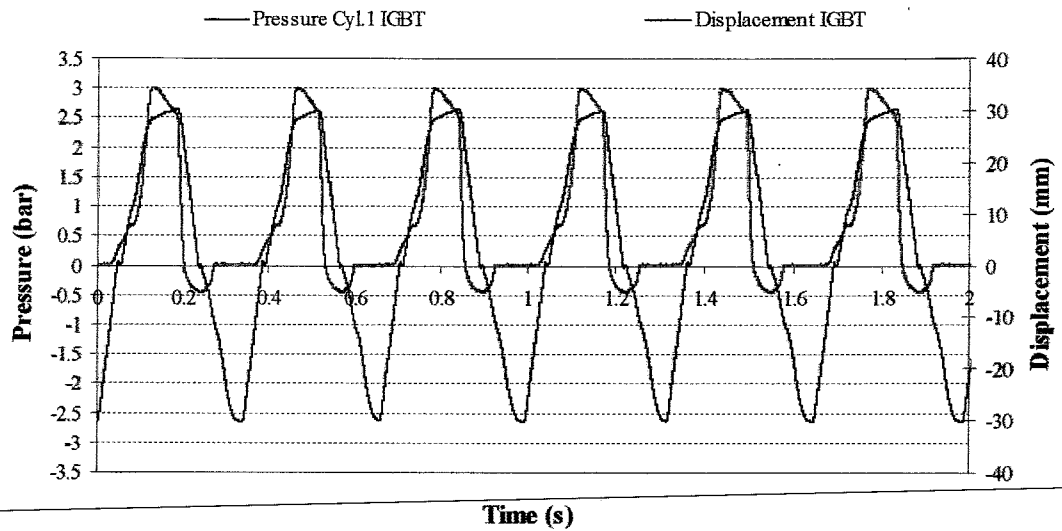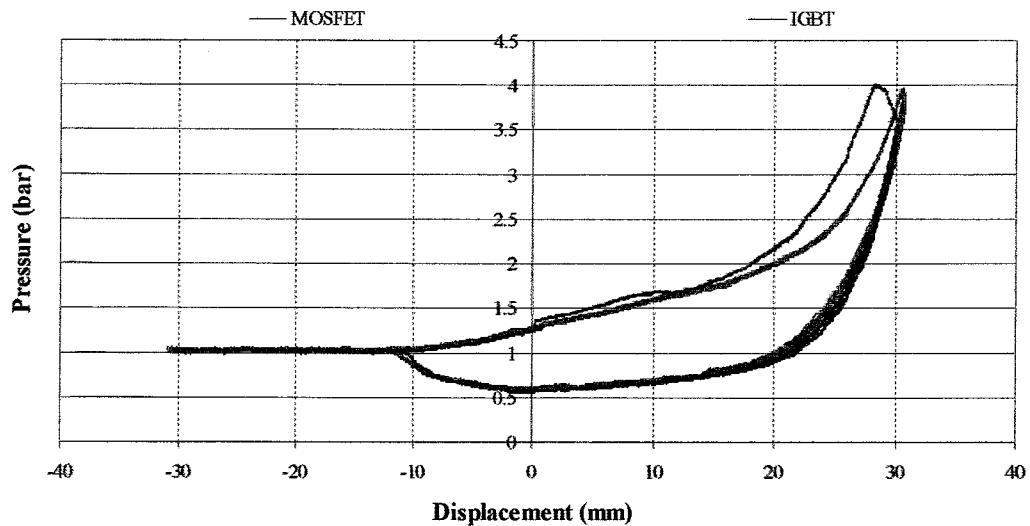

Figure 4.6: Motoring using IGBT with 36 V

Figure 4.7: Motoring Comparison between IGBT and MOSFET with 36 V

Figure 4.6 shows motoring with 36 V using IGBT. Pressure and Displacement is plotted against time. Initial data shows that the motion of LG is not smooth. The peaks are slightly flat compared to motoring 36 V using MOSFET. Pressure peaks are affected as well due to non smooth reciprocating motion. LG manage to produce 4 bar peak compression pressure, almost similar to previous setup using the MOSFET. Area

in the graphs denotes the work in into the system. The wider the area, the more work is being done to compress the air to a certain value or pressure. Comparing both PV as shown in figure 4.7, 36 V using IGBT have wider graph indicating more work is being done to compress up to 4 bar of compression pressure. The major differences are the motion of the piston which MOSFET driven LG produce slightly higher frequency compared to IGBT driven. LG driven by MOSFET operates at a frequency of 4 Hz while with IGBT is at 3 Hz. The non-smooth linear motion contributes to lower operating frequency. Lower operating frequency is not favorable due to higher air leakage through piston rings.

4.2.2 Motoring with 60 V

Following the completion of the previous experimental works, next is to proceed with motoring at higher voltage at 60 V.
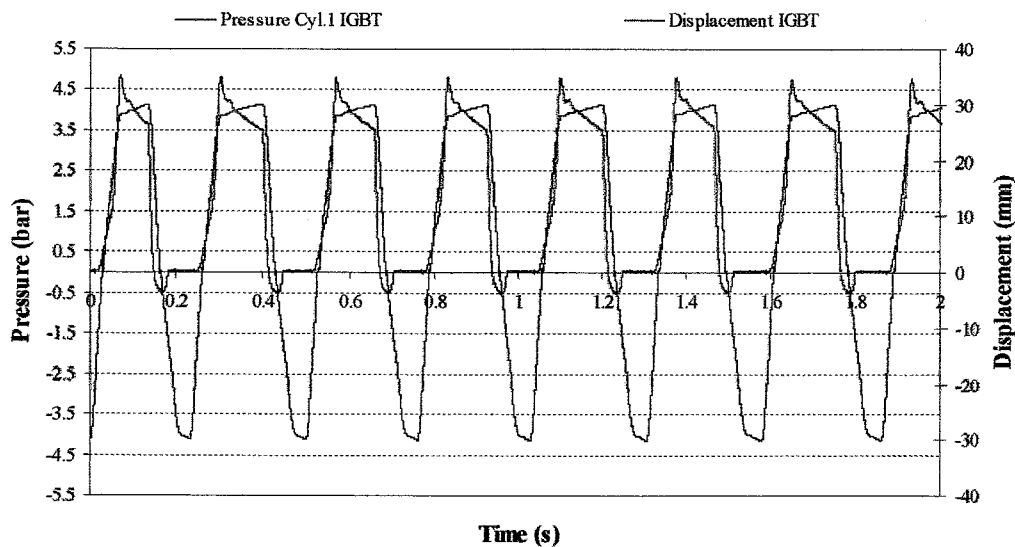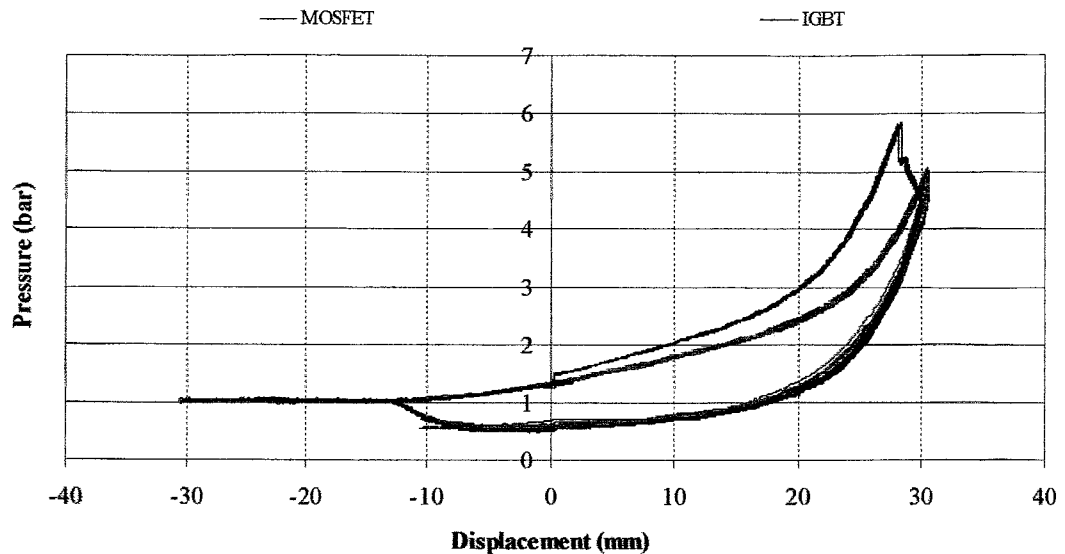

Figure 4.8: Motoring using IGBT with 60 V

60

Figure 4.9: Motoring Comparison between IGBT and MOSFET with 60 V

Figure 4.8 shows motoring profile for 60V using IGBT. It shows similar trend like 36 V with IGBT, flat peaks with not smooth linear motion and unstable operations. With these operating conditions, the IGBT manage to resonate the LG at 4.06 Hz while previous MOSFET driven LG resonates at 5.87 Hz. Peak pressure for IGBT is high at 5.8 bar compared to MOSFET, 4.11 bar. It also can be seen that area of the graph produced by IGBT is wider than the MOSFET as shown in figure 4.9. As previously mention, this indicates the work required to compress the air is higher than the MOSFET. During the experiment running at 60V with IGBT, the engine stalls frequently compare to 36 V. This phenomenon hardly occurred during MOSFET driven LG.

4.2.3 Motoring with 72 V

The attempt to motor LG at 72 V is very much anticipated. This is the first time LG have reach motoring voltage higher than 60 V.
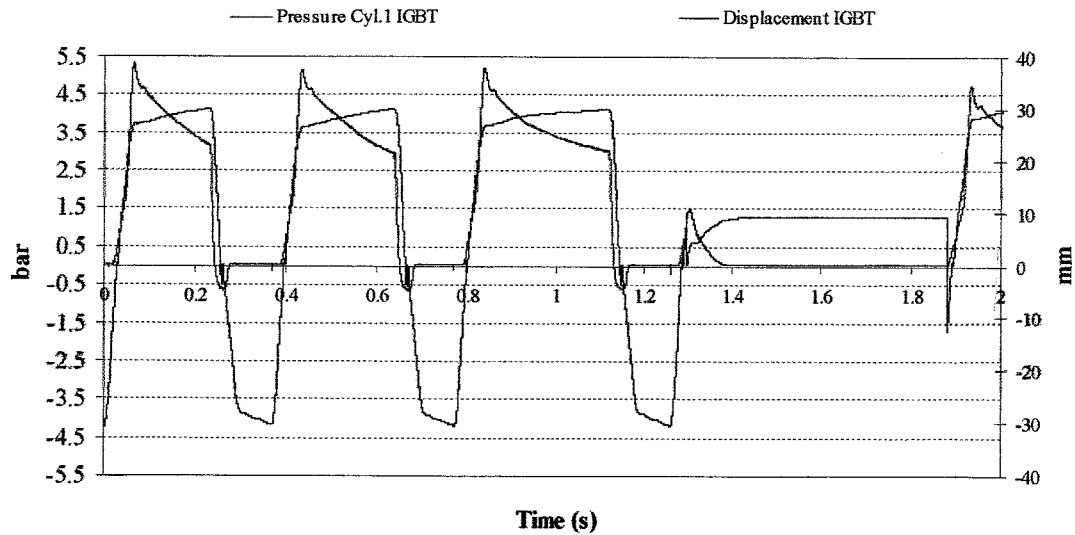
Time (s)

Figure 4.10: Motoring using IGBT with 72 V
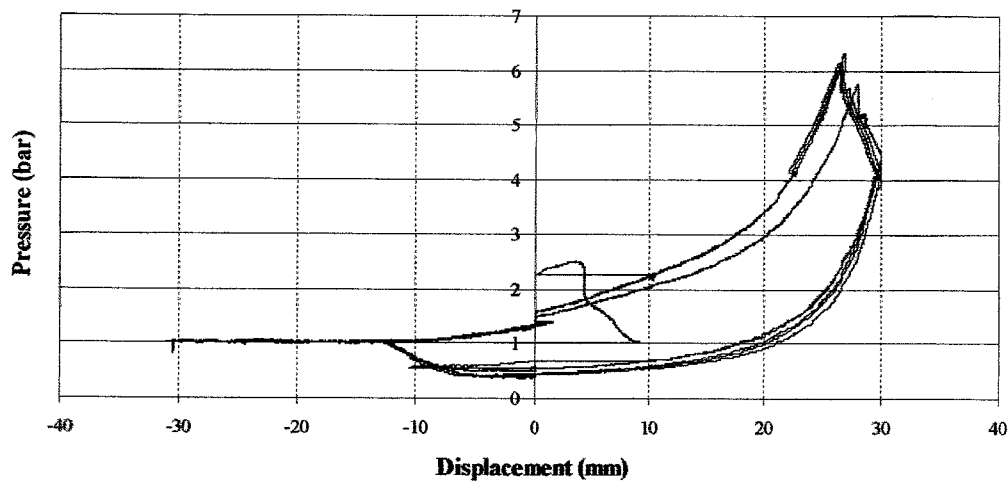

Displacement (mm)

Figure 4.11: PV diagram for motoring using IGBT with 72 V

This is the very first attempt to motor LG using higher than 60 V. The specification for the previous MOSFET only allows the maximum operation of 60 V. Due to that, current work is done to use IGBT (which can support up to 900V) to allow LG to be motor at higher than 60 V. Motoring using IGBT with 72 V is very unstable. LG managed to produce only few cycles before it stalled. Only 3 to 4 cycles managed to be recorded and plotted. Base on the graph above, it manage to produce 6.2 bar compression pressure. The motion is even worst to compare it with previous experiment running at 36V and 60 V using IGBT. From the PV curve, it could be seen that exist a foreign line. Analysis is done on the line and it is found that it is due to false home signal which later will be discussed.

4.2.4 Problem Faced with IGBT

When using IGBT to drive the LG, it became unstable and it is very difficult to get a consistent pressure curve. Figure 4.12 shows a pressure profile having two pressure peaks within one cycle which is abnormal. It is also shown that during its three cycles operations, the last cycle illustrate two pressure peaks then it leads to engine stall and stop. This phenomenon was never encountered when MOSFET was the primary driver for the LG. Additional graphs need to be plotted in order to determine what is the main caused to this irregularity.
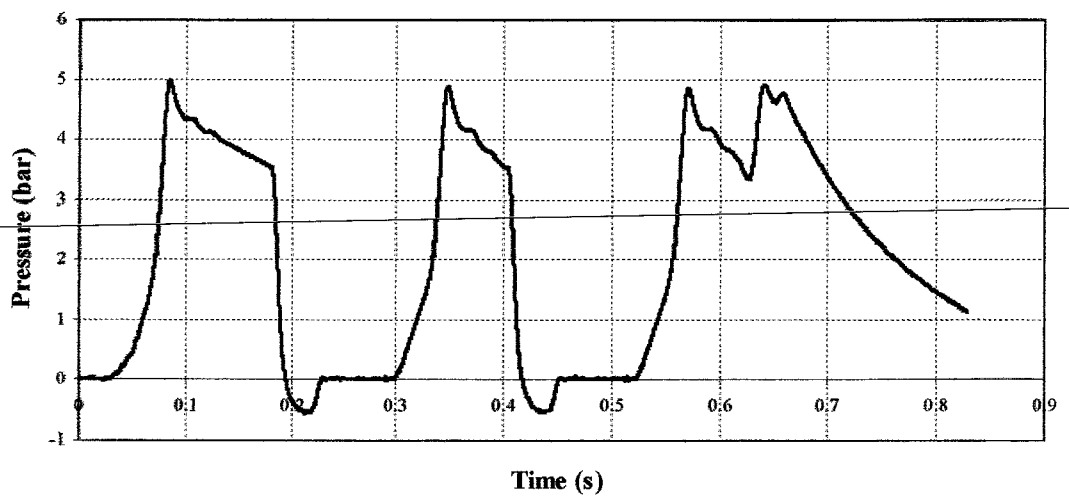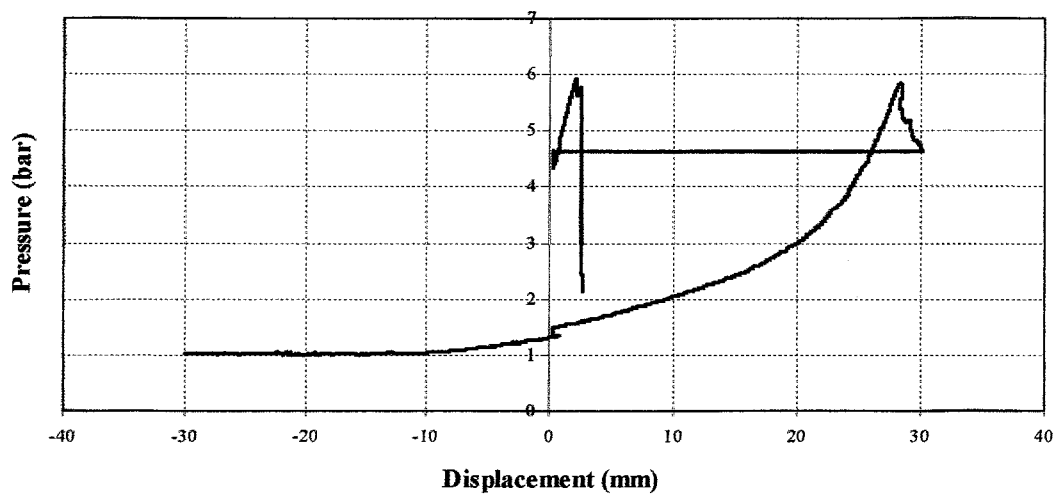

Figure 4.12: Effect of Noise on Pressure Profile

Figure 4.13: Effect of Noise on PV Diagram

PV diagram shown in figure 4.13 was plotted to analyze the behaviour. From the PV diagram, the piston seems to be changing the displacement/volume by moving from displacement of 30 mm to 0 mm at a constant pressure of 4.6 bar and start to increase the pressure from 4.6 bar to 5.9 bar at 0 mm to 2.1mm. This explains why two peak pressures within one cycle is achieved in previous graph (figure 4.12). The pattern doesn't show a normal behavior.
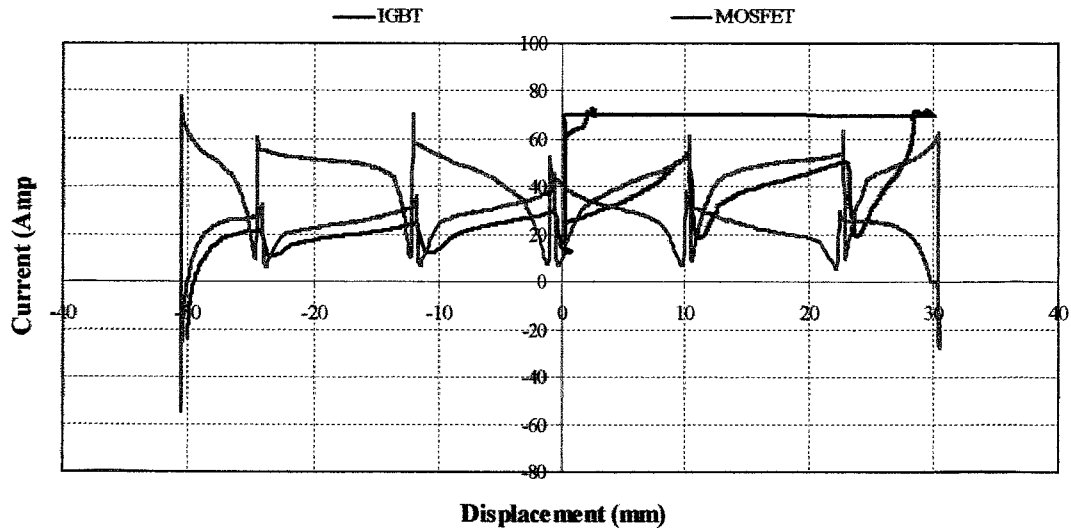

Figure 4.14: Effect of Noise towards Current Profile

Figure 4.14 above shows a comparison of current profile between IGBT and MOSFET. There is slight change in amplitude of the current due to minor drain of battery power during experimentation but this is still within acceptable limit. The main issue here is the major differences in current profile at displacement 0 mm to 30 mm on IGBT. There is an unexpected sudden change of displacement value and this is due to the electromagnetic interference that exists in the control system of LG whenever switching of IGBT gates. It is suspected due to home sensor that resets the position of the piston from 30 mm to 0 mm while the piston is still at 30mm .This can be observed in the next figure 4.15.
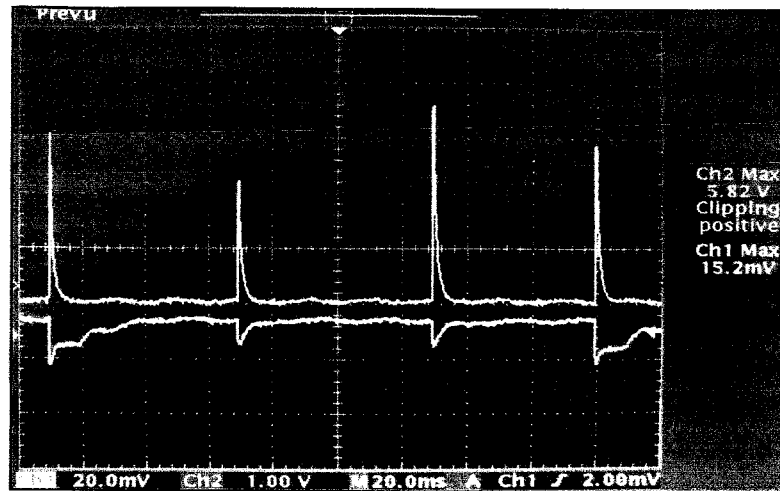
Figure 4.15: Oscilloscope showing existence of noise in the system occurring at the same moment as the IGBT switching (home sensor is taken out from LG)
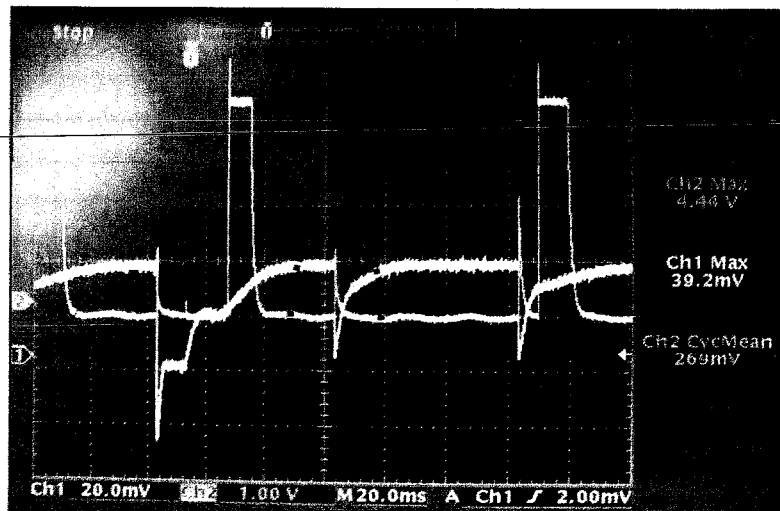

Figure 4.16: Oscilloscope showing existence of noise when home sensor place back to original position

Figure 4.16 above is taken from an oscilloscope which measures electrical properties of LG and it is define by y-axis represents voltage value and x-axis represent time. The figure shows two signals that are being measured which is the current being injected into LG (yellow line) and one more is the home signal (blue line) which tells the position of LG piston to the control system. Clearly it can be seen that both peaks are occurring at the same time without miss. This indicates noise is being produced in the system every time switching of the IGBT gates. The magnitude of the noise produced is related to supply voltage to LG and for this case, it is around 5.8V which is near to the home signal value that is 5V and this would cause

LG control system to be mistakenly read the position of LG piston thus causing instability of engine operations. Further methods have been done to remove the noise in the system and it is successful for the home signal as shown in figure 4.17 but it requires centralized noise filtering method to be able to filter noise from all signals and not only for home signal, which is complicated and requires more time. Due to this, IGBT was no longer chosen to be the primary driver for LG.
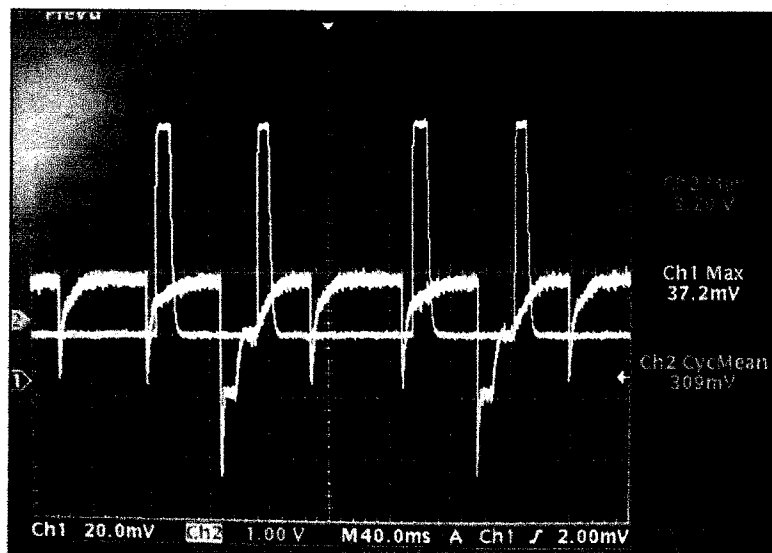

Figure 4.17: Clean home signals without any noise after installing noise filter

Figure 4.18: Clean home signal for control system

4.3 Experimenting with New MOSFET

Previous works have shown how IGBT works and it is not suitable for LG due to the noise it emits during switching of IGBT gates and causing instability to LG. Next is to install and to test the new MOSFET IRFB4110PRB and to analyze LG performance using this new selected primary driver for LG. Firstly, motoring using 36 V and 60 V are done and to compare it with the PV diagram of the previous MOSFET and next is to continue motoring with higher battery capacity. After that is completed, combustion is introduced while motoring at different battery capacity and the combustion pressure are analyzed.

4.3.1 Comparison between previous and new MOSFET

With the new MOSFET in place, motoring at a displacement of 30mm using 36 V is done. In cylinder 1 pressure is captured during the motoring process and the data is as shown in figure 4.19.
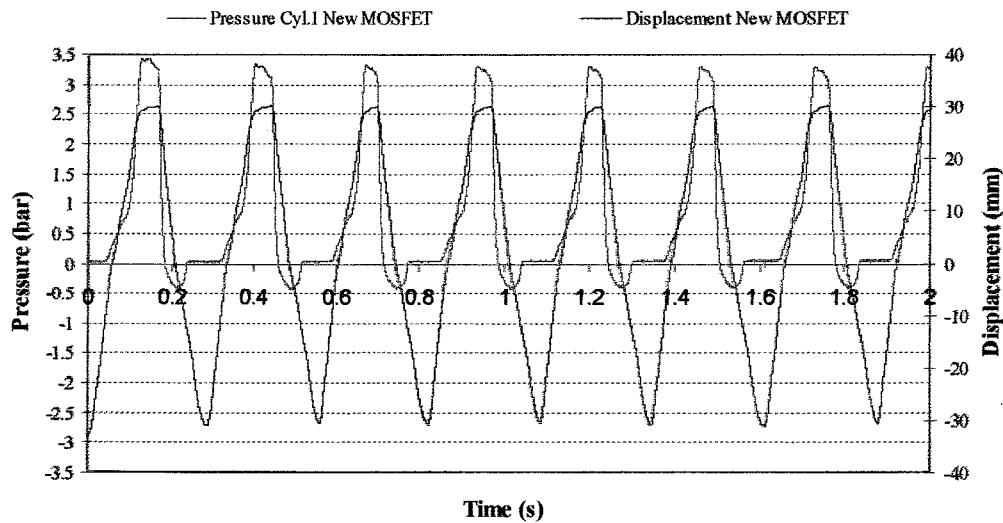

Figure 4.19: Pressure and Motion profile during motoring using 36 V

As shown in figure 4.19, peak cylinder pressure produced is at 3.3 bar and moving with a frequency of 3.7 Hz. The operation is very smooth and having high repeatability rate with varying pressure of ±0.3bar. It can be also seen that the peak pressure occurs around 28mm displacement while the piston travels up to 31mm

67

TDC. During the compression from point 28mm to 31mm, the pressure drops due to leakage through the piston ring since the piston movement is slow.
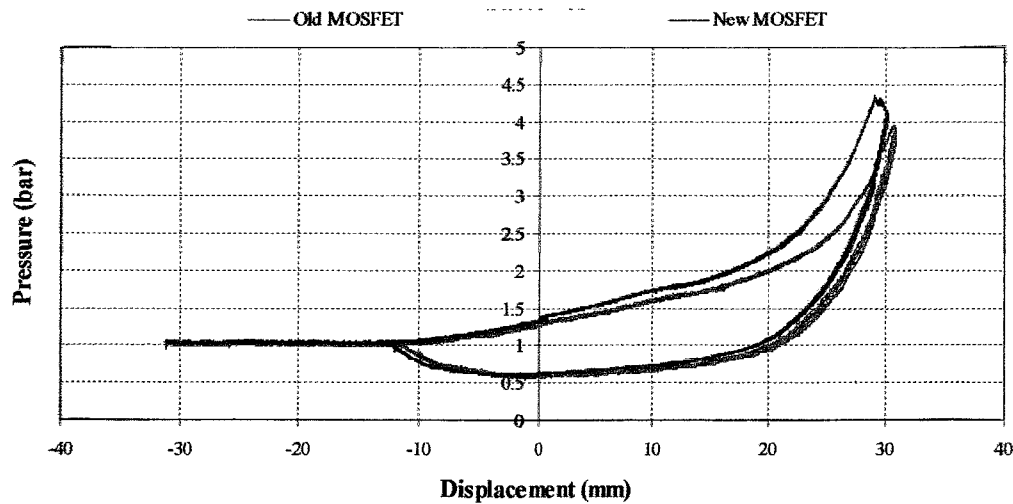

Figure 4.20: Motoring comparison between previous and new MOSFET with 36 V

As shown above in Figure 4.20, the comparison for both new and previous MOSFET. New MOSFET produce slightly higher pressure due to better MOSFET ratings and faster switching. Higher compression pressure relates to higher air density at point of ignition which is preferable. The piston travels further for the previous MOSFET (higher TDC) due to low compression pressure thus low resistance force during compression. Both graphs showing same pattern and profile. Up to this point, the new MOSFET is reliable and showing exact behaviour from the previous MOSFET setup.
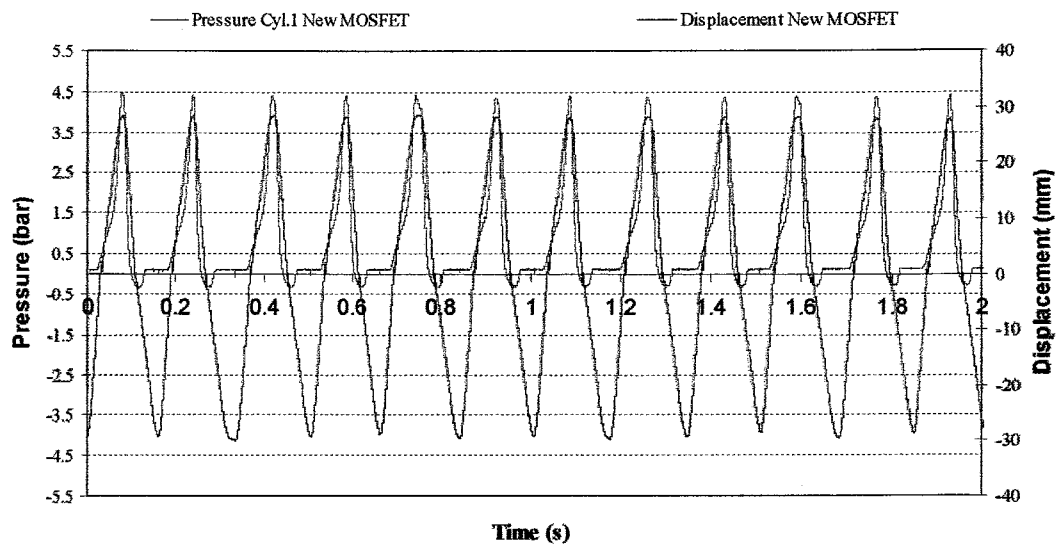
Figure 4.21: Pressure and Displacement vs Time with 60 V

Motoring at 60 V as shown in figure 4.21 allows higher power during motoring thus producing higher pressure with higher speed at 7.25Hz. TDC is at 28mm. The pressure and motion peaks are very smooth and sharp showing good motoring behaviour.
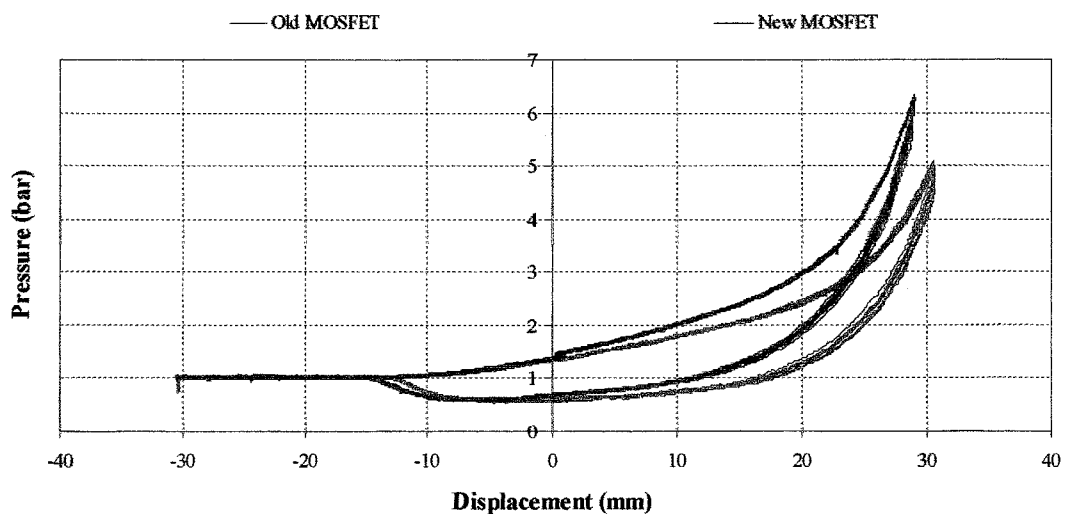

Figure 4.22: Motoring comparison between previous and new MOSFET with 60 V

With the new MOSFET, higher compression pressure can be achieve with lower TDC point as in figure 4.22. This indicates the piston is moving much faster and able to reduce air leaks through piston rings thus making higher pressure at earlier TDC point. Overall comparing 36 V and 60 V motoring using previous and new MOSFETs discovers that new components shows great improvement while maintaining its

standard profile and behaviour thus making further experiment works desirable and achievable.

4.3.2 Motoring using 36 V , 60 V, 72 V and 84 V

Previously, several experiments was done to verify the performance of the new MOSFET and the results are promising. Further experiment was taken place to motor Motoring is carried out using 36V, 60V, 72V and 80V respectively.
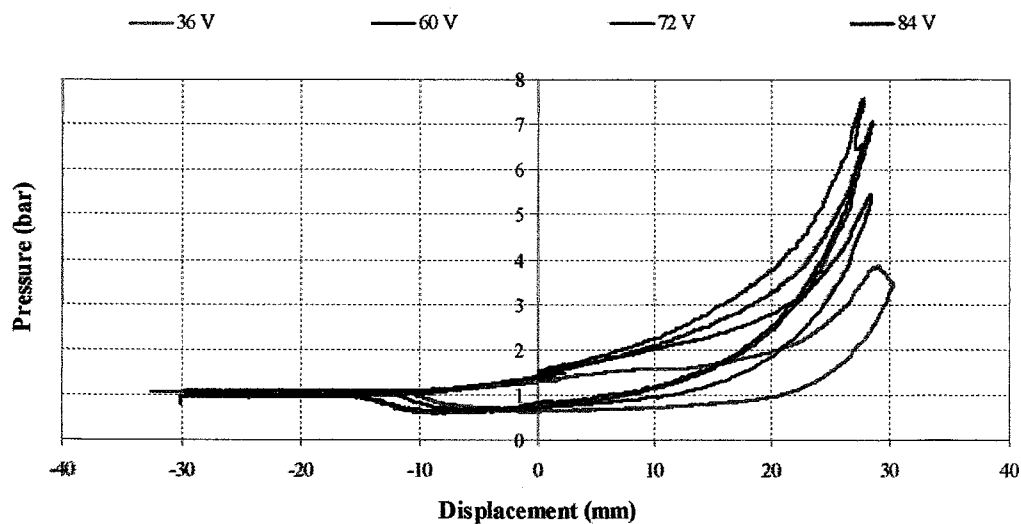
Figure 4.23: Motoring comparison on PV diagram for 36, 60, 72 and 84 V

Figure 4.23 above shows the motoring of LG using new MOSFET by varying the battery capacity from 36 V to 84 V. It can be seen that 84 V have the highest compression pressure which is at 7.58 bar and followed by 72 V 7 bar, 60 V 5.43 bar and 36 V 3.85 bar respectively. It is also noticed that for 84 V, it reaches 7.58 bar earlier than others meaning, it achieves higher compression peak pressure at shorter stroke (lower TDC) compared to others which is at 27.5mm. Higher battery capacity achieve high pressure earlier compared to others and can be seen from the TDC line. This is due to higher velocity which decreases air leakage through piston rings.
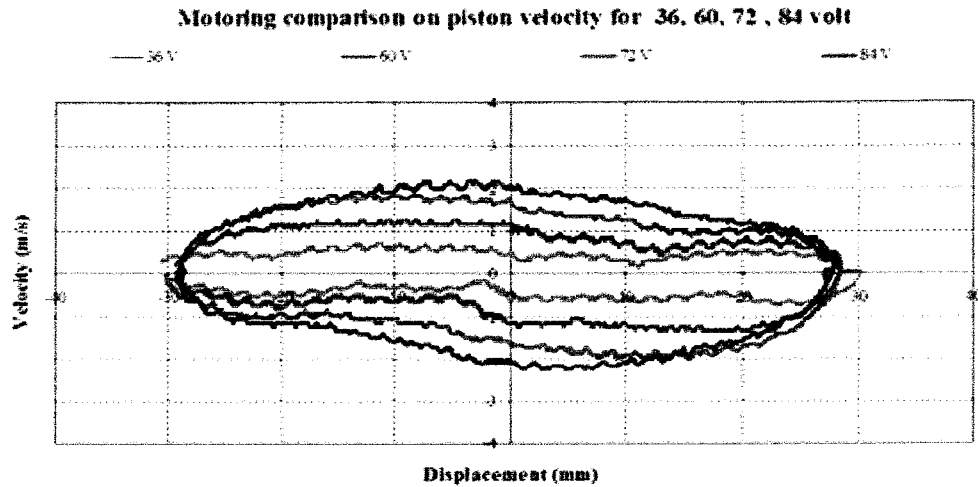
Figure 4.24: Motoring comparison on piston velocity for 36, 60, 72 and 84V

Motoring with 84 V have the highest piston velocity at 0mm which is at 2 m/s and followed by 72 V 1.6m/s, 60 V 1.1m/s and 36 V 0.5m/s. The velocity will decrease towards both ends due to resistance during compression stroke. Motoring with higher battery capacity is able to produce higher compression pressure due to less air leakage through piston rings during high piston velocity motion.

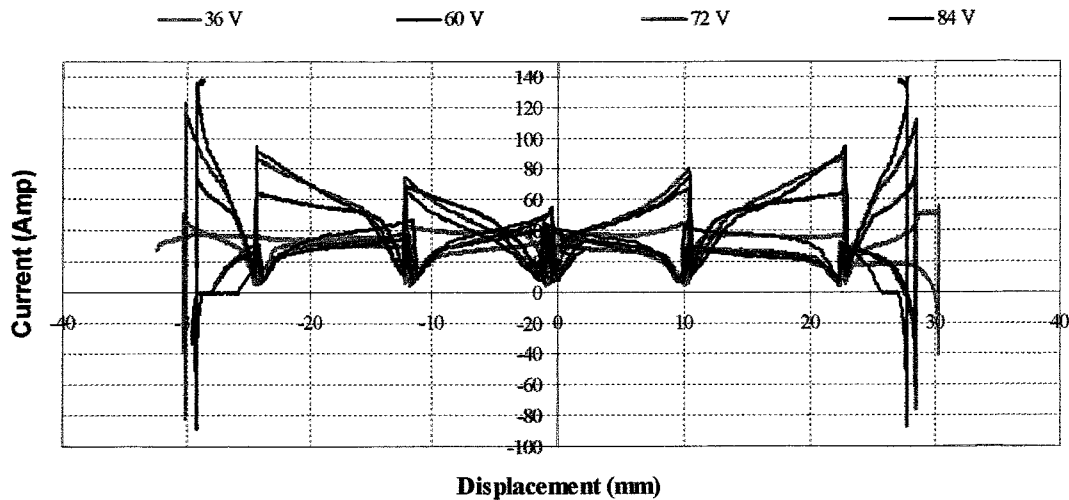Figure 4.25: Motoring comparison on current profile for 36, 60, 72 and 84 V

Figure 4.25 above shows 4 types of current profile. As the battery capacity increases, total current would increase there for showing differences in the profile. The biggest difference can be seen at the end of every stroke. At that point is the highest resistance force towards the piston (compression stroke), due to that the

71

current will be at its peak. Immense profile difference also can be seen for 36V, 60V and 72V while for 72V and 84V doesn't show much different. This is due to the limitation of hardware that restricts the maximum current flow.
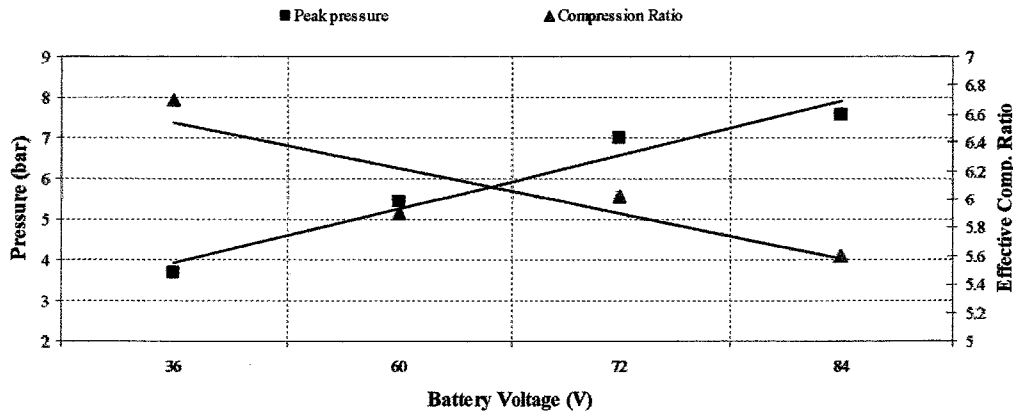

Figure 4.26: Relation between peak pressure and effective compression ratio

Figure 4.26 above shows two types of graph which explains how peak pressure and effective compression ratio is affected by battery capacity during motoring. Peak pressure reacts linearly with battery capacity, higher battery capacity will increase the cylinder peak pressure and it is the inverse relation for the effective compression ratio since increased in battery capacity will reduce the effective compression ratio.

Higher battery capacity will increase the piston speed and this will reduce air leakage through piston rings thus producing higher compression pressure at earlier displacement. Less air leakage will increase the effectiveness to absorb and release energy during reciprocation process. By achieving high compression pressure at earlier displacement will significantly decrease the effective compression ratio. The main target is to achieve higher compression ratio with high compression pressure but it is yet to achieve due to lacking in motoring force.

4.4 Experimenting with combustion

After conducting series of experiments on LG motoring, combustion experiment is next to carry out. As previously explain, combustion characteristic will be analyze by looking at PV diagram, IMEP, MFB and ROHR. Parameters such as injection

timing, equivalence ratio, and battery capacity are varied to look at the effects towards the combustion behaviour.

4.4.1 Coefficient of Variance

Analysis on coefficient of variance is done to show the reliability and consistency of combustion data. One set of data was taken from the experiment and a COV value is produced.
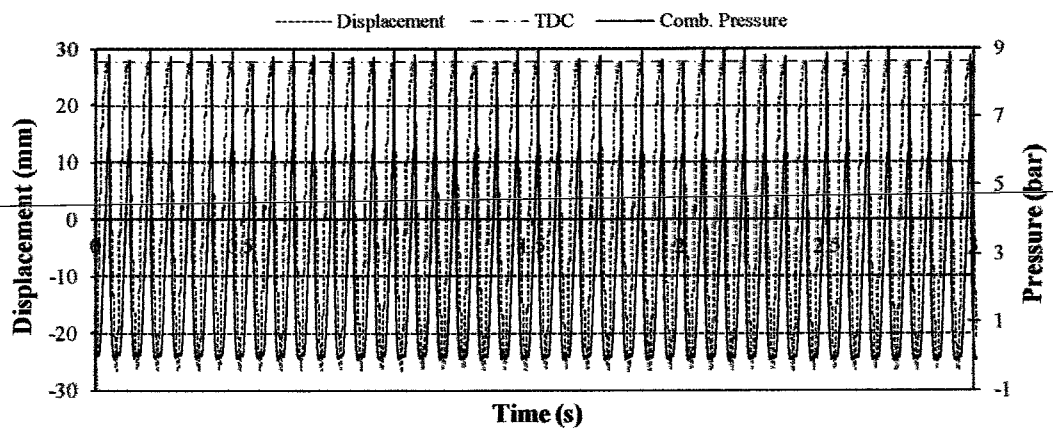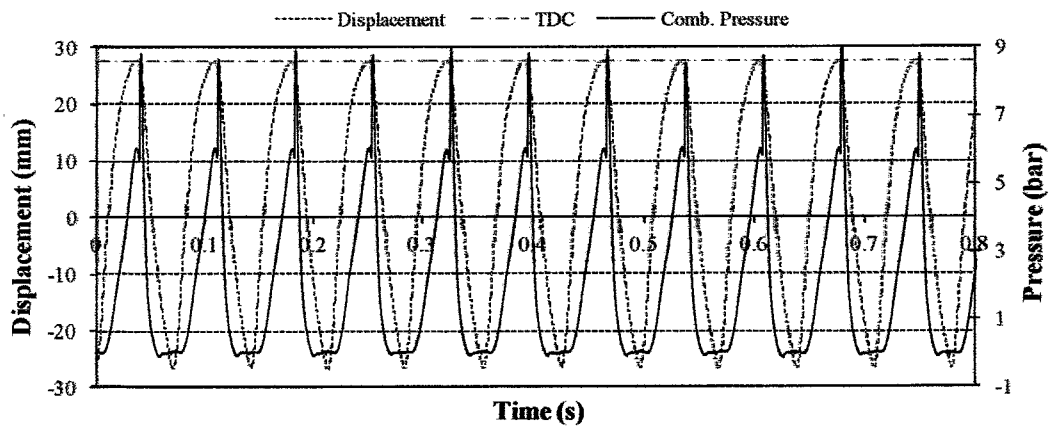

Figure 4.27: Pressure and Displacement vs Time

Figure 4.28: Pressure and Displacement vs Time (close up)

Figure 4.27 shows a continuous cycle of LG with combustion. This is a sample data taken from 72 V combustion experiment. Figure 4.28 is a close up of figure 4.27.

From the data above, a COV value of 1.54% is obtained. This proves that LG manage to run smoothly and reliable with many cycles using the new MOSFETs.

4.4.2 Combustion with 36 V

While motoring with 36 V, fuel is injected at 3 variation of timing and ignited at a point which produces the highest combustion pressure. Few experiments were done on different injection points.
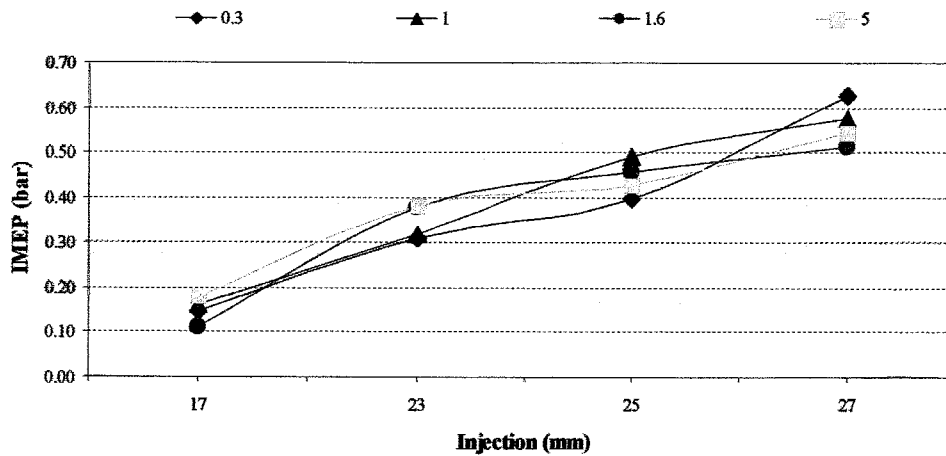

Figure 4.29: Overall IMEP for combustion with 36 V

IMEP is a good approach to study overall combustion behaviour. Figure 4.29 shows overall IMEP for 36 V. For almost all conditions, IMEP increase linearly towards late injection at 27mm. Late injection improves volumetric efficiency therefore producing better combustion, hence higher IMEP.
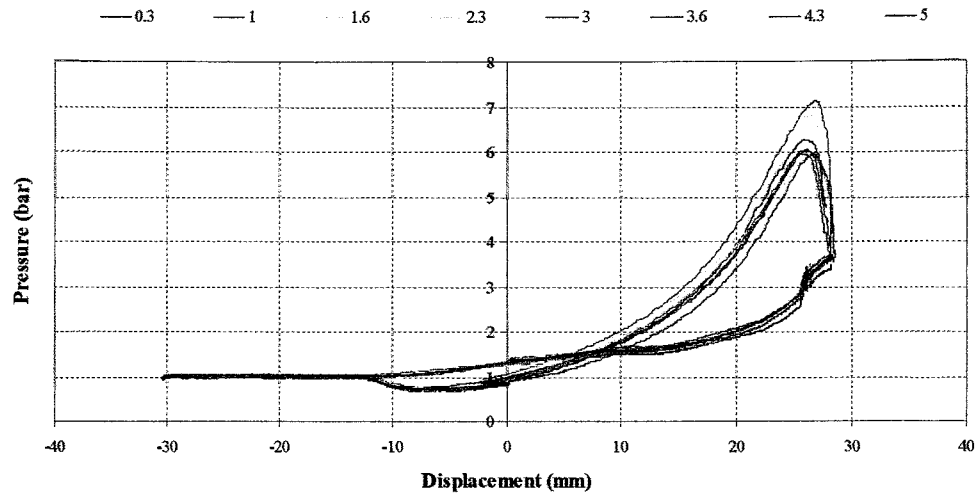
Figure 4.30: PV diagram for constant 25mm injection and vary equivalence ratio

Figure 4.30 above shows the effect of equivalence ratio towards combustion pressure while injection point is set to constant. Equivalence ratio is varied from 0.3 up to 5.0. It can be clearly seen that most of the combustion pressure produced are around 6 bar but different pressures for 1 and 1.6 equivalence ratio. The two categories manage to produce 7.1 bar and 6.8 bar respectively.

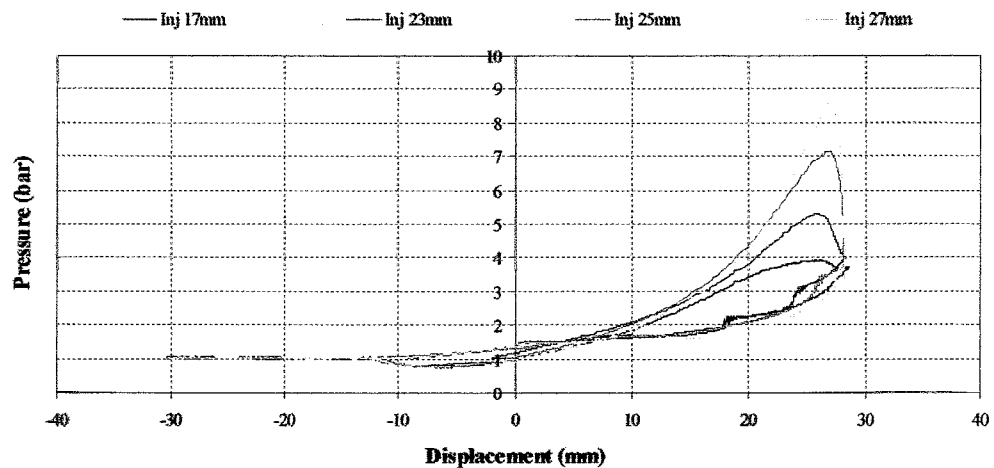**Figure 4.31**: PV diagram for constant 1 equivalence ratio and vary injection timing

In figure 4.31, comparison of combustion pressure by varying injection point is done while injecting constant fuel at 1 equivalence ratio. These managed to produce four different types of curve and injection at 27mm produced highest combustion pressure which is at 8.6 bar followed by 25mm (7.1 bar), 23mm (5.28 bar) and 17mm (3.91 bar) respectively.
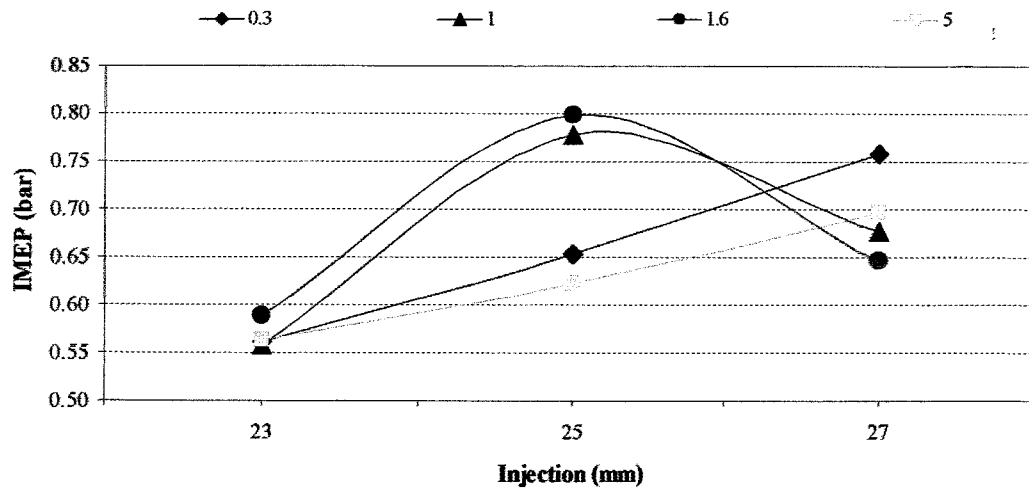
4.4.3 Combustion with 60 V

Figure 4.32: Overall IMEP for combustion with 60 V

IMEP in figure 4.32 above shows 2 different trends for 4 types of equivalence ratio which is linear and parabolic relation. For equivalence ratio of 0.3 and 5, IMEP increase linearly from 23mm injection to 27mm ranging from 0.56 bar to 0.76 bar. While for equivalence ratio 1 and 1.6, peak IMEP occurred at 25mm with values of 0.77bar and 0.8 respectively. Highest IMEP is recorded at 25mm is due to sufficient time for air fuel mixing which is around 12 ms [64]. The time taken from injection 25mm and to ignition 27.625mm is 12.7 ms, which is good compared to 27mm to 27.625mm at only at 2.2 ms. Since highest IMEP occurred at 25mm injection with 1.6 equivalence ratio, further analysis will be concentrated on constant 25mm injection and constant 1.6 equivalence ratio.
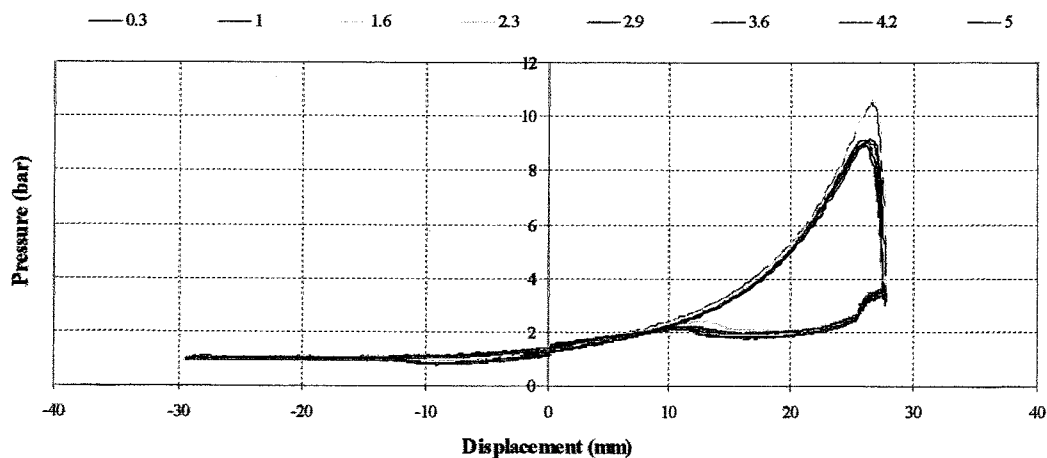

Figure 4.33: PV for constant injection 25mm and vary equivalence ratio

Figure 4.33 plots pressure against displacement for constant injection at 25mm. The highest peaks pressures are recorded by equivalence ratio of 1 and 1.6. Peak pressure is one of the reason it is able to produce higher IMEP and the duration of the combustion plays an important role as well which will be explain in later part of this chapter.

Figure 4.34: PV diagram for constant fuel 1.6 equivalence ratio and vary injection timing

Figure 4.34 above shows a PV curve with a constant 1.6 equivalence ratio while varying injection timing. As shown, 3 peaks are visible showing 3 types of injection was experimented. Injection at 27mm produce highest peak pressure which is at 12 bar, followed by 25mm 10.4bar and 23 mm 8 bar respectively. The 27mm injection is labeled as late injection due to TDC is at 28 mm and ignition is at 27.625mm. This late injection produce higher peak pressure but produce less IMEP due to air fuel mixing. Injection at 25mm allows more time for air and fuel to mix when motoring at 60 V. It can be seen when the curve crossing point for 27mm is at 10mm while for 23 mm and 25mm is partially further at 7mm displacement. This crossing line tells apart the positive and negative work produced by the combustion.

4.4.4 Combustion with 72 V
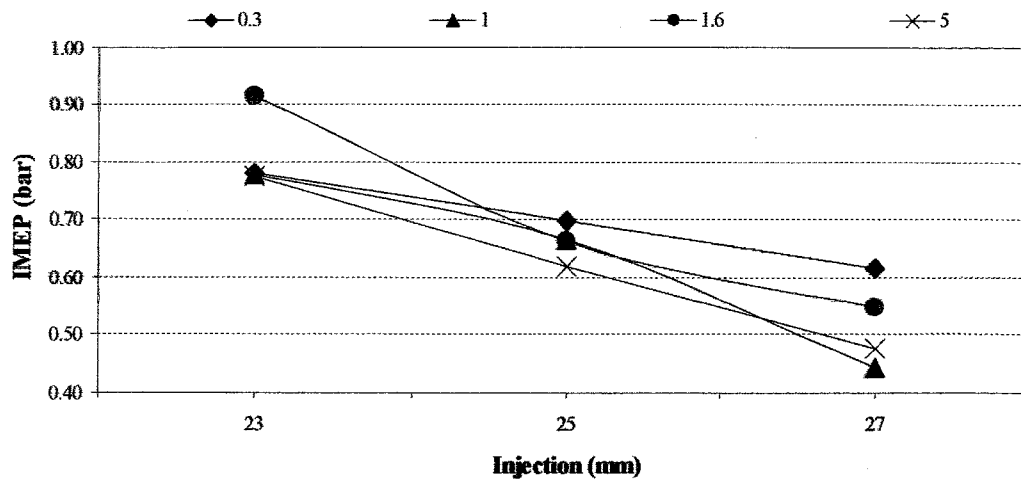
Figure 4.35: Overall IMEP for combustion with 72 V

Figure 4.35 shows a negative linear trend. Early injection (23mm) having highest IMEP and decrease in performance as injection timing is moving near TDC (28.375mm). These indicates the faster the piston travels, early injection is favorable to allow air fuel mixing and to produce good IMEP.
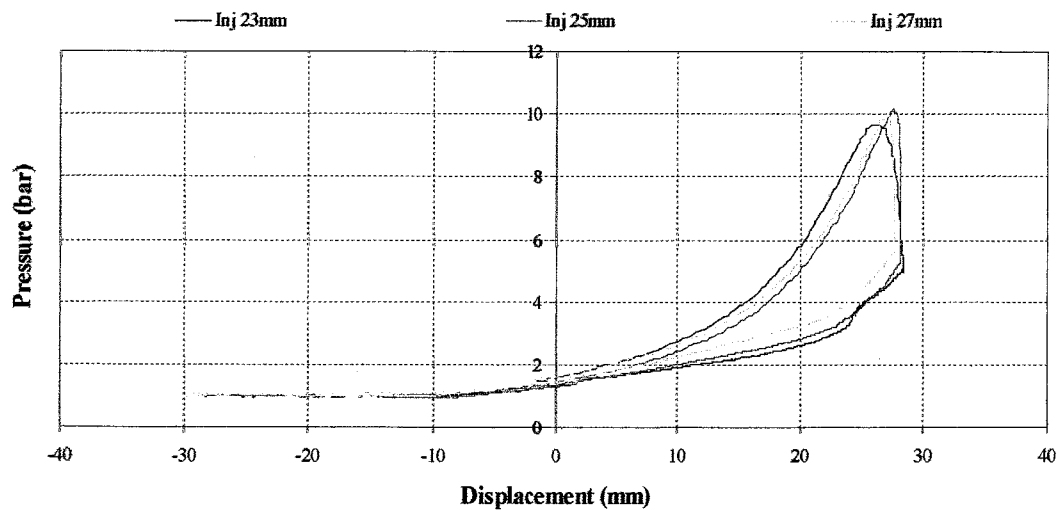
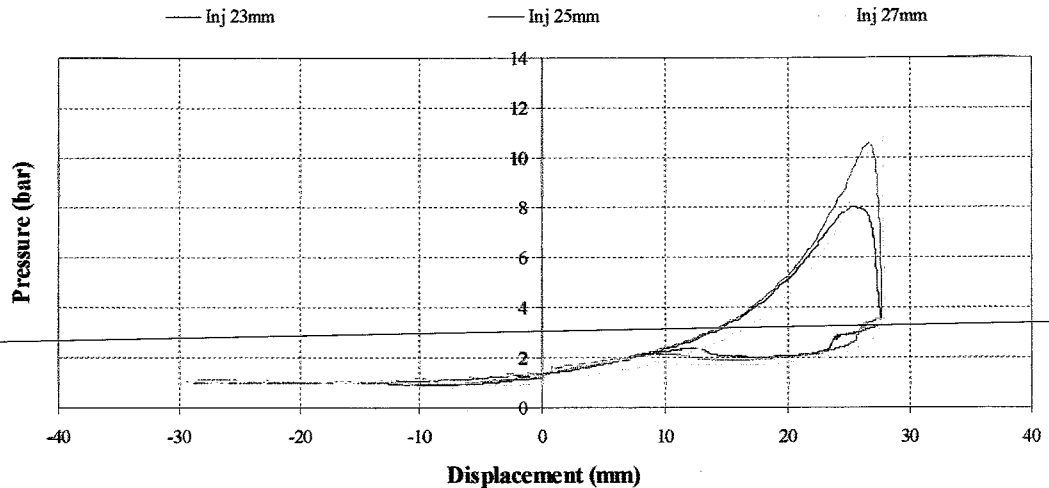Figure 4.36: PV diagram for constant 1.6 equivalence ratio and vary injection

Figure 4.36 above shows PV for constant 1.6 equivalence ratio. Comparing the 3 graphs, it can be seen that the peak pressure for 27mm injection timing is the highest at 10 bar and decreasing for 25mm and 23mm injection respectively. While 27mm injection having the highest peak pressure, the highest IMEP is produced by 23mm

injection. This is true since the area of the PV graph for 23mm injection is larger compared to the other 2 graphs. This also is visible through the 'crossing point' which divides positive work from negative work. Graph for 25 mm and 27 mm have earlier crossing point while 23 mm is later than the other two which indicates more work is being produced by 23mm injection timing.

4.4.5 Combustion with 84 V
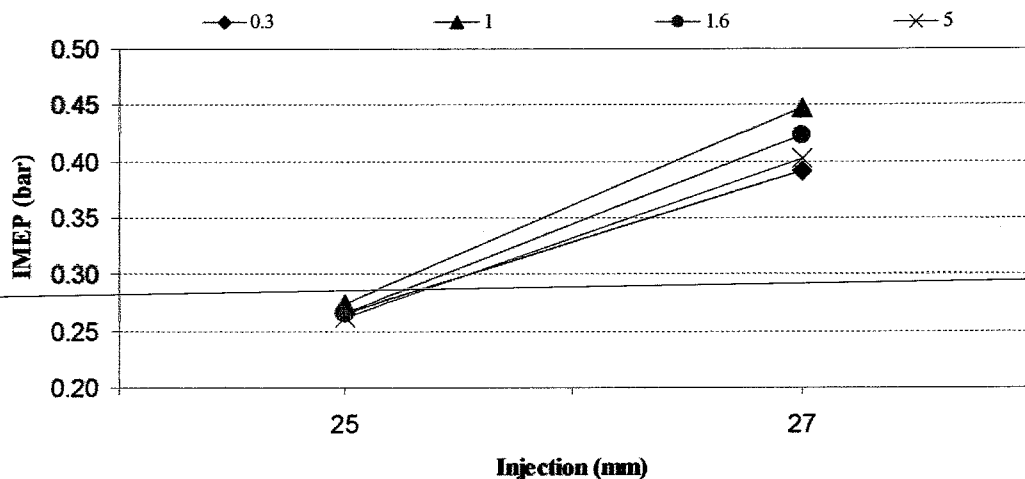
Figure 4.37: Overall IMEP with 84 V

Figure 4.37 above shows LG performance at 84 V. For both 25mm and 27 mm is using a different ignition point. The same engine parameters setting used on 25mm injection is not suitable for 27mm and vice versa. This is mostly due to the control system when running at 84V. At 84V, piston speed increases and control lagging is witnessed when injection and spark is delayed from what is set to be. Due to this, controlling LG at 84V is very much complicated.
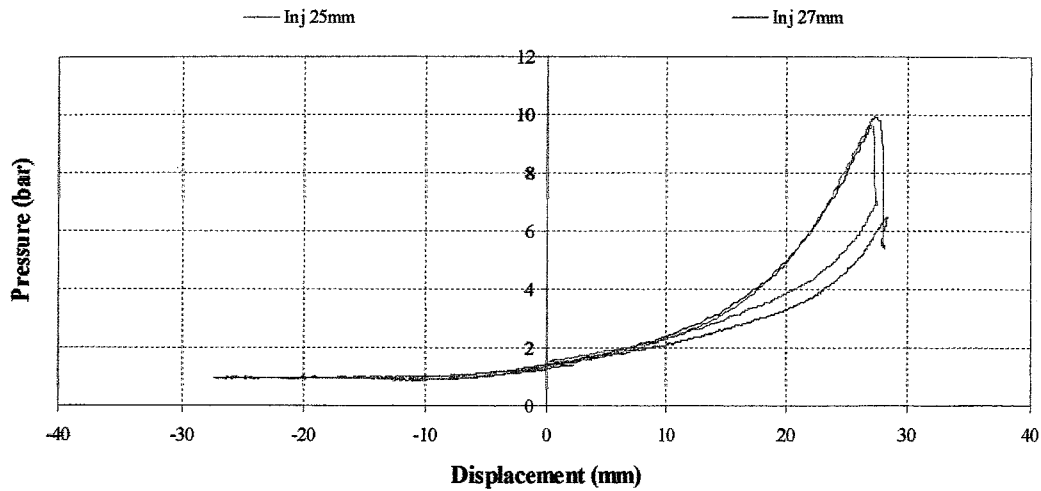
Figure 4.38: PV diagram for constant fuel of 1 equivalence ratio and vary injection

timing

Figure 4.38 shows a comparison between different injection timing. As previously described, the ignition point is different for 25mm and 27mm. A p-V curve for 27mm injection shows a little distortion at the 28mm (TDC). The reason behind this is due to delayed operations of ignition and injection which required complicated control strategy to control LG at 84 V and it is being described below.

4.4.6 Control System Lagging

Data in figure 4.39 display a close up version from a PV diagram comparing 36 V and 84 V combustion process. Both is set at 23mm injection and 1 equivalence ratio. As can be seen, the start of injection for both is delayed from 23mm.
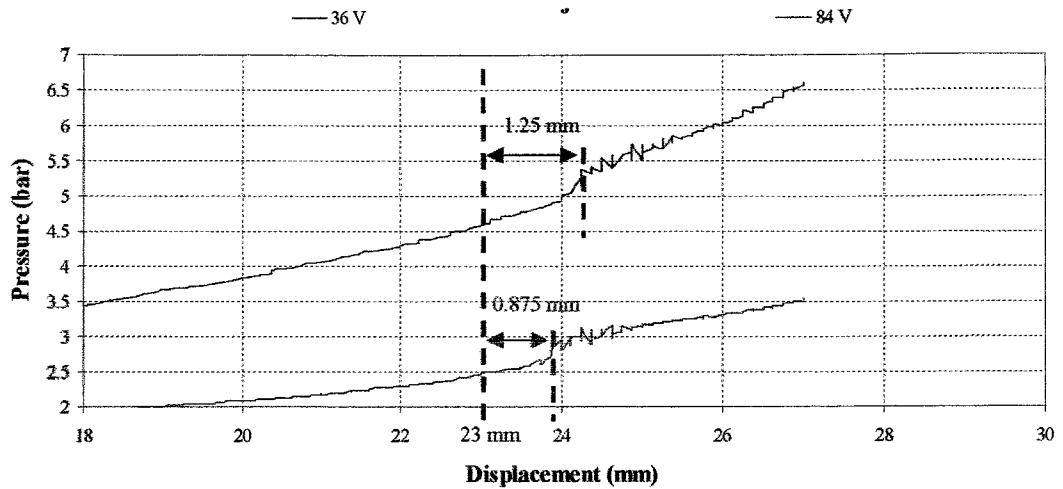
Figure 4.39: Effect of battery capacity on injection delay with constant 23mm and 1 equivalence ratio
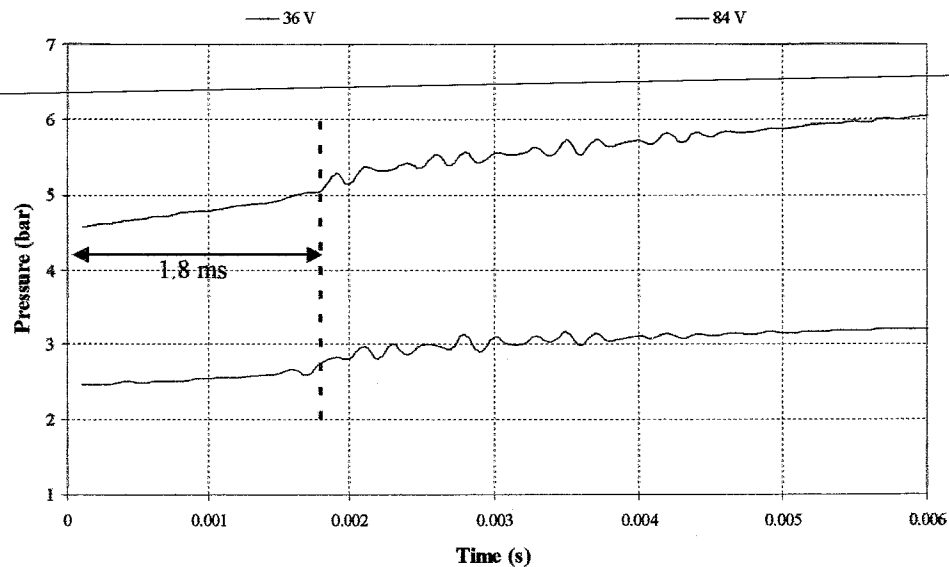
Figure 4.40: Effect of battery capacity on injection delay with constant 23mm and 1 equivalence ratio.

A detailed analysis is done in figure 4.40 and it is found out that the time required from output signal to injecting fuel is 1.8ms. From that 1.8ms, it will affect the accuracy of injection at different piston speeds. As previously explained, higher battery capacity will increase piston speed. For 36 V, start of injection is at 23.875mm (delayed by 0.875mm) and 24.25mm (delayed by 1.25mm) for 84 V. Injection accuracy for 84 V is offset by 5.4 % which causes engine instability and difficulty to control.

4.5 Combustion Analysis

Combustion occurs when combustible react with oxygen to produce heat. The heat later will expand the gases in a cylinder and push a piston thus generating mechanical output. The combining of oxygen and the fuel to generate heat is an intricate process, requiring the exact mixing turbulence and time for the reactants to come in contact and mix appropriately.

Combustion analysis is part of a process intended to improve many factors and one of it is the performance. By looking at several analysis such as the IMEP, mass fraction burn, rate of heat release and thermal efficiency, LG behaviour can be studied to see the what parameters that will affect the performance.

4.5.1 Overall Indicated Mean Effective Pressure (IMEP)

IMEP is a useful relative measurement on engine performance, hence an overall engine performance was tested from 36V up to 84V and the data was plotted in figure 4.41.
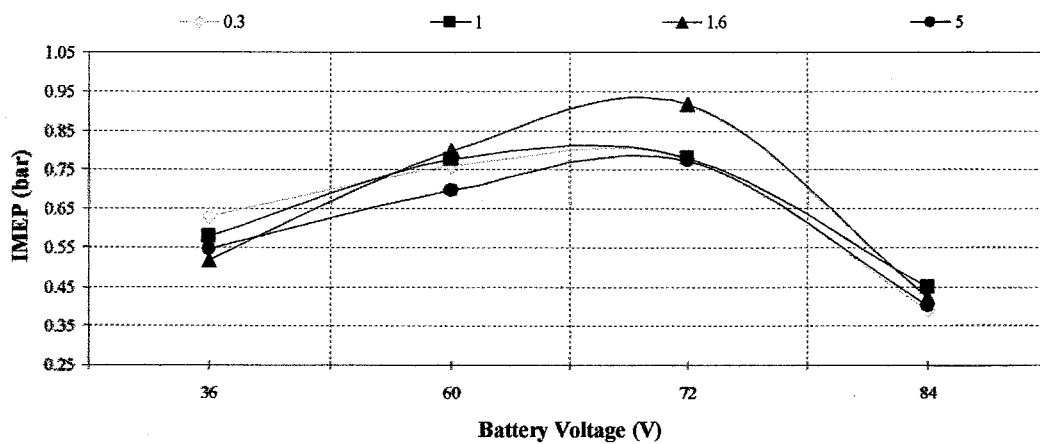

Figure 4.41: Overall IMEP for LG

From figure 4.41, IMEP increase gradually from 36 V to 72 V and drop at 84 V. Data which represent 72 V scores the highest IMEP which is at 0.92 bar with equivalence ratio of 1.6. For the first 3 sets of data (36 V, 60 V and 72 V), the IMEP performance is increasing linearly and decrease at 84 V. As previously discussed,

when operating at higher battery voltage (84 V), complicated control system is required to be able to implement precise control strategy. Further studies will be concentrated on constant 60 V and constant 1.6 equivalence ratio respectively. Studies will include mass fraction burn, rate of heat release and thermal efficiency, and will look how these 3 characteristic effects overall engine performance, IMEP.

4.5.2 Mass Fraction Burned and Rate of Heat Release

The energy from an internal combustion engine derives from the heat released during the combustion of the air fuel mixture. The process of converting chemical energy from a fuel is a complex phenomenon that takes place is transient thermodynamic condition. Evaluation of these processes is the key to engine optimization and effective control.

Mass fraction burned (MFB) is a method which is commonly used to determine the burn rate analysis. It is a standard quantity with a scale of 0 to 1 which describes the chemical process of energy release. It is a ratio of the cumulative heat release to the total heat release.
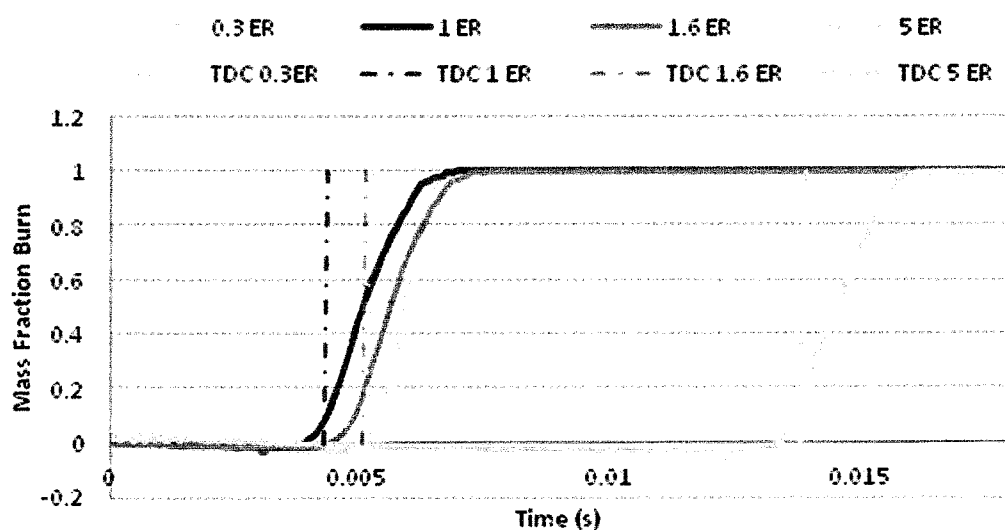
4.5.2.1 Constant 60 V

Figure 4.42: Mass Fraction Burn with Constant 60 V

From figure 4.42, 4 types of data are plotted to look at the effect towards the burning process by varying the equivalence ratio while motoring at a constant 60 V. With this method, the behaviour of the performance will relate to combustion performance. Equivalence ratio is varied from 0.3 to 5 (lean to rich). At 0 second, it represents the start of ignition point which is constant for all 4 sets of data. When comparing between 0.3, 1 and 1.6 equivalence ratio, these 3 curves shows almost similar trend but for 0.3, it shows a steeper curve. This indicates it is going through a rapid burning process which can be confirm by analyzing rate of heat release in figure 4.43 below. The curve that represents 5.0 equivalence ratio displays the longest ignition lag from spark to combust due to difficulty to ignite in too rich air fuel mixture which is noted by Razali [16]. If it was to analyse from the TDC point of view, it does not show any combustion lag but due to free piston behaviour, the TDC point is dependent on several factors and one of it is because of combustion pressure. For all the cases above, flames start to build up before TDC point. Stoichiometric mixture which is at 1 equivalence ratio shows the least ignition lag compared to all the other 3 graphs. IMEP for 1.6 equivalence ratio records slightly higher than others due to more percentage of fuel was burn before TDC.
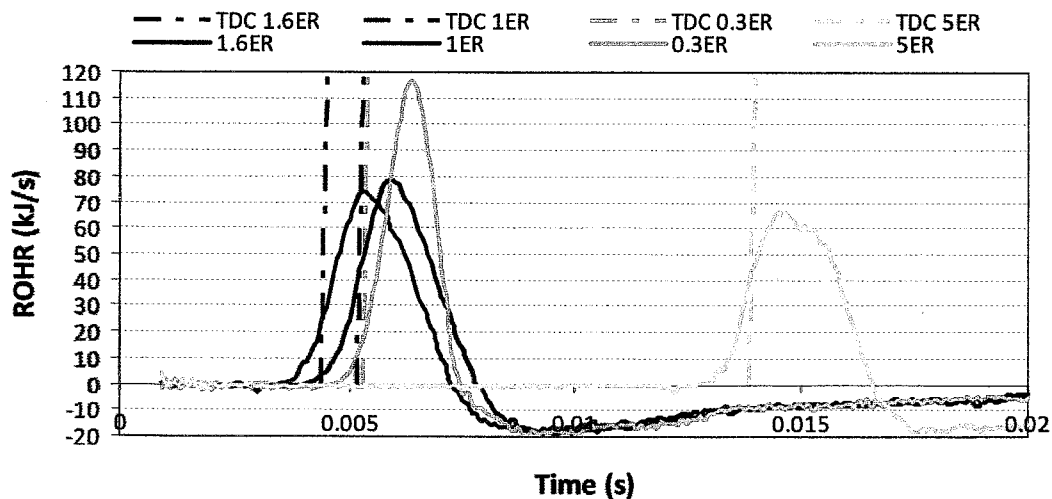

Figure 4.43: Rate of heat release with constant 60 V

Figure 4.43 shows the 0.3 equivalence ratio having the highest heat release value at 115 kJ/s with fastest burning rate. Due to the fast burning rate, steeper curve was produced on mass fraction burn graph. Combustion duration for 1.6 and 1.0 equivalence ratio shows almost similar trend and duration. Both of these experiments

produced almost the same value of IMEP. Combustion for 1.6 equivalence ratio produce slightly higher IMEP, 0.8 bar compared to 0.78 bar for 1.0 equivalence ratio. This is due to slightly higher heat release value which is at 79 kJ/s for 1.6 equivalence ratio in contrast to 74 kJ/s for 1.0 equivalence ratio.

4.5.2.2 Constant 1.6 Equivalence Ratio
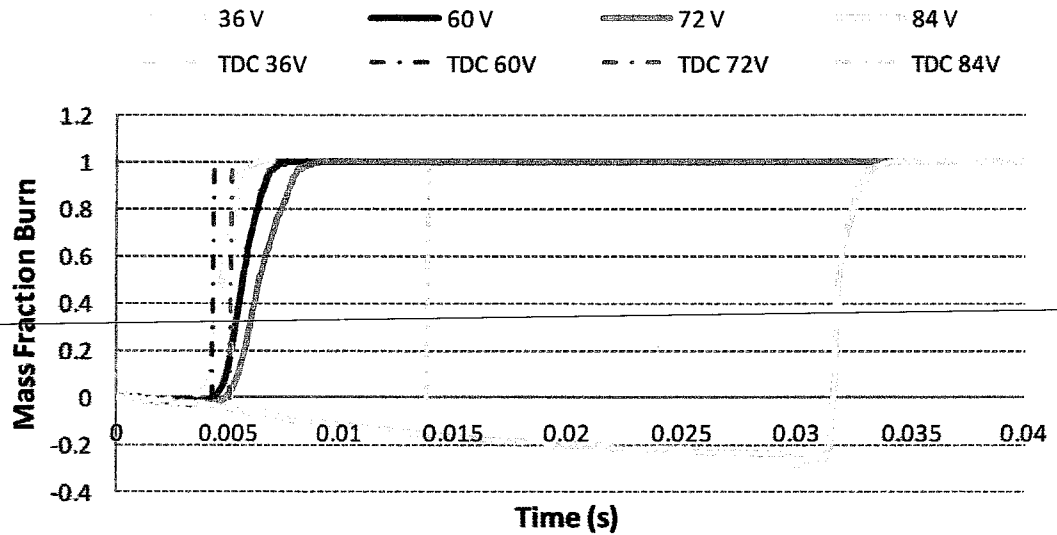
Figure 4.44: Mass fraction burn with constant 1.6 equivalence ratio

Figure 4.44 compares the combustion characteristics based on constant 1.6 equivalence ratio while varying battery capacity. Battery capacity is varied from 36 V up to 84 V. With this approach, any kind of behaviour would relate to factors such as the piston speed and control system capabilities. At 0 second mark the time for start of ignition. From analysing the trend, one could see that the battery capacity relates directly to the ignition lag, 36 V data shows the least ignition lag compared to 84 V which shows the most obvious lag. It can also be seen that it travels to -0.2 before going to 1. This is due to volume expansion which occurred after TDC, before actual ignition takes place. This phenomenon is caused by the lagging in the control system when running at higher battery capacity which was discussed previously. Hence, IMEP for 84 V is the lowest among other sets of data which is at 0.42 bar compared to the highest IMEP 0.92 bar for 72 V.
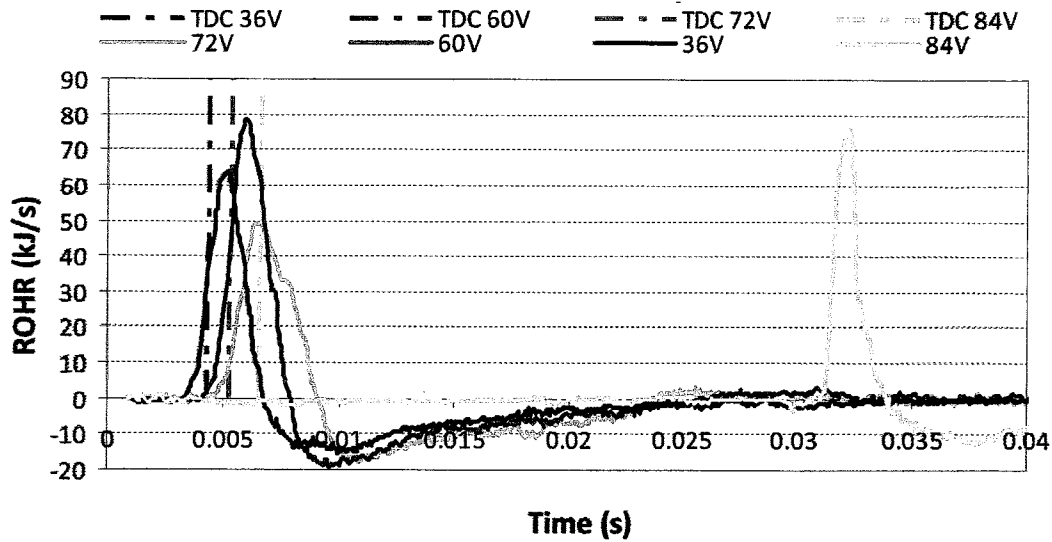
Figure 4.45: Rate of heat release for constant 1.6 equivalence ratio

Rate of heat release is plotted in figure 4.45 to analyze on the effect of battery capacity towards combustion process. It is obvious that 84 V have the longest ignition lag due to control system lag as mention previously. In the same figure above, even thou the highest peak at 79 kJ/s is recorded by 60 V curve, it did not manage to produce the highest IMEP. Looking at 72 V data, it have the lowest heat release value 50 kJ/s but having the longest combustion duration for about 4.7 ms compared to 60 V, 3.7ms. Due to this reason, it managed to produce higher IMEP 0.92 bar compared to 60 V, 0.8 bar.

4.5.3 Thermal Efficiency

Thermal efficiency measures the engine thermal performance base on a simple Wout over Qin equation. It is the ratio of useful output energy (IMEP) over input energy (fuel flow rate).
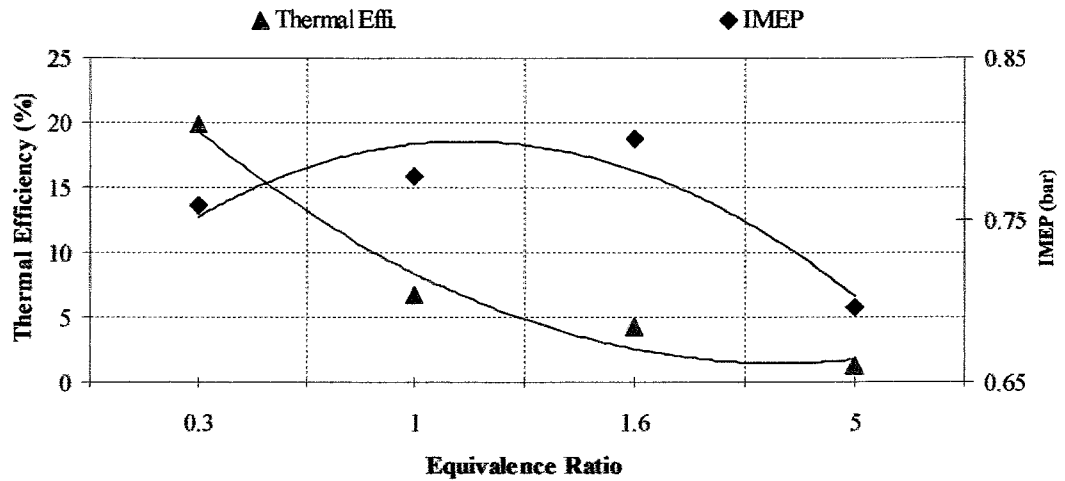
Figure 4.46: Thermal efficiency for constant 60 V

In figure 4.46, thermal efficiency is plotted together with the IMEP to compare the engine performance. Theoretically, thermal efficiency relates inverse to the mass flow rate of fuel. The higher the mass flow rate, the lower the thermal efficiency provided that the workout is not significantly affected by the amount of fuel. That phenomenon can be seen in figure 4.46 where by 0.3 ER produce higher thermal efficiency at 19% and decreases to 3% when equivalence ratio/fuel is increasing. Combustion with 0.3 equivalence ratio is the best setting since the IMEP and thermal efficiency does not have a big difference while still producing reasonable IMEP in this case. While for 1.6 equivalence ratio, it produces highest IMEP at 0.92 bar but having low thermal efficiency at 4%.

4.5.3.2 Constant 1.6 Equivalence Ratio
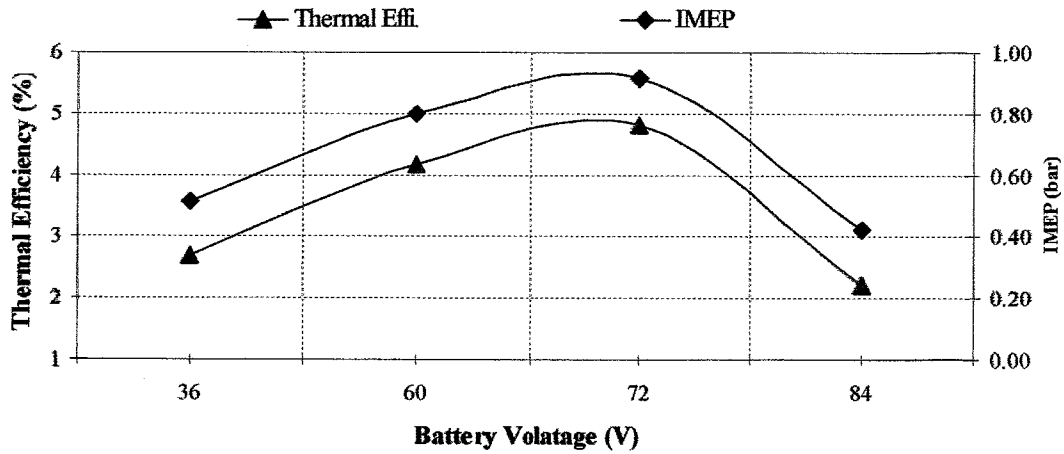
Figure 4.47: Thermal efficiency with constant 1.6 equivalence ratio

Figure 4.47 shows the thermal efficiency with constant 1.6 equivalence ratio and varies battery capacity. By increasing the battery capacity, one could see that the thermal efficiency increases to a point and starts to drop. It shows the similar trend as the IMEP. As explained previously, the reason why the IMEP is low at 84 V is due to control system lagging which have affected the thermal efficiency as well. From 36 V to 72 V and with a constant equivalence ratio, it can be said that the thermal efficiency increase with increasing battery capacity. It is predicted that with higher battery capacity (provided that control system could support high speed operations), the thermal efficiency will increase.

CHAPTER 5

CONCLUSION AND FUTURE WORKS

This chapter will conclude the overall findings and the future recommendation works of this project. The background of the prototype, together with literature review, project methodology and finally the discussion of the experimental results are presented in the previous chapters. After analyzing the experimental results, the conclusions are drawn and stated in this chapter together with future recommendation works.

5.1 Conclusion

A large number of experimental works are done and later the performances and behaviours of the prototype were analyzed. Finally, conclusions are formed based on the analyzed data and it is as listed below:

a) IRFP4110PBF MOSFETs are more stable and reliable inverter driver to motor FPLG compared to SKiiP 342 GB120-3DUL IGBT.

b) Late injection at 27mm produces better efficiency thus producing higher IMEP with a condition that the air and fuel mixture have optimum time to mix.

c) Equivalence ratio of 1.0 and 1.6 produces the best IMEP values throughout all experimental works.

d) Air and Hydrogen fuel requires 12ms to achieve optimum mixing and it is crucial to attain good combustion pressure and IMEP.

e) Motoring with combustion using higher battery capacity from 36V to 72V increases IMEP but the performance drop at 84V due to engine instability.

f) Crossing point in p-V curve can be used as an approximation approach to differentiate the positive and negative work of the prototype.

g) Peak combustion pressure does not necessarily produce higher IMEP value. This phenomenon can be referred to Figure 4.34 and 4.36.

h) Highest IMEP is at 0.92 bar with equivalence ratio 1.6 and battery capacity 72V.

i) At 84V battery capacity, spark and injection delay is offset by 5.4% which contributes to engine instability and low IMEP.

j) In MFB and ROHR analysis, TDC is dependent on combustion timing and combustion delay. The faster the combustion is will caused earlier TDC and slower combustion will cause further TDC.

k) Equivalence ratio 0.3 produces highest thermal efficiency at 19%.

5.2 Main Contribution

The main contribution of this thesis is that by motoring with higher battery capacity, it will increase compression pressure and cycles per minute (cpm) but will reduce stroke length thus lower effective compression ratio as shown in Figure 4.26. The maximum piston velocity achieved is at 2m/s when motoring at 72V. This phenomenon is due to less air leakage through piston ring during high speed motoring.

5.3 Future Works

Several improvements of the current prototype are identified and can be the future works as listed below:

a) FPLG predictive motion control which could predict the end position of the piston and take necessary action such as controlling the switching, injection and ignition parameters in order to create good combustion to push the piston to the opposite side and maintain idling.

b) The switching programming can be redesign to make sure accurate control of the LG position and to obtain precise TDC point.

c) The processing power of the control system need to be boosted up in order to cater for high speed operations of FPLG without causing the injection and ignition delay.

d) State of Charge (SOC) of the battery bank needs to be the input to the data acquisition system in order to monitor precise voltage drop during motoring and voltage increase during generation.

e) A different type of battery bank which supplies higher voltage with lower current ratings can be used to achieve higher compression ratio but lower motoring speed.

f) Since Hydrogen is a fast burning gas and CNG is a slow burning gas, a combination of these gases is a suitable fuel for FPLG in order to produce higher IMEP by prolonging the flame propagation up until the exhaust port.

g) Petrol injectors can be installed on the air intake line in order to implement experiments with gasoline.

Finally, with accurate control, higher compression ratio and higher IMEP, idling of FPLG can be achieved. Once this is done, more focus can be concentrated on power generation mode.

REFERENCES

[1]   R. Gorham, "Air pollution from ground transportation: An assessment of causes, strategies and tactics, and proposed actions for the international community," Division for Sustainable Development Department of Economic and Social Affairs, United Nations2002.

[2]   IEO, "The international energy outlook 2010 (IEO2010)," July 27 2010.

[3]   L. Guzzella and C. H. Onder, *Introduction to modeling and control of internal combustion engine systems*. Verlag Berlin Heidelberg: Springer, 2010.

[4]   R. Mikalsen and A. P. Roskilly, "A review of free-piston engine history and applications," *Applied Thermal Engineering,* vol. 27, pp. 2339-2352, 2007.

[5]   H. T. Aichlmayr, "Design considerations, modeling and analysis of micro-homogenous charge compression ignition combustion free-piston engine," PhD thesis, University of Minnesota, Minnesota, 2002.

[6]   G. Flynn, "Some principles and applications of the free-piston engine," *General Motors Engineering Journals,* pp. 22-27, 1958.

[7]   A. L. London and A. K. Oppenheim, "The free-piston engine development-present status and design aspects," *Trans. ASME,* vol. 74, pp. 1349-1361, 1952.

[8]   P. Van Blarigan, "Homogeneous charge compression ignition with a free piston: A new approach to ideal Otto cycle performance," in *Proceedings of the 1999 U.S. DOE Hydrogen Program Review*, 1999.

[9]   J. Hansson and M. Leksell, "Performance of a series hybrid electric ehicle with a free-piston energy converter," in *Vehicle Power and Propulsion Conference, 2006. VPPC '06. IEEE*, Windsor, 2006, pp. 1-6.

[10]   S. Nandkumar, "Two-stroke linear engine," M.Sc. thesis, Department of Mechanical and Aerospace Engineering, West Virginia University, Morgantown, West Virginia, 1998

[11]   Saiful Azrin, "Modeling, Simulation and Implementation of Rectangular Commutation for Starting of Free-Piston Linear Generator", MSc Thesis, Universiti Teknologi PETRONAS, 2007.

[12]   P.Němeček, M.Šindelka, and O.Vysoký, "Modeling and Control of Linear Combustion Engine," IFAC Symposium on Advances in Automotive Control, 2003.

[13]   Němeček, P., and Vysoký, O., "Control of Two-Stroke Free-Piston Generator," Proceedings of the 6th Asian Control Conference, VOL.1, 2006.

[14]   Hansson, J., Leksell, M., Carlsson, F., and Sadarangani., C., 2005, "Operational Strategies for a Free Piston Energy Converter.", 2005.

[15]   Abdulwehab Adem Ibrahim, "An Experimental and Analytical Investigation of Free-Piston Linear Generator Engine", PhD Thesis, Universiti Teknologi PETRONAS, 2012.

[16]   M. Razali, "Combustion process in a Two-Storoke, H2-DI Linear Generator Free-Piston Engine during starting", MSc Thesis, Universiti Teknologi PETRONAS, 2008.

[17]   Farmer, H. O., "Free-Piston Compressor-Engines," Proceedings of the Institution of Mechanical Engineers, 156, 1947.

[18]   S. A. Zulkifli, et al., "Starting of a free-piston linear engine-generator by mechanical resonance and rectangular current commutation," in IEEE Vehicle Power and Propulsion Conference (VPPC 2008), Harbin, China, 2008, pp. 1-7.

[19]   Brunt, M. F. J., and Emtage, A. L., "Evaluation of IMEP Routines and Analysis Errors," Society of Automotive Engineers, 1996.

[20] H. T. Aichlmayr, *et al.*, "Miniature free-piston homogeneous charge compression ignition engine-compressor concept-Part I: Performance estimation and design considerations unique to small dimensions," *Chemical Engineering Science,* vol. 57, pp. 4161-4171, 2002.

[21] H. T. Aichlmayr, *et al.*, "Miniature free-piston homogeneous charge compression ignition engine-compressor concept-Part II: Modeling HCCI combustion in small scales with detailed homogeneous gas phase chemical kinetics," *Chemical Engineering Science,* vol. 57, pp. 4173-4186, 2002.

[22] J. J. McMullen and W. G. Payne, "Performance of free-piston gas generators," *Trans. ASME,* vol. 76, pp. 1-13, 1954.

[23] H. O. Farmer, "Free-piston compressor-engines," *Proceedings of the Institution of Mechanical Engineers,* vol. 156, pp. 253-271, 1947.

[24] E. Sher, "Design considerations of an airborne free piston compressor," *Proceedings of the Institution of Mechanical Engineers,* vol. 201, pp. 177-184, 1987.

[25] H. O. Farmer, "Free-piston compressor-engines," *Proceedings of the Institution of Mechanical Engineers,* vol. 156, pp. 253-271, 1947.

[26] E. Sher, "Design considerations of an airborne free piston compressor," *Proceedings of the Institution of Mechanical Engineers,* vol. 201, pp. 177-184, 1987.

[27] S. Tikkanen, *et al.*, "First cycles of the dual hydraulic free piston engine," *SAE Paper,* vol. 2000-01-2546, 2000.

[28] G. E. M. Vael and P. A. J. Achten, "The Innas fork lift truck, working under constant pressure," in *Internationales Fluidtechnisches Kolloquim,* Aachen, Germany, 1998.

[29] P. A. J. Achten, "The development of the Innas free piston engine: The art of choosing the right moment," University of Linköping, Sweden1995.

[30]   A. K. Oppenheim and A. L. London, "Design analysis of free-piston engines," *Automotive Industries,* pp. 46-50, 76, 1950.

[31]   F. A. I. Muntz and R. Huber, "The free-piston gas-generator turbine as a power plant for ship propulsion," *Institute of Marine Engineers Transactions,* vol. 66, pp. 946-952, 1954.

[32]   P. A. J. Achten, "A review of free piston engine concepts," *SAE Paper,* vol. 941776, 1994.

[33]   C. Tóth-Nagy and N. N. Clark, "The linear engine in 2004," *SAE paper* vol. 2005-01-2140, 2005

[34]   P. A. J. Achten, *et al.,* "Horsepower with brains: The design of the chiron free piston engine," *SAE Paper,* vol. 2000-01-2545, 2000.

[35]   A. J. Ehrat, "Free-piston gas-turbine prime movers: A review of basic principles," *ASME Paper No. 54-A-67,* vol. 77, pp. 212-216, 1955

[36]   C. W. Herbert, "Free piston-gas turbine machinery," in *Turbine main engines,* ed: Pergamon Press, 1965, pp. 161-257

[37]   H. G. Spier, "Supercharging in the free-piston cycle," *SAE Transactions,* vol. 67, pp. 281-288, 1958.

[38]   T. A. Johansen, *et al.,* "Free-piston diesel engine timing and control towards electronic cam-and crankshaft," *IEEE Trans. Control Systems Technology,* vol. 10, pp. 177–190, 2002.

[39]   R. Huber, "Operational stability of free piston gasifiers," *Journal of the American Society for Naval Engineers,* vol. 62, pp. 257-272, 1950

[40]   W. R. Cawthorne, "Optimization of a brushless permanent magnet linear alternator for use with a linear internal combustion engine," PhD thesis, Department of Computer Science and Electrical Engineering, West Virginia University, Morgantown, West Virginia, 1999

[41]   K. D. Annen, *et al.*, "Miniature internal combustion engine (MICE) for portable electric power," presented at the Proc. of the 23rd Army Science Conference, Florida, 2002

[42]   Rasswieler, G.M., and Withrow, L.,"Motion Pictures of Engine Flames Correlated with Pressure Cards", Society of Automotive Engineers Transactions, p33, 1938.

[43]   D. Houdyschell, "A diesel two-stroke linear engine," M.Sc. thesis, Department of Mechanical and Aerospace Engineering, West Virginia University, Morgantown, West Virginia, 2000.

[44]   H. Arof, *et al.*, "On the issues of starting and cogging force reduction of a tubular permanent magnet linear generator " presented at the Proc. of Australasian Universities Power Engineering Conference (AUPEC 2004), Brisbane, Australia, 2004.

[45]   A. Braun, "The potential in the free-piston engine principle," *The Engineering Journal,* vol. 43, pp. 57-61, 1960

[46]   J. B. Heywood, *Internal combustion engine fundamentals*: McGraw-Hill, 1988.

[47]   C. Tóth-Nagy, "Linear engine development for series hybrid electric vehicles," PhD, Department of Mechanical and Aerospace Engineering, West Virginia University, Morgantown, West Virginia, 2004

[48]   C. M. Atkinson, *et al.*, "Numerical simulation of a two-stroke liner engine-alternator combination," *SAE Paper,* vol. 1999-01-0921, 1999

[49]   E. Shoukry, *et al.*, "Numerical simulation for parametric study of a two-stroke direct injection linear engine," *SAE Paper,* 2002

[50]   E. F. Shoukry, "Numerical simulation for parametric study of a two-stroke compression ignition direct injection linear engine," PhD thesis, Department

of Mechanical and Aerospace Engineering, West Virginia University, Morgantown, West Virginia, 2003.

[51] N. N. Clark, *et al.*, "Fundamental analysis of a linear two-cylinder internal combustion engine," *SAE Paper,* vol. 982692, 1998

[52] N. Clark, *et al.*, "Operation of a small bore two-stroke linear engine," in *ASME 98-ICE-120*, 1998, pp. 33-42.

[53] F. Stelzer, "Two-stroke internal combustion engine," 1983.

[54] S. S. Goldsborough and P. Van Blarigan, "A numerical study of a free piston IC engine operating on homogeneous charge compression ignition combustion," *SAE Paper,* vol. 1999-01-0619, 1999

[55] P. Van Blarigan, "Advanced hydrogen fueled internal combustion engines," *Energy & Fuels,* vol. 12, pp. 72-77, 1998.

[56] P. Van Blarigan, *et al.*, "Homogeneous charge compression ignition with a free piston: A new approach to ideal Otto cycle performance," *SAE Paper,* vol. 982484, 1998.

[57] Mendera, K. Z. Spyra, A., and Smereka, M., "Mass Fraction Burned Analysis", Journal of KONES Internal Combustion Engine, 2002.

[58] Pulkrabek, W. W., Engineering Fundamentals of the Internal Combustion Engine, Prentice-Hall, Inc, 1997.

[59] Stone, R., Introduction to Internal Combustion Engines, Society of Automotive Engineers, Inc., Warrendale, Pa, 1999.

[60] Heywood, J. B., and Sher, E., The Two-Stroke Cycle Engine: Its Development, Operation, and Design, Society of Automotive Engineers, Inc., Warrendale, PA, USA, 1999.

[61] Blair, G. P., The Basic Design of Two-Stroke Engines, Society of Automotive Engineers, Inc., 1990.

[62]   Tom Denton, 2000, Automobile Electrical and Electronic Systems, Arnold, London

[63]   Challen, B., and Baranescu, R., 1999, Diesel Engine Reference Book, Butterworth-Heinemann, Massachusetts

[64]   C.M White, R.R Steeper, A.E Lutz " The hydrogen-fueled internal combustion engine: a technical review" Combustion Research Facility, Sandia National Laboratories, 2006

[65]   Youngmind Woo, Youngjae Lee, Yonggyun Lee " The performance characteristics of a hydrogen-fuelled free piston internal combustion engine and linear generator system" Automobile Energy and Environment Research, Korea Institute of Energy Research,2009.

[66]   J. Warnatz, U. Maas, and R.W. Dibble, 2006, Combustion, Springer.

[67]   Baumgarten, C., 2006, Mixture Formation in Internal Combustion Engines, Springer-Verlag Berlin Heidelberg New York.

[68]   Mavinahally, N. S., 2004, "An Historical Overview of Stratified Scavenged Two-Stroke Engines – 1901 through 2003," SAE(2004-32-0008).

[69]   Ned Mohan, Tore M. Undeland, William P. Robbins, "Power Electronics" John Wiley & Sons, Inc, 2003

[70]   C. Abbate, G. Busatto, L. Fratelli, F. Iannuzzo, "The High Frequency Behaviour of High Voltage and Current IGBT Modules", University of Cassino, Science Direct, 2006.

[71]   Satoki Takizawa, " A New di/dt Control Gate Drive Circuit for IGBTs to Reduce EMI noise and Swithcing Losses", Fuji Electric Corporate Research and Development Ltd, IEEE, 1998.

[72]   B, Majumdar, "IGBT Gate Drive Circuit with in-built Protection and Immunity to Transcient Fault", Jadavpur University, IEEE, 2000.

[73]   Q.Liu, W.Shen, F. Wang, "On Discussion of Motor Drive Conducted EMI Issues" Virginia Polytechnic Institute and State University, 2002.

[74]   Han-Chang Tsai, Kuo-Chang Wang, "Investigation of EMI-induced noise spectrum in an enhancement-type MOSFET", Cheng-Shiu University, Science Direct, 2008.

[75]   W. P. Hew, *et al.*, "Fabrication and testing of linear electric generator for use with a free-piston engine," in *Pro. of National Power and Energy Conference (PECon 2003)*, Bangi, Malaysia, 2003, pp. 277-282.

[76]   K. M. Nor, *et al.*, "Design of a 5 KW tubular permanent magnet linear generator," in *Proc. 39th International Universities Power Engineering Conference (UPEC 2004)*, University of the West of England (UWE) Bristol, UK, 2004, pp. pp. 528-532.

[77]   H. W. Ping, *et al.*, "Design of a permanent magnet linear generator," in *Proc. of the 1st International Forum on Strategic Technologies (IFOST 2006)*, Ulsan, 2006, pp. 231-234.

[78]   Mendera, K. Z., Spyra, A., and Smereka, M., "Mass Fraction Burned Algorithm Based On the pV Product", Journal of KONES Internal Combstion Engine, 2002.

[79]   A. R. A.Aziz, "Design and development of a prototype free piston linear generator engine," presented at the National R & D Symposium, Tronoh, 2003.

[80]   A. A. Ibrahim, et al.,

PUBLICATIONS

1. Ezrann Zharif Zainal Abidin, Abdulwehab A. Ibrahim, A. Rashid A. Aziz and Saiful A. Zulkifli, Investigation of Starting Behaviour of a Free-Piston Linear Generator, Journal of Applied Sciences 12 (24): 2592-2597, 2012. ISSN 1812-5654

2. Abdulwehab A. Ibrahim, A. Rashid A. Aziz, Ezran Zharif B. Zainal Abidin and Saiful A. Zulkifli, The Operation of Free Piston Linear Generator Engine Using MOSFET and IGBT Drivers, Journal of Applied Sciences, 11(10): 1791-1796, 2011.

3. Abdulwehab A. Ibrahim, Ezrann Zharif b. Zainal Abidin, A. Rashid A. Aziz and Saiful A. Zulkifli, Effect of Injection Timing on the Operation of Hydrogen-Fuelled Free-Piston Linear Generator Engine during Starting, International Journal of Automotive Engineering 4 (2013) 47-53, Society of Automotive Engineers of Japan (JSAE)

4. Abdulwehab A. Ibrahim, Ezran Zharif B Zainal Abidin, A. Rashid A. Aziz and Saiful A. Zulkifli, Motoring of Free-Piston Linear Generator Engine Using MOSFET and IGBT Drivers, Asia Pacific Symposium of Applied Electromagnetics and Mechanics (APSAEM2010), Kuala Lumpur, Malaysia, 28-30th July 2010.

5. Abdulwehab A. Ibrahim, A. Rashid A. Aziz, Saiful A. Zulkifli, and Ezran Zharif B Zainal Abidin, Investigation of Free-Piston Linear Generator Engine, The 2nd International Conference of the Institution of Engineering and Technology (IETBIC 2010), Bandar Seri Begawan, Brunei Darussalam, 21-23th June 2010.

6. Abdulwehab A. Ibrahim, Ezran Zharif B. Zainal Abidin, A. Rashid A. Aziz and Saiful A. Zulkifli, Studying the Operation of Free Piston Linear Generator

Engine Using MOSFET and IGBT Drivers, International Conference on Plant Equipment and Reliability (ICPER 2010), Kuala Lumpur, Malaysia, 15-17th June 2010.

APPENDIX A

EXPERIMENTAL MATRIX

Table A.1: Experimental matrix for 36V

Injection Timing (mm)

Fuel (mg)	17	20	23	25	27
1	Test 1a	Test 1a	Test 1a	Test 1	Test 1
3	Test 2a	Test 2b	Test 2	Test 2b	Test 2
5	Test 3b	Test 3a	Test 3	Test 3	Test 3a
7	Test 4	Test 4	Test 4a	Test 4	Test 4b
9	Test 5	Test 5b	Test 5c	Test 5	Test 5
11	Test 6	Test 6b	Test 6b	Test 6	Test 6c
13	Test 7	Test 7	Test 7a	Test 7c	Test 7a
15	Test 8b	Test 8c	Test 8a	Test 8	Test 8

Table A.2: Experimental matrix for 60V

Injection Timing (mm)

Fuel (mg)	17	20	23	25	27
1	Exp 22	Exp 12	Exp 13	Exp 2	Exp 1
3	Exp 23	Exp 13	Exp 14	Exp 3	Exp 2
5	Exp 24	Exp 14	Exp 15	Exp 5	Exp 3
7	Exp 25	Exp 15	Exp 16	Exp 6	Exp 6
9	Exp 26	Exp 17	Exp 17	Exp 8	Exp 7
11	Exp 27	Exp 18	Exp 18	Exp 9	Exp 9
13	Exp 28	Exp 19	Exp 19	Exp 10	Exp 10
15	Exp 29	Exp 20	Exp 20	Exp 11	Exp 11

Table A.3: Experimental matrix for 72V

Injection Timing (mm)

Fuel (mg)	17	20	23	25	27
1	Exp 26	Exp 34a	Exp 18	Exp 10	Exp 10
3	Exp 27	Exp 35	Exp 19	Exp 11	Exp 11
5	Exp 28	Exp 36	Exp 20	Exp 12	Exp 12
7	Exp 29	Exp 37	Exp 21	Exp 13	Exp 13
9	Exp 30	Exp 38	Exp 22	Exp 14	Exp 14
11	Exp 31	Exp 39	Exp 23	Exp 15	Exp 15
13	Exp 32	Exp 40	Exp 24	Exp 16	Exp 16
15	Exp 33	Exp 41	Exp 25	Exp 17	Exp 17

Table A.4: Experimental matrix for 84V

Injection Timing (mm)

Fuel (mg)	17	20	23	25	27
1	Exp 17	Exp 9	Exp 1	Exp 40	Exp 25
3	Exp 18a	Exp 10	Exp 2	Exp 41	Exp 26
5	Exp 19	Exp 11	Exp 3	Exp 42	Exp 27
7	Exp 20	Exp 12	Exp 4	Exp 43	Exp 28
9	Exp 21	Exp 13	Exp 5	Exp 44	Exp 29
11	Exp 22	Exp 14	Exp 6	Exp 45	Exp 30
13	Exp 23	Exp 15	Exp 7	Exp 46	Exp 31
15	Exp 24	Exp 16	Exp 8	Exp 47	Exp 32

APPENDIX B

RAW EXPERIMENTAL DATA
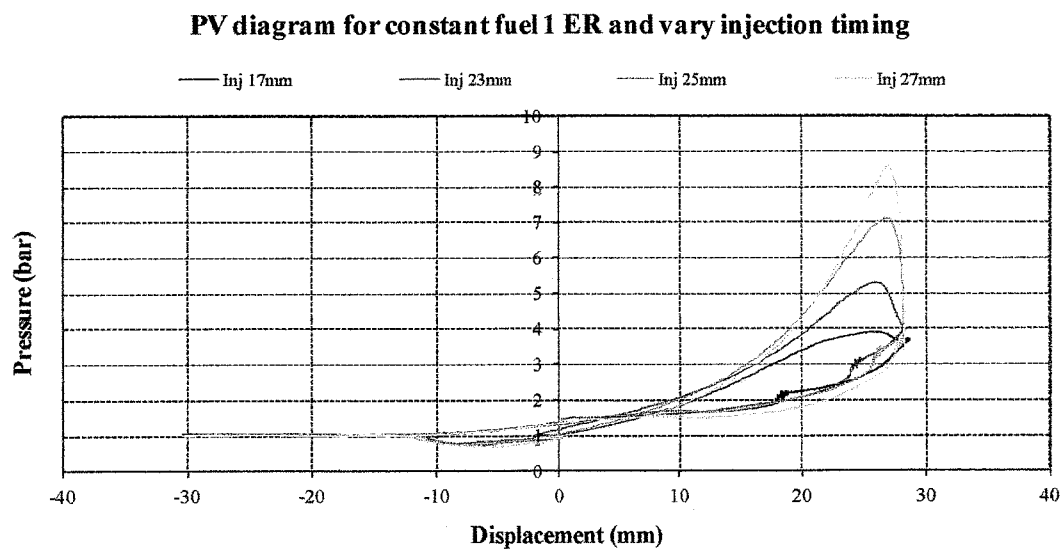
Figure B.2: PV diagram constant 1.0 ER while vary injection timing (36 V)
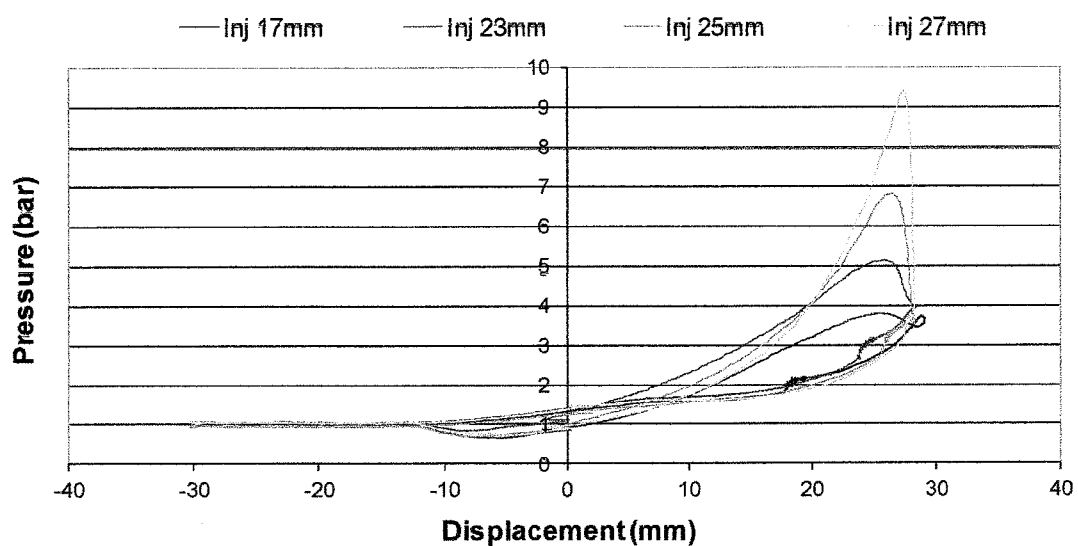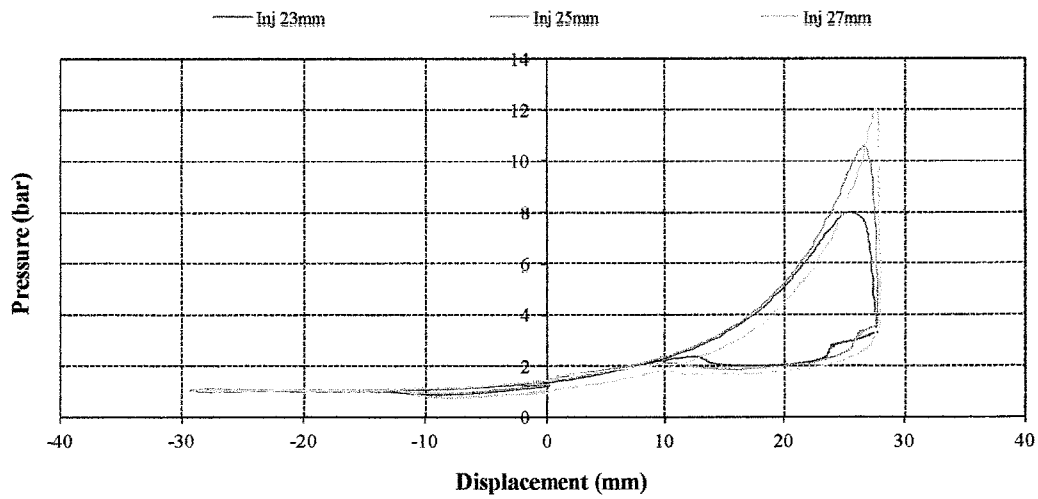

Figure B.2: PV diagram constant 1.6 ER while vary injection timing (36 V)

106
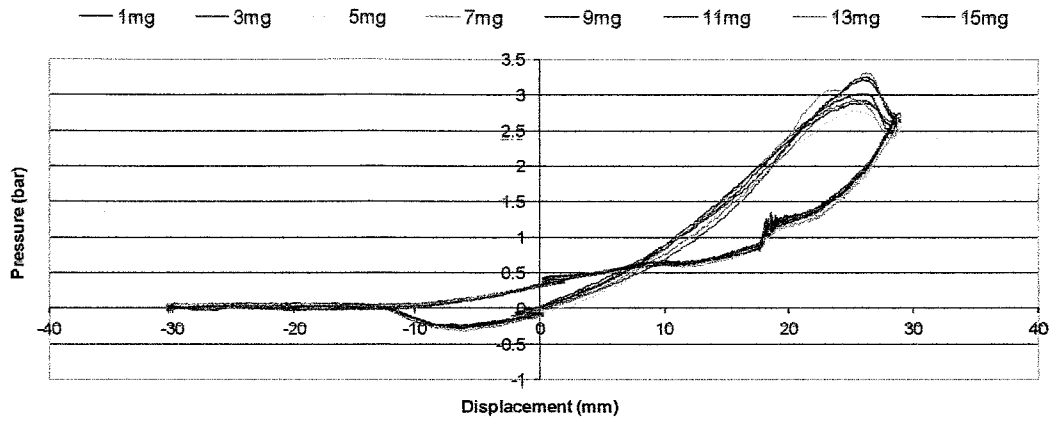
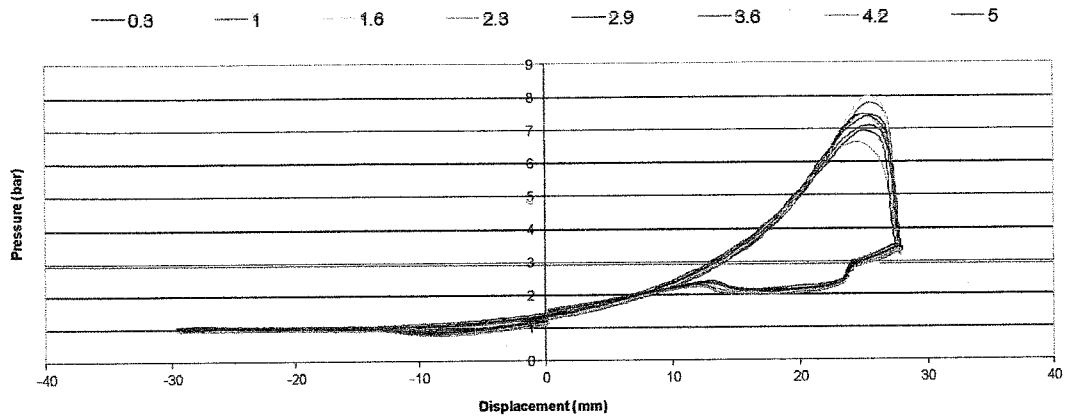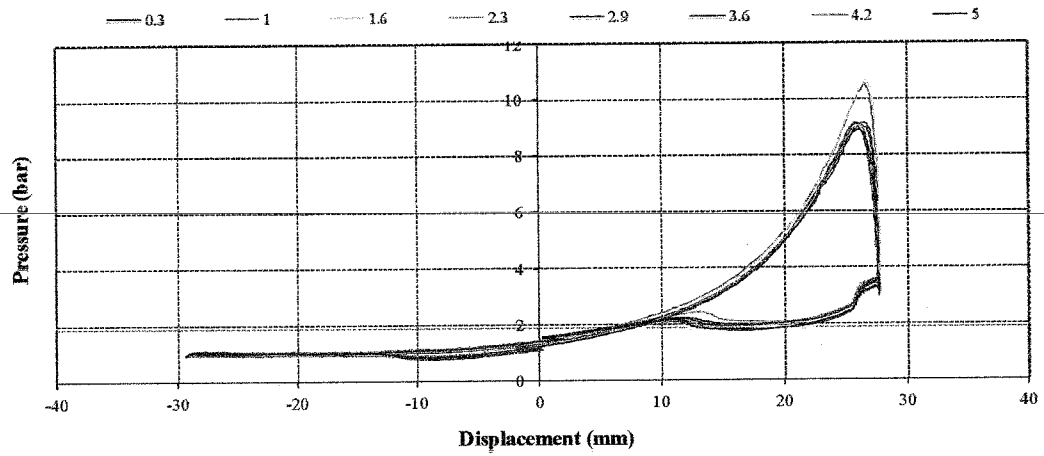Figure B.3: PV diagram constant 17 mm injection while vary equivalence ratio (36 V)
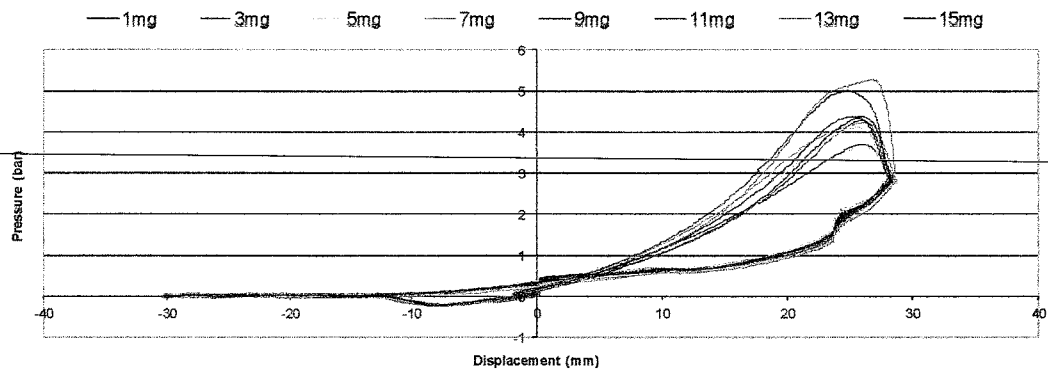
Figure B.4: PV diagram constant 23 mm injection while vary equivalence ratio (36 V)
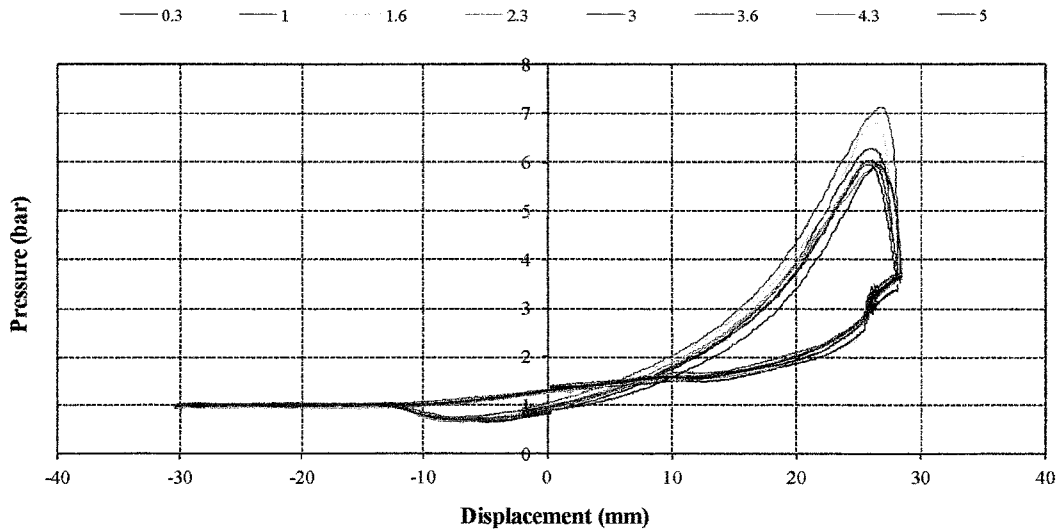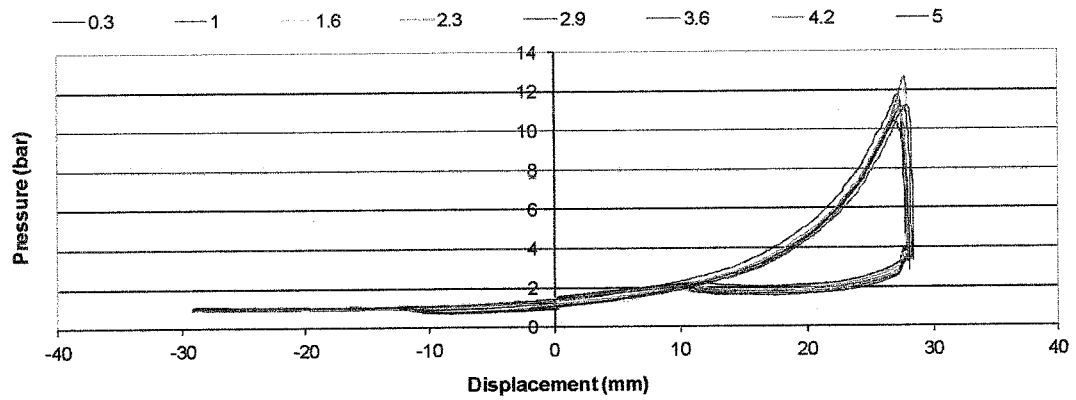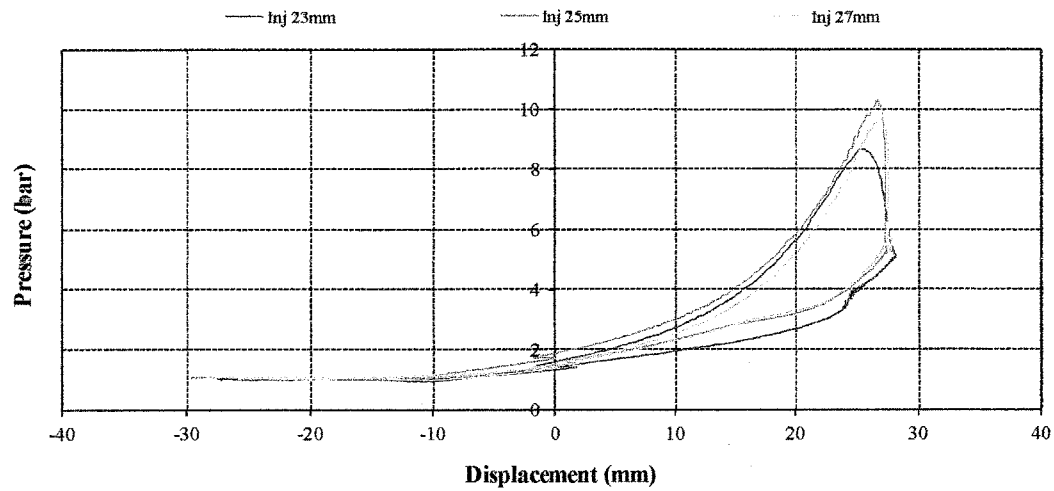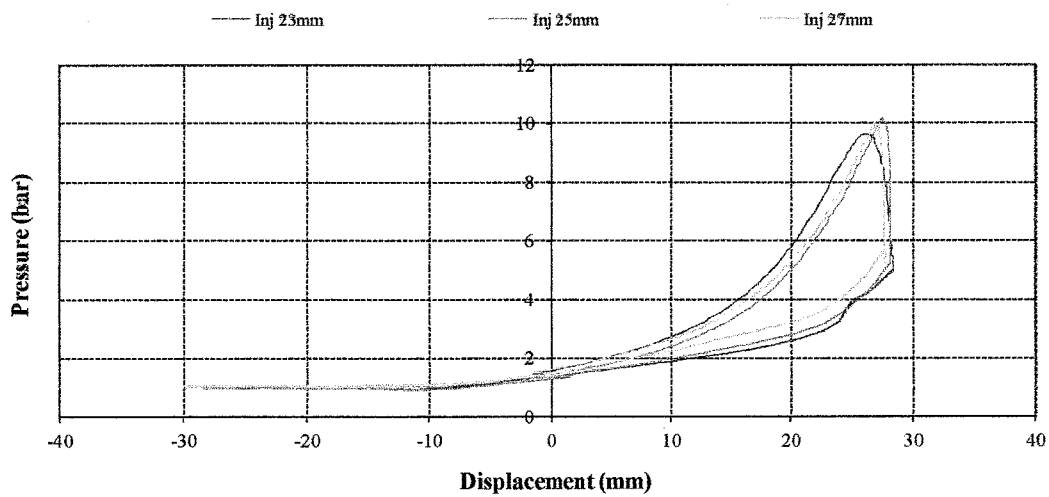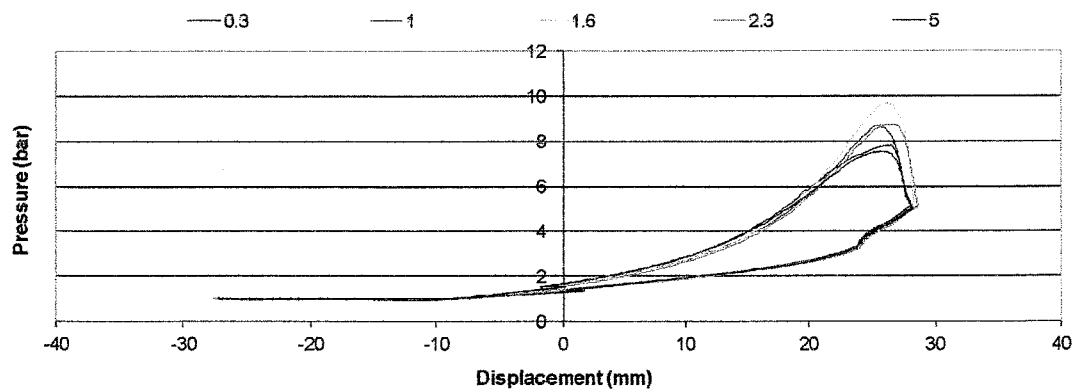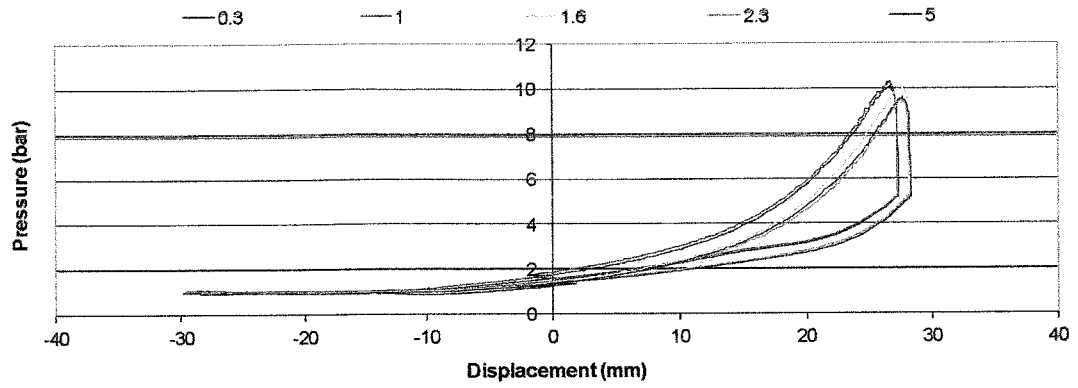

Figure B.5: PV diagram constant 25 mm injection while vary equivalence ratio (36 V)
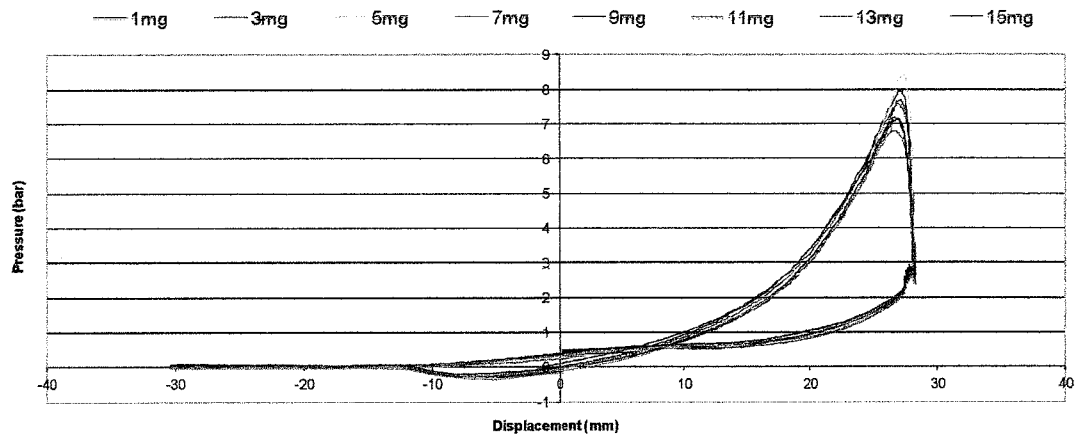
Figure B.5: PV diagram constant 27 mm injection while vary equivalence ratio (36 V)
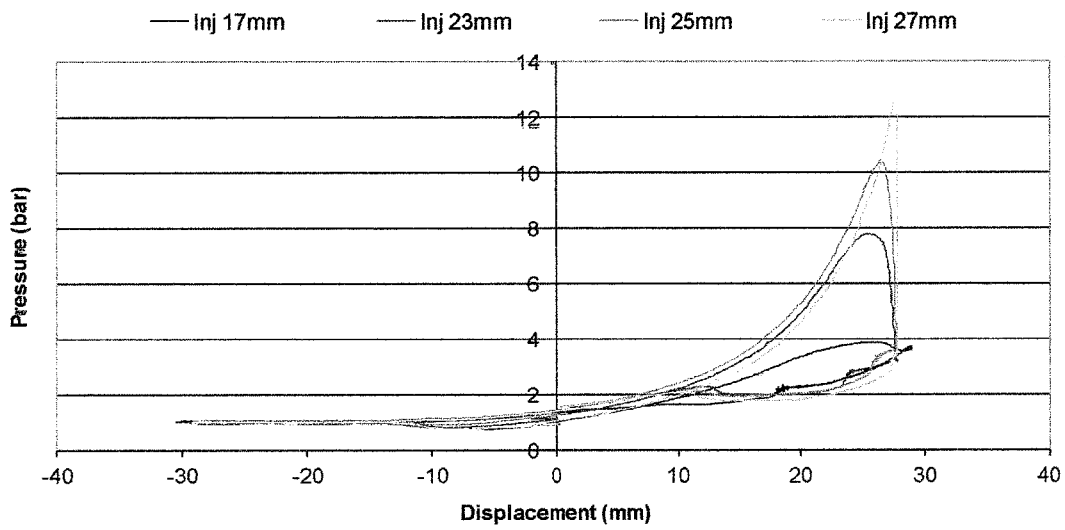
Figure B.6: PV diagram constant 1 ER while vary injection timing (60 V)

Figure B.7: PV diagram constant 1.6 ER while vary injection timing (60 V)

Figure B.8: PV diagram constant 23 mm injection while vary equivalence ratio (60 V)

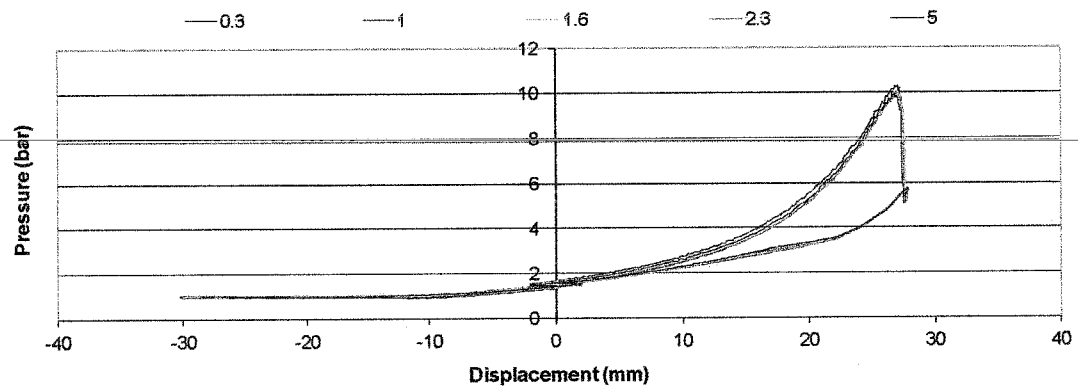Figure B.9: PV diagram constant 25 mm injection while vary equivalence ratio (60 V)

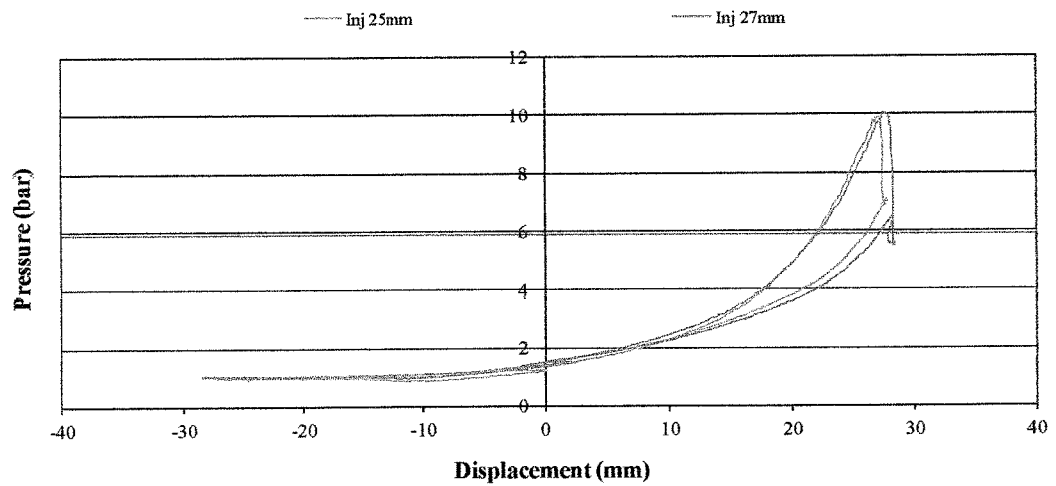Figure B.10: PV diagram constant 27 mm injection while vary equivalence ratio (60 V)

Figure B.11: PV diagram constant 1 ER while vary injection timing (72 V)

Figure B.12: PV diagram constant 1.6 ER while vary injection timing (72 V)

Figure B.13: PV diagram constant 23 mm injection while vary equivalence ratio (72 V)

Figure B.14: PV diagram constant 25 mm injection while vary equivalence ratio (72 V)

Figure B.15: PV diagram constant 27 mm injection while vary equivalence ratio (72 V)

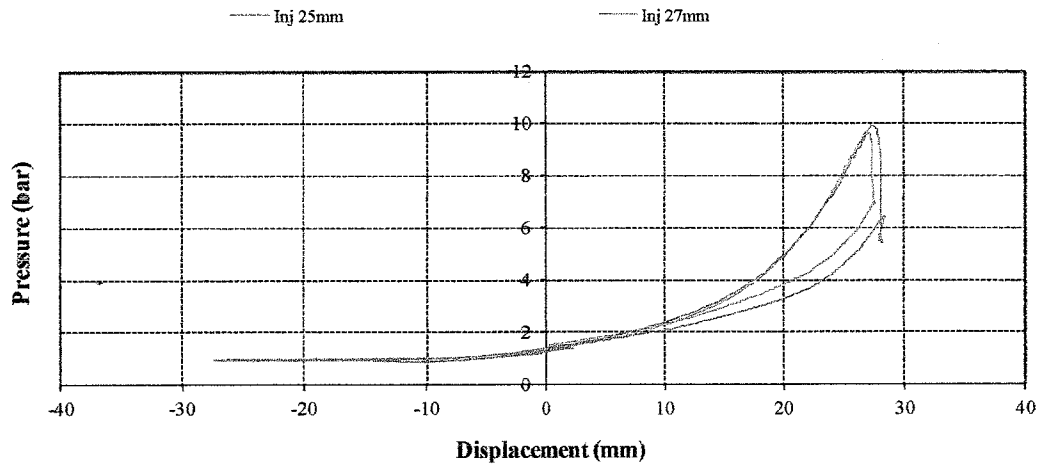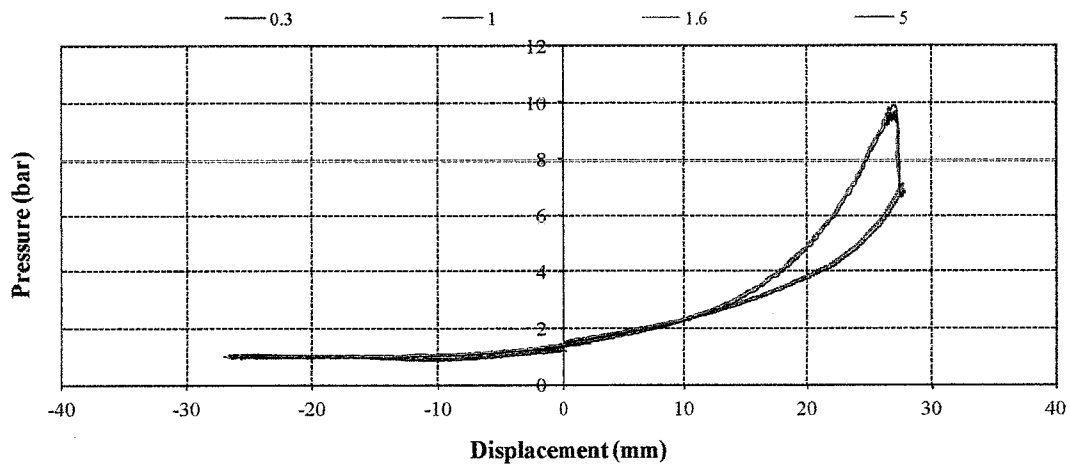Figure B.16: PV diagram constant 0.3 ER while vary injection timing (84 V)

111

Figure B.17: PV diagram constant 1 ER while vary injection timing (84 V)

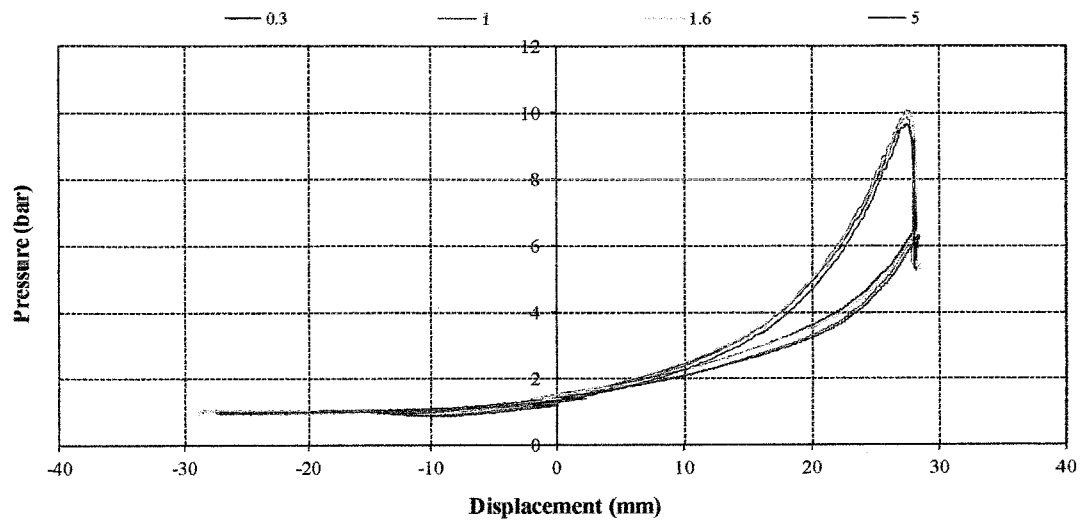Figure B.18: PV diagram constant 25 mm injection while vary equivalence ratio (84 V)

Figure B.19: PV diagram constant 27 mm injection while vary equivalence ratio (84 V)